

Spring 2018

INTEGRATED STRATIGRAPHIC CONTROLS FOR FLOW SIMULATION OF THE WALL CREEK MEMBER OF FRONTIER FORMATION: WESTERN POWDER RIVER BASIN, WYOMING

Tuan Le
Montana Tech

Follow this and additional works at: https://digitalcommons.mtech.edu/grad_rsch



Part of the [Petroleum Engineering Commons](#)

Recommended Citation

Le, Tuan, "INTEGRATED STRATIGRAPHIC CONTROLS FOR FLOW SIMULATION OF THE WALL CREEK MEMBER OF FRONTIER FORMATION: WESTERN POWDER RIVER BASIN, WYOMING" (2018). *Graduate Theses & Non-Theses*. 159.
https://digitalcommons.mtech.edu/grad_rsch/159

This Thesis is brought to you for free and open access by the Student Scholarship at Digital Commons @ Montana Tech. It has been accepted for inclusion in Graduate Theses & Non-Theses by an authorized administrator of Digital Commons @ Montana Tech. For more information, please contact sjuskiewicz@mtech.edu.

INTEGRATED STRATIGRAPHIC CONTROLS FOR FLOW SIMULATION
OF THE WALL CREEK MEMBER OF FRONTIER FORMATION:
WESTERN POWDER RIVER BASIN, WYOMING

by
Tuan Le

A thesis submitted in partial fulfillment of the
requirements for the degree of

Master of Science in Petroleum Engineering

Montana Tech

2018



Abstract

The Frontier Formation in the Powder River Basin has been re-discovered for oil and gas potential with the development of long horizontal wells and multi-stage hydraulic fracturing. Over the last decade, the Upper Cretaceous Wall Creek Member (WCM) of the Frontier Formation has proven to be a successful hydrocarbon-producing target, yet a full understanding of the flow behavior in this complex stratigraphic unit has not been fully achieved.

The fluid and rock properties have uncertainty and are not well defined due to the low permeability rocks. This study aims to describe the fluid flow behaviors of these features and create an integrated outcrop model that includes all the reservoir properties and geologic features to better understand hydrocarbon recovery. This project consists of two distinct aspects: (1) defining the reservoir properties through a well flow model and (2) upscaling the permeability of the reservoir models with different geologic features into an outcrop model for the WCM.

A single horizontal well flow simulation model was created to estimate the reservoir properties. Using well logs from three offset vertical wells, a 32 foot-thick interval was selected to represent the net pay zone of the WCM. The porosity was estimated using neutron porosity and density porosity well logs, and permeability was established by applying a correlation of porosity and permeability from core data. The historical production data was matched by modifying the initial fluid saturations and the rock physics parameters such as relative permeability and capillary pressure. As a result, representative fluid and rock physics models were obtained for the integrated outcrop model.

From the outcrop study, high-resolution models with different geologic facies of WCM were created to include abundances and orientations of mud drapes as the most impacted features that may affect the fluid flow ability. An integrated outcrop model captures fine heterogeneities of all the facies using flow-based upscaling of the high-resolution models. The effective directional permeabilities of each facies were obtained to integrate into a model to capture the geologic features that may have a large impact on the hydrocarbon recovery.

In this work, we developed methods to incorporate fine-scale (cm) geologic observations from the outcrop with well scale properties from the field in an integrated study that was ultimately used to help determine field level decisions such as well spacing and fracture spacing.

Keywords: Reservoir, characterization, fluid, behavior, Wall Creek Member, Frontier Formation, Powder River Basin

Dedication

This dissertation is dedicated to my sweet and loving Father and Mother who have raised and supported me with all their hearts. I also want to dedicate to my Brother who has been taking care of my parents entire time to allow me pursue education in United States with ease.

Acknowledgements

I wish to thank the members of my thesis committee for their consistent support, encouragement, constructive criticism and direction during the course of this dissertation:

Professor Todd Hoffman, who has continually and convincingly conveyed a spirit of adventure in regard to research and scholarship, and an excitement in regard to teaching. Without his guidance and persistent help this dissertation would not have been possible.

Professor David Reichhardt, who has been very patient in teaching and enthusiastic in learning new knowledge everyday and very willing to share it to his students.

Professor Larry Smith, whose teaching has been always efficient and very dedicated in helping students with his great knowledge.

I would like to thank for the supports of all Montana Tech faculty and friends for the past 5 years. They have helped my education at Montana Tech become more joyful and meaningful.

This project was funded in part of master thesis study by SM Energy Company. I thank for all engineers and geologists of Western Powder River basin team from SM Energy for providing the data, financial support and encouragement for this project. Special thanks for graduate student Nathan LaFontaine and Professor Michael Hofmann from University of Montana for their cooperations in this study

Table of Contents

| | |
|----------------------------------------------------------------------|--------------|
| ABSTRACT | II |
| DEDICATION | III |
| ACKNOWLEDGEMENTS | IV |
| TABLE OF CONTENTS..... | V |
| LIST OF TABLES | VIII |
| LIST OF FIGURES..... | IX |
| LIST OF EQUATIONS | XVIII |
| 1. INTRODUCTION | 1 |
| 1.1. Goal of Research | 2 |
| 1.2. Methodology..... | 3 |
| 2. BACKGROUND..... | 6 |
| 2.1. Wall Creek Member, Frontier Formation, Powder River Basin | 6 |
| 2.2. Porosity and Permeability | 10 |
| 2.3. Soave-Redlich-Kwong Equation of State | 11 |
| 2.4. Relative Permeability | 12 |
| 2.5. Flow Based Upscaling..... | 14 |
| 3. WELL SCALE MODELING | 16 |
| 3.1. Single Horizontal Well Reservoir Model | 16 |
| 3.2. Reservoir Properties | 19 |
| 3.2.1. Porosity | 20 |
| 3.2.2. Permeability | 23 |
| 3.2.3. Water Saturation..... | 26 |
| 3.3. Fluid Properties | 28 |

| | | |
|----------|------------------------------------------------------------------------|----|
| 3.4. | <i>Relative Permeability and Capillary Pressure</i> | 29 |
| 3.5. | <i>Well Completion</i> | 33 |
| 3.6. | <i>Preliminary Run and Sensitivity Analysis</i> | 34 |
| 3.6.1. | Preliminary run for history matching | 34 |
| 3.6.2. | Sensitivity analysis..... | 36 |
| 3.6.2.1. | Porosity | 38 |
| 3.6.2.2. | Permeability | 39 |
| 3.6.2.3. | Hydraulic Fractures | 41 |
| 3.6.2.4. | Relative Permeability | 43 |
| 3.6.2.5. | Summary of Sensitivity Analysis..... | 47 |
| 3.7. | <i>History Matching</i> | 48 |
| 3.7.1. | Logarithmic grid refinement application..... | 48 |
| 3.7.2. | Modification of reservoir properties | 49 |
| 3.7.3. | History matching results..... | 51 |
| 3.8. | <i>Field Analysis</i> | 53 |
| 3.9. | <i>Summary of Well Scale Model</i> | 57 |
| 4. | INTEGRATION OF THE OUTCROP OBSERVATION AND SUBSURFACE PROPERTIES | 58 |
| 4.1. | <i>High-Resolution Models</i> | 58 |
| 4.2. | <i>Flow Based Upscaling</i> | 60 |
| 4.3. | <i>Integrated Outcrop Model</i> | 63 |
| 4.4. | <i>Sensitivity Analysis of Integrated Outcrop Models</i> | 67 |
| 4.4.1. | Structural models vs Stratigraphic models..... | 67 |
| 4.4.2. | Field Development Analysis | 71 |
| 5. | DISCUSSION AND CONCLUSION | 77 |
| 6. | RECOMMENDATION | 79 |
| 7. | REFERENCES CITED..... | 80 |
| 8. | APPENDIX A: WELL SCALE MODEL | 84 |
| 9. | APPENDIX B: HIGH-RESOLUTION MODELS AND FLOW BASED UPSCALING..... | 91 |

| | |
|--------------------------------------------------------|----|
| 10. APPENDIX C: INTEGRATED OUTCROP MODEL ANALYSIS..... | 95 |
|--------------------------------------------------------|----|

List of Tables

| | |
|-------------------------------------------------------------------------------------------------------------|----|
| Table I: Reservoir properties taken from PVT report of Rush State well at 7,260 feet below sea level..... | 20 |
| Table II: Initial parameter for relative permeability curve | 30 |
| Table III: Values to generate a capillary pressure function using correlation for oil-water in Petrel | 32 |
| Table IV: Fracture Depth on Well Scale Model | 33 |
| Table V: Sensitivity analysis cases | 37 |
| Table VI: Modified parameter for relative permeability curve | 49 |
| Table VII: Characteristics of facies observed from the Tisdale Anticline outcrop (LaFontaine, 2018) | 60 |
| Table VIII: Properties of fresh water for flow-based upscaling | 61 |
| Table IX: Results of flow-based upscaling for each facies of WCM. | 63 |
| Table X: Color description of each facies for the Integrated Outcrop model..... | 63 |
| Table XI: Porosity/Permeability input for geologic structural and stratigraphic models .. | 69 |
| Table XII: Porosity/Permeability input for geologic structural and stratigraphic models. | 69 |
| Table XIII: Porosity/Permeability input for proxy models (Model 3B-1 and 3D-1)..... | 69 |
| Table XIV: Color description and initial assigned permeability of the Integrated Outcrop model. | 72 |
| Table XV: Initial properties for fluid components before matching | 84 |
| Table XVI: Properties for fluid components after matching using Soave-Redlich-Kwong EOS | 85 |

List of Figures

| | |
|----------------------------------------------------------------------------------------------------------------------------------------------------------------------------------------------------------------------------------|----|
| Figure 1: Workflow study to integrate the subsurface data and outcrop observation into full outcrop model. | 4 |
| Figure 2: (A) Cross-section of geologic study and location of Frontier outcrop at the surface in Wyoming that associated with Frontier Formation in PRB. (B) Tisdale Mountain outcrop study area. (C) Reservoir model study..... | 6 |
| Figure 3: Generalized east-west cross section of Powder River Basin showing a west side basin axis. (Anna and others, 2010) | 7 |
| Figure 4: Stratigraphic column of Upper Cretaceous strata in the Powder River Basin | 8 |
| Figure 5: 3D outcrop exposure (LaFontaine, 2018)..... | 10 |
| Figure 6: Well scale model boundary from WOGCC and modeled on Petrel showing Rush State well inside the boundary. | 16 |
| Figure 7: Location of Rush State well and three vertical offset wells (Moore Federal Fee 23-1, Bozeman Trail 25-1-A, and Taylor 25) in Johnson County, Wyoming (Map taken from WOGCC, 2018) | 17 |
| Figure 8: Geosteering data provided by SM Energy showing the Rush State well drilled inside the preferred target zone of WCM to indicate the 32-foot interval for reservoir model. | 18 |
| Figure 9: Upper and lower boundary surface of Well Scale model with Rush State well on Petrel. | 19 |
| Figure 10: Well log pickings from three vertical offset wells. | 21 |
| Figure 11: Porosity estimation from three vertical offset wells with 2 foot interval from formation top..... | 21 |

| | |
|---------------------------------------------------------------------------------------------------------------------------------------------------------------------------------------------------------------------------------------------------------------------------------------------------------------------------------------------------------------------------------------------------------------------------------------------------------|----|
| Figure 12: Porosity distribution ranging from 0.05 to 0.091 on Well Scale model..... | 22 |
| Figure 13: Permeability and porosity cross plot provided by SM Energy. One trend line (dashed) has one slope, and the other (black lines) has two different slopes changing at a porosity of 3.9%. (A) Core samples of WCM from different wells within study area. (B) Concentration cross plot for most common values distribution in core analysis. (PHIE = porosity measured from cores, Core_K _{max} = Permeability measure from cores). . | 24 |
| Figure 14: Permeability estimation from porosity-permeability cross plot. | 25 |
| Figure 15: Permeability distribution ranging from 0.0382 md to 0.7806 md on Well Scale model. | 25 |
| Figure 16: Water saturation logs of three vertical offset wells interpreted by SM Energy geologists. | 27 |
| Figure 17: Water saturation model ranging from 45% to 65%..... | 27 |
| Figure 18: PVT matching results for fluid model. Red dots are PVT data, blue lines are matched model..... | 29 |
| Figure 19: Relative permeability for the preliminary run. | 31 |
| Figure 20: Capillary pressure for the preliminary run. | 32 |
| Figure 21: Rush State well completion using the completion report from SM Energy. Entire horizontal portion of 4 ½ inch liner (grey) inside a 6-inch open hole (green). Each hydraulic fracture is represented by the single red rectangular box that penetrated through formation..... | 34 |
| Figure 22: Preliminary results of history matching with reasonable match for water production and water cut | 35 |

| | |
|----------------------------------------------------------------------------------------------------------------------------------------------------------------------------------------------------------------------------------------------------------------------------------------------------|----|
| Figure 23: Preliminary results of history matching with reasonable match for oil and gas production and bottomhole pressure. | 36 |
| Figure 24: Test run for sensitivity analysis using bottom hole pressure constrained from preliminary run for Rush State data. Oil, gas, and water cumulative production from two cases are matched on top of each other. | 37 |
| Figure 25: Porosity sensitivity analysis with 30% offset from average porosity with 2-foot interval. | 38 |
| Figure 26: Oil production cumulative and oil production rate for porosity sensitivity analysis. | 39 |
| Figure 27: Water production cumulative and water production rate for porosity sensitivity analysis. | 39 |
| Figure 28: Permeability sensitivity analysis with 12 cases of random distribution, minimum and maximum ranges of permeability. (A) A graph illustrates random permeability values within the minimum and maximum ranges. (B) Concentration porosity-permeability cross plot for core samples. | 40 |
| Figure 29: Top view (A) and side view (B) of random permeability distribution model. | 41 |
| Figure 30: Oil production cumulative and oil production rate for permeability sensitivity analysis. | 41 |
| Figure 31: Hydraulic fractures sensitivity analysis. | 42 |
| Figure 32: Oil production cumulative and oil production rate for hydraulic fractures sensitivity analysis. | 42 |
| Figure 33: Oil/Water relative permeability curves for oil Corey exponent sensitivity analysis. | 44 |

| | |
|-------------------------------------------------------------------------------------------------------------------------------|----|
| Figure 34: Oil production cumulative and oil production rate for oil Corey exponent sensitivity analysis..... | 44 |
| Figure 35: Oil/Water relative permeability curves for water Corey exponent sensitivity analysis. | 45 |
| Figure 36: Water production cumulative and water production rate for water Corey exponent sensitivity analysis. | 45 |
| Figure 37: Oil/gas relative permeability curves for gas Corey exponent sensitivity analysis. | 46 |
| Figure 38: Gas production cumulative and gas production rate for gas Corey exponent sensitivity analysis..... | 46 |
| Figure 39: K_{ro} at S_{omax} for oil/water relative permeability curves sensitivity analysis. | 47 |
| Figure 40: Oil production cumulative and oil production rate for K_{ro} at S_{omax} sensitivity analysis | 47 |
| Figure 41: Top (A) and side (B) view of the Petrel reservoir model for a single horizontal well showing LGR application. | 49 |
| Figure 42: Modified relative permeability for the historical production matching. | 50 |
| Figure 43: Modified permeability for history matching. | 51 |
| Figure 44: History matching results for with reasonable match for water production and water cut..... | 52 |
| Figure 45: History matching results for with reasonable match for oil and gas production and bottom hole pressure. | 52 |
| Figure 46: Fracture spacing analysis with 5 cases for different number of fracture stages and fracture spacing. | 53 |

| | |
|-------------------------------------------------------------------------------------------------------------------------------------------------------------------------------------------------------------------|----|
| Figure 47: Fracture spacing analysis results for oil cumulative production. | 54 |
| Figure 48: Fracture spacing analysis results for oil production rate. | 54 |
| Figure 49: Well spacing analysis with 5 cases for different number of wells and well spacing in a same reservoir. | 55 |
| Figure 50: Well spacing analysis results for oil cumulative production..... | 56 |
| Figure 51: Well spacing analysis results for oil production rate of a middle well in each case (right) | 56 |
| Figure 52: An example of defined geologic model for 5 feet thick tidal bar top. (Arrow illustrates the direction of the model)..... | 59 |
| Figure 53: Examples of flow-based upscaling in three directions for tidal bar top model | 61 |
| Figure 54: Example of permeability reduction of tidal bar top with T_m from 0 to 1 | 62 |
| Figure 55: Integrated Outcrop model (Model 3A) including architectural stratigraphy of Wall Creek member based on the measured points taken at the outcrop. (Arrow illustrates the direction of model)..... | 64 |
| Figure 56: Proxy structural model (Model 3B) including the simplification of facies distribution of the outcrop. (Arrow illustrates the direction of model) | 65 |
| Figure 57: Integrated Outcrop models with flattened structure: (A) geologic stratigraphic model (Model 3C) and (B) proxy stratigraphic model (model 3D). (Arrow illustrates the direction of model)..... | 66 |
| Figure 58: Permeability graph with boundary line between two distinct sedimentary facies. | 67 |
| Figure 59: Well placement for outcrop analysis – Vertical wells (red) and Horizontal wells (teal) (Arrow illustrate the direction of the model). | 68 |

| | |
|--------------------------------------------------------------------------------------------------------------------------------------------------------------------------------------------------------------------------------------------------------------------------------------------------------------------------------------|----|
| Figure 60: A horizontal well was modeled at the middle of the reservoir that penetrated the first two tidal bar layers of the geologic model. (Arrow illustrates the direction of the model) | 73 |
| Figure 61: Cumulative oil production of three model scenarios..... | 74 |
| Figure 62: Modified fracture height well penetrate only into the first two layers of interested zones. (Arrow illustrates the direction of model) | 75 |
| Figure 63: (A) Cumulative oil production and (B) cumulative water production of four scenarios in fracture height analysis on production using integrated outcrop model with and without permeability reduction. ((ModifiedHBasecase and ModifiedHReducedCase are the cases with reduced fracture height for model 3a and 3b))...... | 75 |
| Figure 64: Three horizontal wells with 440 feet spacing for well spacing analysis. (Arrow illustrates the direction of model). | 76 |
| Figure 65: Well spacing analysis compares the effect of stratigraphic system on field development. Upper three lines simulate three wells production. Lower three lines simulate one well production. (WS = Well spacing case) | 76 |
| Figure 66: Gas production cumulative and gas production rate for porosity sensitivity analysis. | 86 |
| Figure 67: Water production cumulative and water production rate for minimum and maximum permeability sensitivity analysis. | 86 |
| Figure 68: Gas production cumulative and gas production rate for minimum and maximum permeability sensitivity analysis. | 86 |
| Figure 69: Water production cumulative and water production rate for random permeability sensitivity analysis. | 87 |

| | |
|-----------------------------------------------------------------------------------------------------------------------|----|
| Figure 70: Gas production cumulative and gas production rate for random permeability sensitivity analysis. | 87 |
| Figure 71: Water production cumulative and water production rate for hydraulic fractures sensitivity analysis. | 87 |
| Figure 72: Gas production cumulative and gas production rate for hydraulic fractures sensitivity analysis..... | 88 |
| Figure 73: Water production cumulative and water production rate for oil Corey exponent sensitivity analysis. | 88 |
| Figure 74: Gas production cumulative and gas production rate for oil Corey exponent sensitivity analysis..... | 88 |
| Figure 75: Oil production cumulative and oil production rate for water Corey exponent sensitivity analysis. | 89 |
| Figure 76: Gas production cumulative and gas production rate for water Corey exponent sensitivity analysis. | 89 |
| Figure 77: Oil production cumulative and oil production rate for gas Corey exponent sensitivity analysis..... | 89 |
| Figure 78: Water production cumulative and water production rate for gas Corey exponent sensitivity analysis | 90 |
| Figure 79: Water production cumulative and water production rate for K_{ro} at S_{omax} sensitivity analysis..... | 90 |
| Figure 80: Water production cumulative and water production rate for K_{ro} at S_{omax} sensitivity analysis..... | 90 |

| | |
|----------------------------------------------------------------------------------------------------------------------------------------------------------------------------------------------------------------------------------|----|
| Figure 81: (A) Thin, interbedded sandstone and siltstone/mudstone facies model, and (B) mud drapes abundance illustrated by black traces. | 91 |
| Figure 82: Flow-based upscaling results for Thin, interbedded sandstone and siltstone/mudstone facies. | 91 |
| Figure 83: Shoreface Parasequences facies models..... | 92 |
| Figure 84: Flow-based upscaling results for Shoreface Parasequences facies. | 92 |
| Figure 85: Tidal bar base and tidal bar top facies models | 93 |
| Figure 86: Flow-based upscaling results for tidal bar top facies. | 93 |
| Figure 87: Flow-based upscaling results for tidal bar base facies. | 94 |
| Figure 88: Results of vertical wells scenarios for geologic structural model (Model 3A) with $T_m=0$ and $T_m=0.5$. (D = Dipping, Vert = Vertical, A = All zones perforated, SW = South-West, NE = North-East, C = Center)..... | 95 |
| Figure 89: Results of vertical wells scenarios for proxy structural model (Model 3B). (D = Dipping, Px = Proxy, Vert = Vertical, A = All zones perforated, SW = South-West, NE = North-East, C = Center). | 95 |
| Figure 90: Results of horizontal wells scenarios for geologic structural model (Model 3A) with $T_m=0$. (D = Dipping, WE = West-East, NS = North-South, L = Lower zone, U = Upper zone, Frac = Hydraulic fractures). | 96 |
| Figure 91: Results of horizontal wells scenarios for geologic structural model (Model 3A) with $T_m=5$. (D = Dipping, WE = West-East, NS = North-South, L = Lower zone, U = Upper zone, Frac = Hydraulic fractures). | 96 |

- Figure 92: Results of horizontal wells scenarios for proxy structural model (Model 3B). (D = Dipping, Px = Proxy, WE = West-East, NS = North-South, L = Lower zone, U = Upper zone, Frac = Hydraulic fractures).97
- Figure 93: Results of vertical wells scenarios for geologic stratigraphic model (Model 3C) with $T_m=0$ and $T_m=0.5$. (Vert = Vertical, A = All zones perforated, SW = South-West, NE = North-East, C = Center).97
- Figure 94: Results of vertical wells scenarios for proxy stratigraphic model (Model 3D). (Px = Proxy, Vert = Vertical, A = All zones perforated, SW = South-West, NE = North-East, C = Center).98
- Figure 95: Results of horizontal wells scenarios for geologic stratigraphic model (Model 3C) with $T_m=0$. (WE = West-East, NS = North-South, L = Lower zone, U = Upper zone, Frac = Hydraulic fractures).98
- Figure 96: Results of horizontal wells scenarios for geologic stratigraphic model (Model 3C) with $T_m=5$. (WE = West-East, NS = North-South, L = Lower zone, U = Upper zone, Frac = Hydraulic fractures).99
- Figure 97: Results of horizontal wells scenarios for proxy stratigraphic model (Model 3D). (Px = Proxy, WE = West-East, NS = North-South, L = Lower zone, U = Upper zone, Frac = Hydraulic fractures).99

List of Equations

Equation (1)11

Equation (2)11

Equation (3)13

Equation (4)13

Equation (5)13

Equation (6)15

Equation (7)15

Equation (8)23

Equation (9)23

Equation (10)26

Equation (11)31

1. Introduction

Early introduction of oil reservoir of Wall Creek sandstone (later named the Wall Creek Member of the Frontier Formation [Merewether, 1996]) was reported by Wegemann (1911) at the Salt Creek oil field in Wyoming to study the hydrocarbon potential of Western Powder River Basin. Wegemann (1911) showed that the Wall Creek sandstone had good quality reservoir rocks including porosity and permeability through core samples taken from wells and evidences of oil production from early wells. More detailed studies of sandstone in Wall Creek Member were reported by Merewether (1996) through core studies of the Wall Creek outcrop found in the southern half of Johnson County to become an initial approach for Wall Creek study in this thesis project. Over the last decade, the Frontier Formation in the Powder River Basin has been re-discovered for oil and gas potential with the development of long horizontal wells and multi-stage hydraulic fracturing. The Upper Cretaceous Wall Creek Member (WCM) of the Frontier Formation has proven to be a successful hydrocarbon-producing target, yet a full understanding of the flow behavior of this complex stratigraphic unit has not been fully achieved. This project was started in 2014 by the University of Montana and SM Energy to study the stratigraphy of the WCM using the Tisdale Anticline outcrop at Wall Creek Road along the western margin of the Powder River Basin, south of Kaycee, Johnson County, Wyoming. Zupanic (2017) built a virtual outcrop model of part of the Wall Creek outcrop. However, studying the multi-scale heterogeneities using quantitative analog studies is not sufficient to understand their effects on reservoir behavior (LaFontaine, 2018). Other aspects such as rock physics and fluid properties from reservoir engineers working with the subsurface data are important to explain the fluid flow behavior in such heterogeneities of the WCM. The outcrop-based modeling has been conducted to build a high-resolution model from the virtual outcrop model to include the impact of multi-

scale heterogeneities (from cm-scale to m-scale). The model describes the main stratigraphic features of the WCM, which is divided by two distinct packages of facies: wave-influenced facies and tidally-influenced facies. Each of the packages contains the set of sequence stratigraphy that includes the related depositional sequences for creating this outcrop model (LaFontaine, 2018). Quantifying the spatial variation of architecture and associated reservoir connectivity at the bed-scale level became a main focus for the outcrop study to understand the fluid flow behavior. Flow-based upscaling has preserved these features in terms of effective permeability in horizontal and vertical directions to represent fine-scale heterogeneities in a coarse-grid reservoir model. Integration of subsurface data into this model improves the reliability for predicting the reservoir capability and reservoir performance under subsurface conditions.

Results from this study includes: (1) creating the workflow to incorporate the geologic features from the outcrop observation with the subsurface data, (2) understanding how the distinct geologic features of the WCM affect the fluid flow behavior, and (3) recommending the well placement strategies for the WCM of the Frontier Formation, Powder River Basin. The outcome will demonstrate that the study of stratigraphy from the outcrop is very important to explain the complexity of the reservoir that will lead to a better subsurface modeling and possibly more efficient well placement, drilling, and completion.

1.1. Goal of Research

The study aims to describe the fluid flow behaviors of the WCM in the Frontier Formation and create an integrated outcrop model that includes all the reservoir properties and geologic features to better understand hydrocarbon recovery. This project consists of two distinct aspects: (1) defining the reservoir properties through a well flow model and (2) upscaling the

permeability of the outcrop models with different geologic features into a reservoir model for the WCM. This work will try to develop the methods to incorporate fine-scale (cm) geologic observations from the outcrop with well scale (m) properties from the field in an integrated study that was ultimately used to help determine field level decisions such as well spacing and fracture spacing.

1.2. Methodology

The project is a collaboration between Montana Tech, University of Montana, and SM Energy. The main task of this research is to build the flow simulation model to capture the complex small-scale stratigraphic heterogeneity of the WCM observed in the Tisdale Anticline on the western margin of the Powder River Basin in Wyoming. The University of Montana provided the high-resolution models including the interpretation from the outcrop, and Montana Tech uses these models to analyze different fluid flow behavior. In this thesis, three different types of models were created:

1. Well Scale model – a horizontal well reservoir model that includes the reservoir properties of WCM in Western Powder River Basin. This model will be referred to as Model 1 (Scale: 5000 ft x 2500 ft x 32 ft)
2. High-Resolution model – Detailed model of each facies presented in WCM. This model will be referred to as Model 2 (Scale: 50 ft x 50 ft x 5 ft)
3. Integrated Outcrop model – Full scale outcrop model with upscaled permeability from the high-resolution model and reservoir properties from well scale model. This model will be referred to as Model 3 (Scale: 2300 ft x 1600 ft x 60 ft)

The Well Scale model (Model 1) for WCM of Frontier Formation in Western Powder River Basin is created using Schlumberger's Petrel software. The model was built based on

information gathered from well logs, core samplings, literature, and production data. This model was used to understand the overall reservoir properties including porosity, permeability, saturation, fluid properties, rock physics, and fluid behavior inside the reservoir. The High-Resolution models (Model 2) for each facies in WCM were created from outcrop observations, and then flow-based upscaling (King and Mansfield, 1999) was used to integrate this information into an outcrop model that includes different geologic features. The outcomes from the Well Scale model (fluid properties and relative permeability) were included into the Integrated Outcrop model (Model 3) to analyze fluid flow behavior with and without applying detailed geologic features. Field analysis was also performed to determine optimal development plans. Figure 1 shows a diagram of the work flow to incorporate the geologic features from the outcrop into the model.

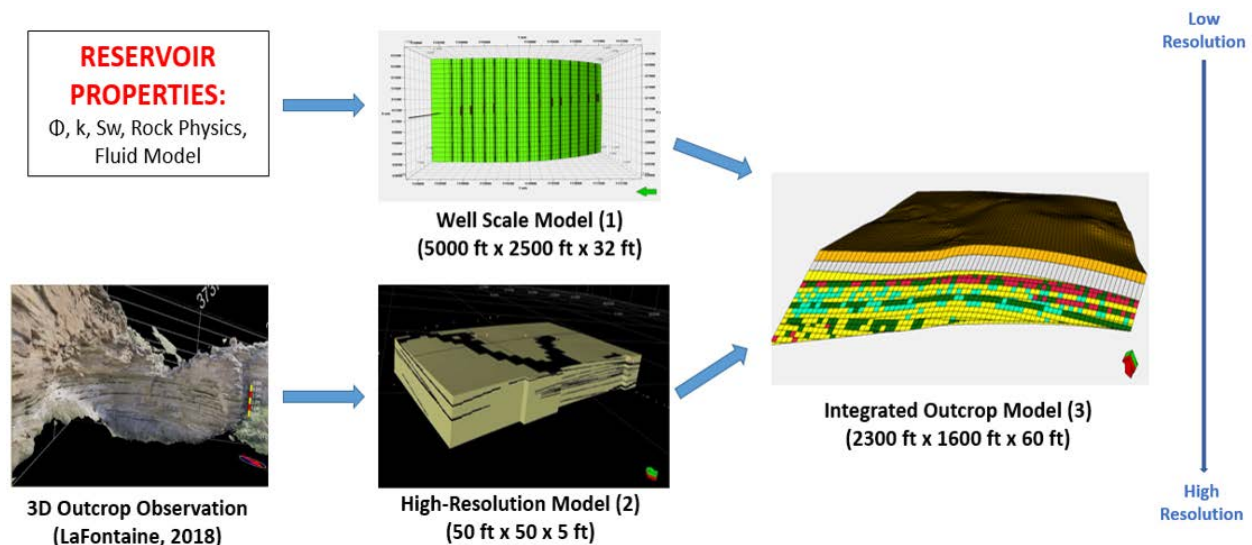


Figure 1: Workflow study to integrate the subsurface data and outcrop observation into full outcrop model.

The workflow to complete the research included:

- Gather data including well logs, core analysis, well completion report, PVT report, and historical production.

- Interpret the well logs to estimate water saturation and porosity, and apply permeability-porosity correlation.
- Build the black oil fluid model using Soave-Redlich-Kwong equation of state (Soave, 1972) to model different fluid behaviors at different pressures.
- Build the Well Scale model based on one horizontal well produced from WCM.
- Estimate the rock physics of WCM using historical production matching.
- Perform sensitivity analysis on reservoir model parameters to ensure the reliability of the final matching model.
- Create High Resolution models from fine-scaled detailed outcrop data.
- Perform flow-based upscaling for high-resolution model with various architectural controls on fluid flow within a hierarchical stratigraphic system implementing the single-phase flow method of Durlafsky (2005).
- Integrate High Resolution models into the Integrated Outcrop model.
- Analyze the fluid flow behavior and field development using the Integrated Outcrop model.

2. Background

2.1. Wall Creek Member, Frontier Formation, Powder River Basin

The Powder River Basin (PRB) is located in northeastern Wyoming and southeastern Montana in the United States. The basin is bounded from West to East by the Bighorn Mountain and the Black Hills, respectively (Figure 2). As shown in Figure 3, the Powder River Basin is an asymmetric basin with near overturned dip on the West side and gentle sub horizontal dip to the East side of the basin. The deepest part of the basin is around 17,000 feet to the top of the Precambrian basement. The uplift dip is about 500 feet per mile to the east side of Casper arch, Bighorn Mountains and about 100 feet per mile to the west side of Black Hills (Anna and others, 2010).

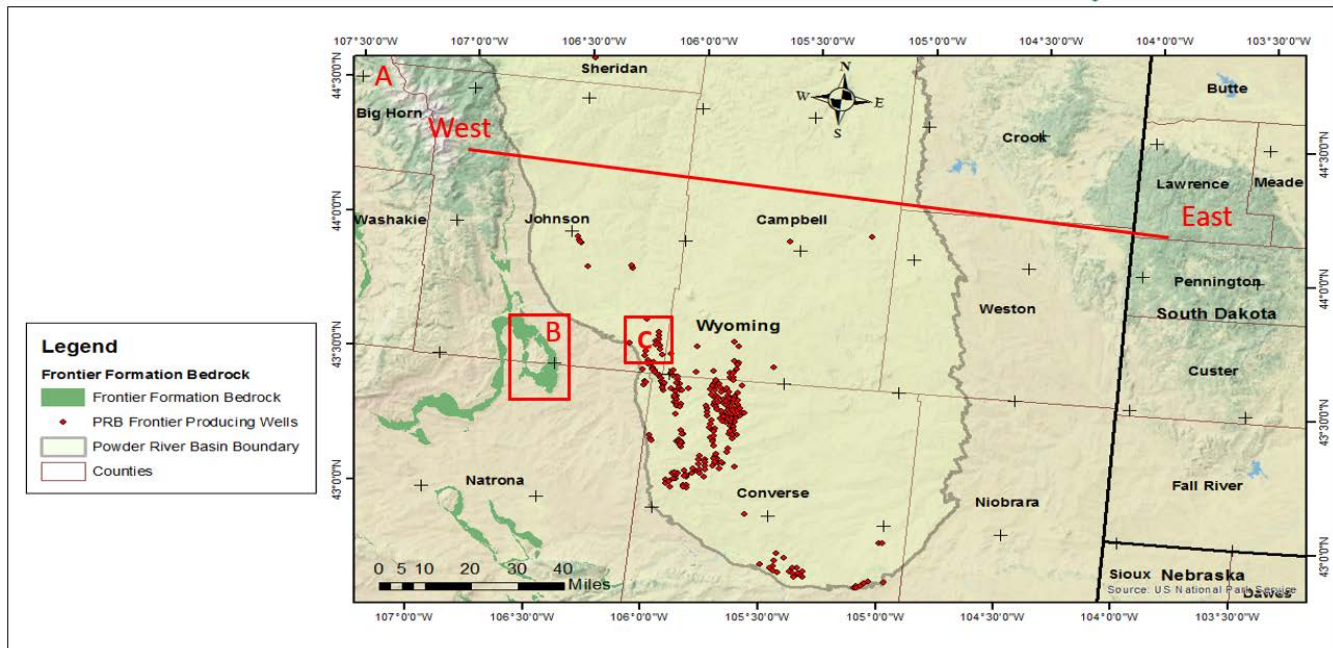


Figure 2: (A) Cross-section of geologic study and location of Frontier outcrop at the surface in Wyoming that associated with Frontier Formation in PRB. (B) Tisdale Mountain outcrop study area. (C) Reservoir model study.

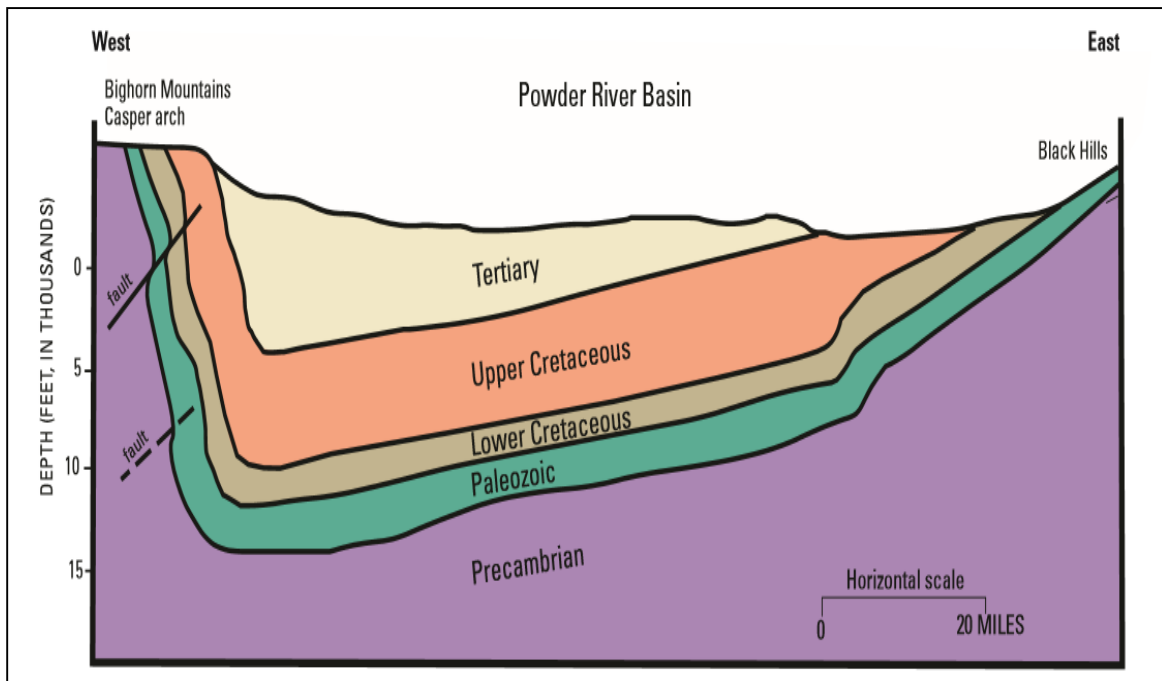


Figure 3: Generalized east-west cross section of Powder River Basin showing a west side basin axis. (Anna et al., 2010)

The Frontier Formation was deposited during Late Cretaceous by an eastward-prograding clastic wedge into a foreland basin during Cenomanian and Turonian Age (Bhattacharya and Willis, 2001). The Frontier Formation is bounded by the upper contact Clay Spur Bentonite bed of Mowry Shale and Carlile shale as part of Cody Shale (Merewether, 1996). Mowry Shale was determined to be the Lower Cretaceous petroleum source rock for the Frontier Formation (Nixon, 1973; Byers and Larson, 1979). Hydrocarbon migrated vertically through connected faults or fracture zones associated with the Belle Fourche arch (Anna et al., 2010). Due to the asymmetrical basin, the depositional environments and sequence stratigraphy of the Powder River Basin are divided into Western and Eastern Powder River Basin shown in Figure 4. An example of this feature is WCM and Turner Sandy Member. They were both deposited during Late Cretaceous. While Turner Sandy Member was described to be deposited in shelf depression (Rice and Keighin, 1989) or reworked from Wall Creek sands through tidal currents and postdeposition transgression (Merewether, 1996), WCM was deposited by consequent

progradation of deltaic environment (Merewether, 1996). Therefore, the study was conducted using the data mainly on Western Powder River Basin.

| System | Series | Stage | West PRB | East PRB |
|------------|---------------|----------------------|---------------------|---------------------|
| CRETACEOUS | Upper | Maastrichtian (part) | Fox Hills Formation | Fox Hills Formation |
| | | Campanian | Mesaverde Fm | Pierre Sh |
| | | | Lewis Sh | |
| | | | Teapot Ss Mbr | |
| | | | unnamed | |
| | | | Parkman Ss Mbr | |
| | | | unnamed | |
| | | | Sussex Ss | |
| | | | Shannon Ss | |
| | | | Steele Sh | |
| | | Santonian | Niobrara Fm | Niobrara Fm |
| | | Coniacian | | |
| | | Turonian | Carlile Sh | Carlile Sh |
| | | | Wall Ck Mbr | Turner Sandy Mbr |
| | | | | Pool Ck Mbr |
| Lower | Albian (part) | Cenomanian | Frontier Fm | Greenhorn Fm |
| | | | Belle Fourche Mbr | Belle Fourche Sh |
| | | | Frontier sandstones | |
| | | | Mowry Shale | Mowry Shale |

Figure 4: Stratigraphic column of Upper Cretaceous strata in the Powder River Basin (modified from (Anna et al., 2010))

According to the initial finding by Zupanic et al. (2016), the heterolithic lowstand system tract has shown to be the primary reservoir interval of interest. This finding was supported by later study of Zupanic (2017) based on the outcrop observation. This study was conducted at the eastern limb of the Tisdale Anticline seen in Figure 1-B on the western margin of the Powder River Basin. Using a sedimentological and modeling approach, the outcrop was analyzed to create the field-scale geocellular model framework and multiple, nested facies models capturing

bed-scale heterogeneities affecting fluid flow (Zupanic, 2017). These heterogeneities were defined as the muddy toesets of bed-scale, migrating dunes. The observed outcrop consisted of a 50 to 66 foot thickness of the WCM which includes the heterolithic, reservoir facies shown in Figure 5. Two distinct sedimentary facies that are discussed in the study of LaFontaine (2018) is: tidally-influenced facies and wave-influenced facies. Within the tidally-influenced facies, there are a series of stacked tidal bars about 16 feet thick that are the basic building blocks of this part of the reservoir and laterally extend across the entire outcrop area. Each of these tidal bars has complex internal structure that likely affects fluid flow. To fully describe the WCM, stratigraphy sequence of wave-influenced facies were also included to analyze the fluid migration vertically. Typical measurements for reservoir properties in these facies cannot account for the impact made by these muddy baffles and barrier, as they cannot be captured in logs or seismic. The integration of geologic, petrologic, petrophysical and geophysical models can help to predict the reservoir heterogeneity better (Samuel and et al., 2015) by adding geologic comprehension of stratigraphic architecture and reservoir distribution into one reservoir model. This research suggests the study by LaFontaine (2018) to analyze the geology of WCM from the outcrop and integrate it with a reservoir model built by actual subsurface data to understand the heterogeneities of WCM. For example, Figure 5 captures the mud-drape visibility (black traces) due to weathering between mud and sand within the tidal bars. These features were interpreted throughout the outcrop, and then imported into a high-resolution model to create a network of truncated muddy toe-sets that may represent the realistic bed geometries, spacing, extent and sand connectivity.

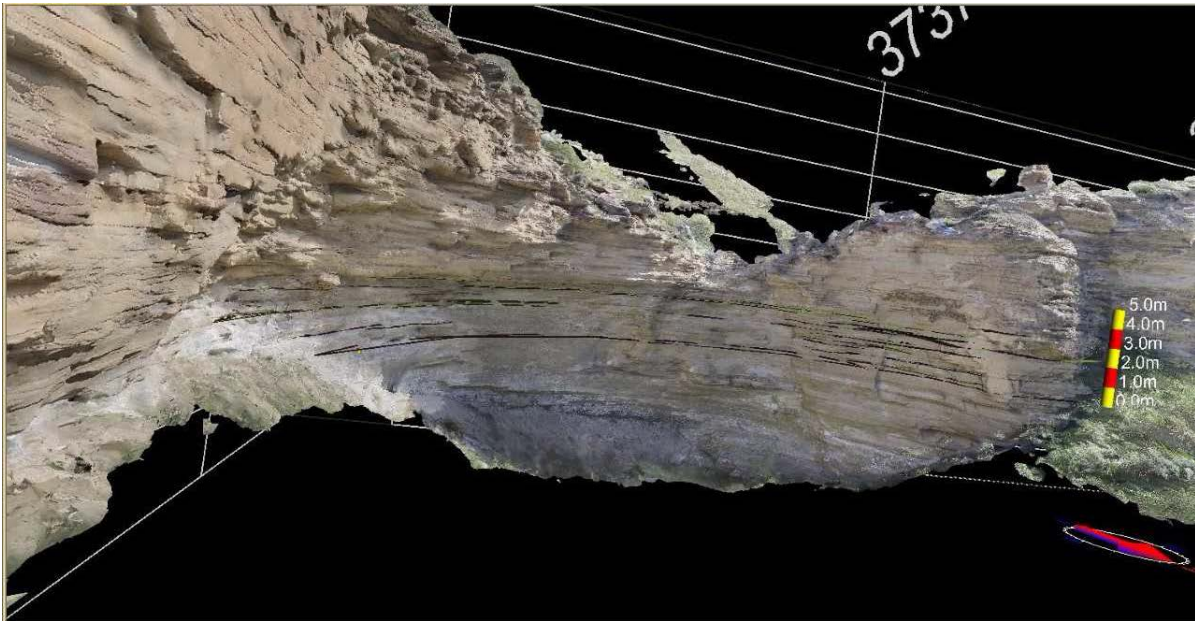


Figure 5: 3D outcrop exposure (LaFontaine, 2018).

2.2. Porosity and Permeability

Porosity and permeability are related properties that are used to describe the capability of fluid inside the sediments. Porosity is the open space in a rock that can be occupied by the fluid inside a rock. Permeability is an ability for fluid to flow through the rock. The values of porosity and permeability often define the capability of the reservoir rocks to hold the oil and gas, as well as a productivity of the reservoir.

Porosity is often measured in laboratory directly from the core samples taken from the drilled wells. However, laboratory measurements for porosity are not very representative due to the heterogeneities of the reservoir on the large-scale model (Dandekar, 2013). For simulation purposes, the porosity estimation is improved by including additional types of information. Well logging has been developed to measure the rock properties while drilling or during completion to capture the lithological properties at every depth inside the well (Schuster and Riboud, 1971). A common method to estimate porosities is based on the neutron porosity and density porosity

from well logs. If the density porosity is less than neutron porosity the porosity is assumed to be equal to the density porosity. In contrast, basic average calculation using density porosity (ϕ_D) and neutron porosity (ϕ_N) is applied to find porosity from the well logs as shown by Hartmann and Beaumont (1999) in the equation below:

$$\Phi = \left(\frac{\Phi_N^2 + \Phi_D^2}{2} \right)^{1/2} \quad (1)$$

Permeability cannot be obtained directly by well logging methods. Permeability must be either measured using core or computed using a correlation with other properties such as water saturation, porosity, stresses, etc. to estimate the permeability values (Dandekar, 2013).

Permeability varies with lithology and location under different overburden stresses inside the reservoir. In this project, SM Energy has provided the permeability and porosity cross plot that was obtained from many core sample analyses around the field.

2.3. Soave-Redlich-Kwong Equation of State

Reservoir fluid properties were obtained from the Pressure-Temperature-Volume (PVT) report of Rush State well located in Johnson County, Wyoming (Figure 2C) that represents the fluid properties of WCM. The PVT data was analyzed using PVTi software with the Soave-Redlich-Kwong equation of state (EOS) to create the fluid model. The mathematical expression (Eq. 1) of Soave-Redlich-Kwong EOS (Soave, 1972) is:

$$P = \frac{RT}{V_m - b} - \frac{a\alpha}{V_m(V_m + b)} \quad (2)$$

Where:

$P = \text{pressure (psia)}$

$R = \text{gas constant } \left(\frac{ft^3 \cdot psia}{^\circ R \cdot lb-mole} \right)$

$T = \text{temperature (degree Rankine or } ^\circ R)$

$V_m = \text{molar volume } (\frac{ft^3}{mole})$

$\alpha = \text{attraction parameter} = (1 + (0.480 + 1.574\omega - 0.176\omega^2)(1 - \sqrt{T_r}))^2$

$a = \text{modified attraction parameter} = \Omega_a \frac{R^2 T_c^2}{P_c}$

$b = \text{repulsion parameter} = \Omega_b \frac{RT_c}{P_c}$

$\Omega_a = \text{constant that corrects for attractive potential of molecules}$

$\Omega_b = \text{constant that corrects for volume}$

$T_c = \text{critical temperature of a component (degree Fahrenheit or } ^\circ F)$

$P_c = \text{critical pressure of a component (psia)}$

$T_r = \text{reduced temperature}$

$\omega = \text{acentric factor}$

The use of an EOS in PVT matching helps to describe the state of fluid in different reservoir conditions such as temperature and pressure (Perrot, 1998). The black oil model describe the fluid properties as a function of pressure (Coats et al., 1998). In this project, the black oil model created from PVT matching by the EOS should be more representative for the reservoir fluid of WCM and allow the simulation to run faster with fewer errors than using the direct PVT data measurements due to the variation of the data.

2.4. Relative Permeability

Fluid behavior in modeling is often described using relative permeability curve, which is expressed by relative permeability of each fluid as a function of a fluid saturation (Dandekar, 2013). In WCM reservoir, three types of fluids are presented: oil, gas, and water. A construction

of the relative permeability curves is necessary in the presence of more than one fluid in porous medium to describe the reservoir flow processes using modified Brook-Corey relations (Brooks and Corey, 1964):

$$k_{ro} = k_{ro,max} \left(\frac{S_o - S_{or}}{1 - S_{or} - S_{wir} - S_{gr}} \right)^{n_o} \quad (3)$$

$$k_{rw} = k_{rw,max} \left(\frac{S_w - S_{wc}}{1 - S_{or} - S_{wir} - S_{gr}} \right)^{n_w} \quad (4)$$

$$k_{rg} = k_{rg,max} \left(\frac{S_g - S_{gc}}{1 - S_{or} - S_{wir} - S_{gr}} \right)^{n_g} \quad (5)$$

Where:

k_{ro} = relative permeability of oil

k_{rw} = relative permeability of water

k_{rg} = relative permeability of gas

$k_{ro,max}$ = maximum relative permeability of oil

$k_{rw,max}$ = maximum relative permeability of water

$k_{rg,max}$ = maximum relative permeability of gas

S_o = saturation of oil

S_w = saturation of water

S_g = saturation of gas

S_{or} = residual saturation of oil

S_{wir} = irreducible saturation of water

S_{gr} = residual saturation of water

n_o = Corey exponent of oil

$n_w = \text{Corey exponent of water}$

$n_g = \text{Corey exponent of gas}$

By observing the historical production, well logs, and literature study of Frontier Formation (Moore, 2016), the end-point fluid saturations such as S_{or} , S_{wir} , and S_{gr} were estimated and modified to be within reasonable ranges that was discussed later. Corey exponent of each fluid was also modified to describe better the interferences of each fluid in the porous medium to achieve the historical production matching.

2.5. Flow Based Upscaling

Upscaling is a process of assigning effective properties to coarse scale cells from properties on a fine scale grid (Warren and Price, 1961). Geological models often contain millions of cells that makes the run time of a simulation longer and can cause more conversion problems. Upscaling will help to reduce the CPU time for uncertainty analysis and risk assessment (Warren and Price, 1961). Many methods have been used for upscaling geologic models (Qi and Hesketh, 2007). The most common is simply averaging the properties, but this often leads to property distributions that are too smooth and not representative of the parameter being modeled (Paterson et al., 1996). Flow based upscaling is a common method that honors the geological characteristics of the field to preserve the connectivity and flow within the reservoir (Samier, 1990; King and Mansfield, 1991; Durlofsky, 2005). The process will upscale the permeability in three directions X, Y, and Z from a fine scale grid to coarse scale grid.

For this project, Petrel was used for the simulation to estimate the permeability in three directions. The simulation allowed the fluid flow through part of reservoir in only one direction. For example, if the fluid flows in the X direction, the boundaries in the Y and Z directions will

be closed (Samier, 1990). This will only be done for the section of the reservoir that is being upscaled. Darcy's law for single phase flow (Muskat and Botset, 1931) was applied to each simulation to calculate the effective permeability in each direction as shown in equation 3.

$$q = \frac{kA(P_{in} - P_{out})}{\mu L} (SI \text{ Unit}) \quad (6)$$

The equation is then formatted with conversion factor from SI unit to field unit and from reservoir condition to surface condition by formation volume factor (β) (Dandekar, 2013).

$$q = \frac{0.001127kA(P_{in} - P_{out})}{\mu L \beta} (Field \text{ Unit}) \quad (7)$$

Where:

$q = \text{flow rate } (\frac{m^3}{s} \text{ in SI Unit or } \frac{bbl}{day} \text{ in Field Unit})$

$k = \text{effective permeability } (m^2 \text{ in SI Unit or milidarcy in Field Unit})$

$A = \text{cross section area } (m^2 \text{ in SI Unit or } ft^2 \text{ in Field Unit})$

$P = \text{pressure } (Pascal \text{ in SI Unit or } psia \text{ in Field Unit})$

$\mu = \text{viscosity } (Pascal.s \text{ in SI Unit or } cp \text{ in Field Unit})$

$L = \text{length } (m \text{ in SI Unit or } feet \text{ in Field Unit})$

$\beta = \text{formation volume factor } (reservoir \text{ barrel}/standard \text{ condition barrel})$

3. Well Scale Modeling

3.1. Single Horizontal Well Reservoir Model

The Well Scale model used the Rush State well (API number 4901929986) located in NW/4 NE/4 of section 36, township 42N, Range 77W in Powder River Basin, Johnson County, Wyoming. The model boundary was based on the actual coordinates according to Wyoming Oil and Gas Conservation Commission (WOGCC, 2016) (Figure 6). The boundary size was about 5000 feet by 2500 feet. The reservoir properties were found based on three vertical offset wells: Bozeman Trail 25-1-A (API Number 4901920972), Moore Federal Fee 23-1 (API number 4901920829), and Taylor 25 (API number 4901920891) that were about one mile distance away from the Rush State well (Figure 7).

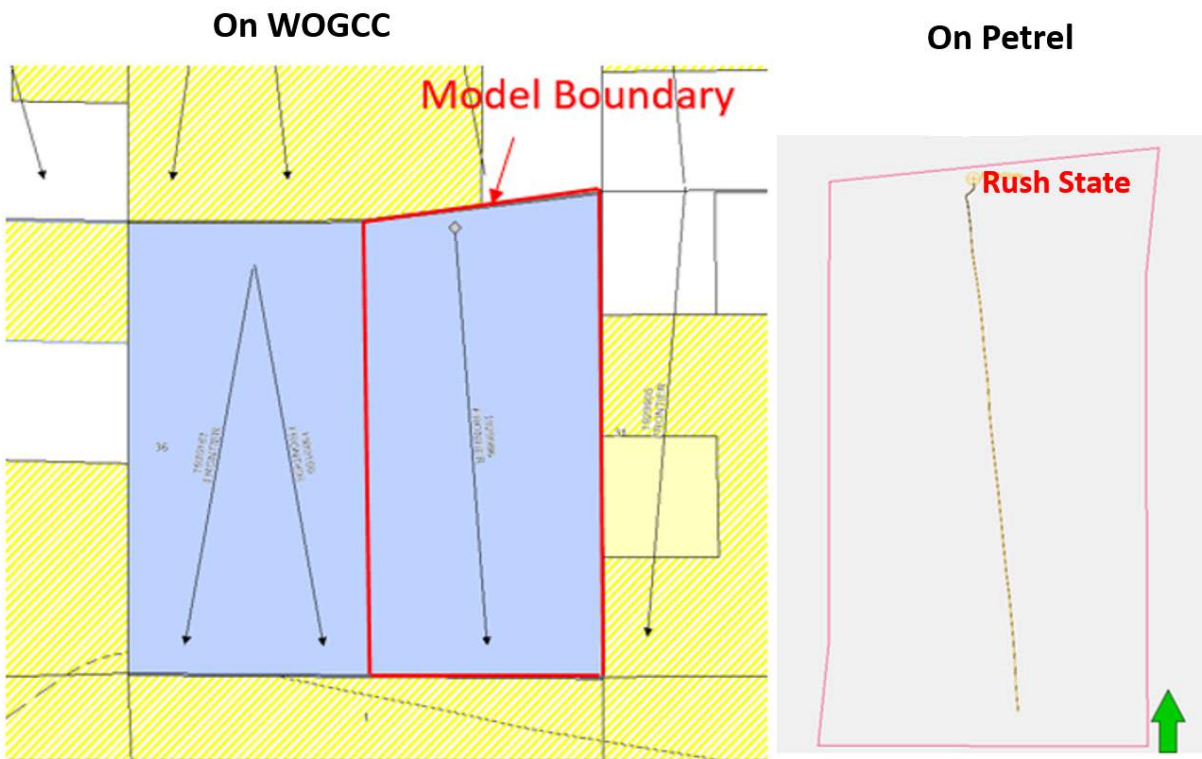


Figure 6: Well scale model boundary from WOGCC and modeled on Petrel showing Rush State well inside the boundary (Arrow illustrates the direction of the model).

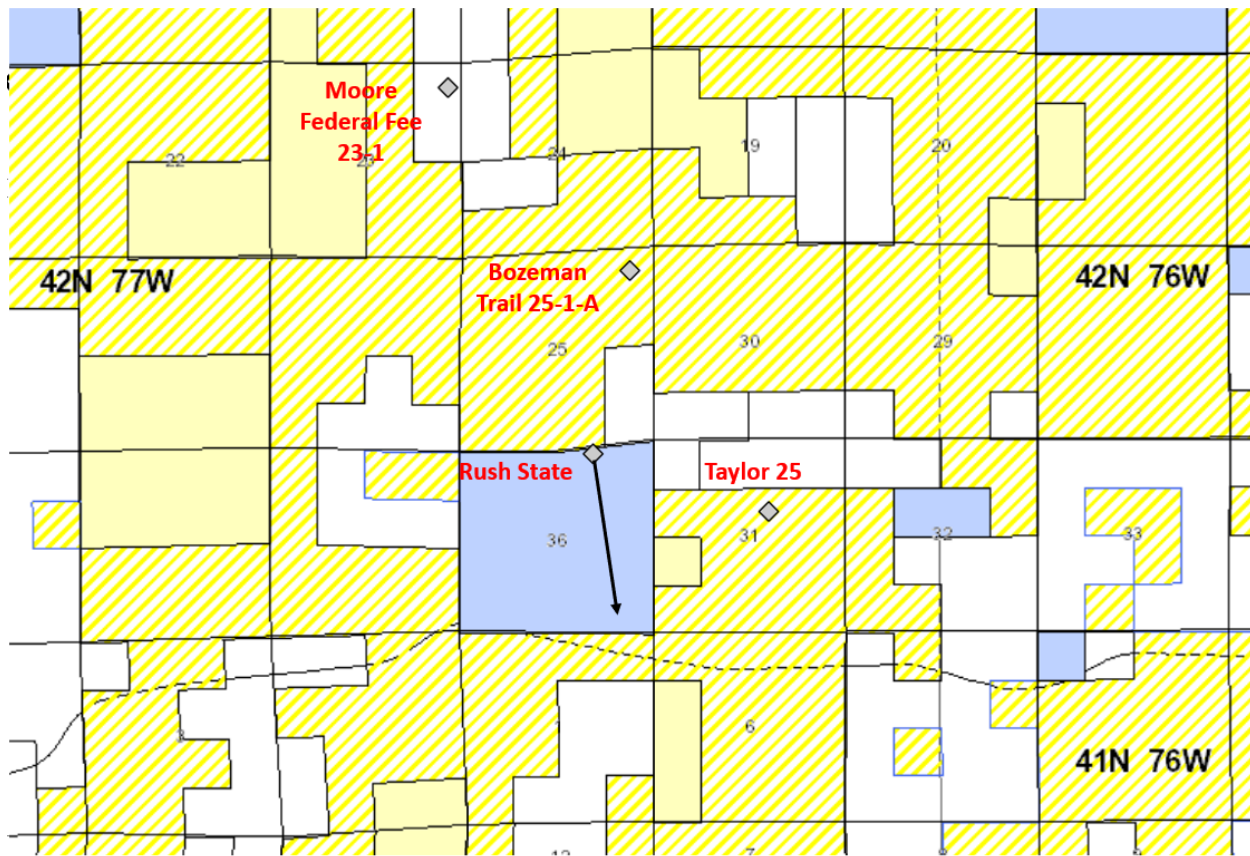


Figure 7: Location of Rush State well and three vertical offset wells (Moore Federal Fee 23-1, Bozeman Trail 25-1-A, and Taylor 25) in Johnson County, Wyoming (Map taken from WOGCC, 2018)

Geosteering data was provided by SM Energy to model the upper and lower limits of the reservoir based on the green target zones as shown in Figure 8. A 32-foot interval was found to be a high-quality reservoir with high porosity and permeability compared to other zones in the Frontier Formation. In Figure 9, the shape of reservoir model was created based on the geosteering data that included the targeted 32-foot production interval of the WCM. The well was modeled according to the completion data obtained from the company including sliding sleeve completion and hydraulic fractures of the well. To confirm the reliability of the model, history matching was performed to match the actual performance of Rush State well for oil, gas, water production, and bottom hole pressure. During the matching, certain reservoir properties needed to be modified to match the actual properties in the reservoir. For each property, a



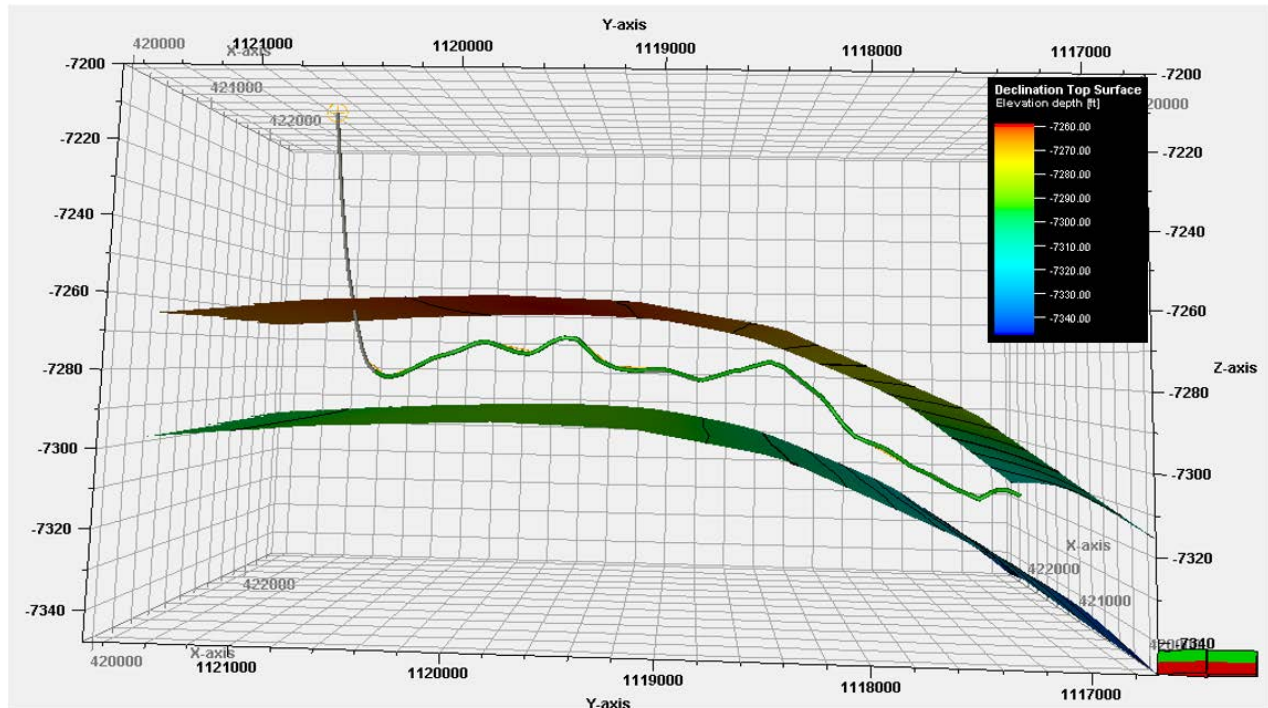


Figure 9: Upper and lower boundary surface of Well Scale model with Rush State well on Petrel. (Arrow illustrates the direction of the model)

For the preliminary run to test the property's input, the reservoir model was created using 100 foot by 100 foot grid blocks and 16 layers with 2 feet per layer. The total number of grid cells is 20800. The reservoir properties for this model are discussed in the following sections.

3.2. Reservoir Properties

To represent the subsurface properties of WCM, the reservoir properties were estimated directly from the well logs, core data, and a literature review (Moore, 2016) in the field. In the following section, the initial input of each property such as porosity, permeability, water saturation, and rock physics used to test the simulation for properties correctness and runtime are presented. Preliminary runs were compared to historical data and a sensitivity analysis was done to test the limit of each property. Changes were applied to certain properties to achieve a good match to historical data. This is shown in history matching section. Other reservoir properties found in PVT report of Rush State well provided by SM Energy in 2017 are shown in Table 1:

Table I: Reservoir properties taken from PVT report of Rush State well at 7,260 feet below sea level

| Properties | Values | Units |
|------------------------|--------|----------|
| Reservoir Pressure | 5,866 | psia |
| Solution gas-oil ratio | 1.1 | mscf/stb |
| Water salinity | 19,730 | mg/L |

3.2.1. Porosity

Three vertical offset logs were used to define the interval of a 50-foot thick section of the WCM for analysis. The gamma ray logs shown in Figure 10 are used to identify of the top of the WCM that is identified as a target zone of the formation. The top picks of WCM were correlated by the change from high gamma ray (shale indicator) to low gamma ray. The base picks were chosen to be 50 feet distance from the top picks because the gamma ray values had increased to the shale indicator values at approximately 50 feet. Even though only the first 32 feet were used for the Well Scale model, the full 50-foot section was used for the overall property observation of the WCM. For the analysis purpose, Density porosity and neutron porosity logs were used to estimate the porosity of the reservoir. The average method (Eq. 1) was used to create the plot in Figure 11, which is an estimate of the average porosity for the 50-foot section of the WCM. Noticed from the estimation, at layer 10 of the Taylor 25 well, the graph shows very high porosity of 0.171 compared to others. This value was kept due to the possible presence of natural fractures in the reservoir.

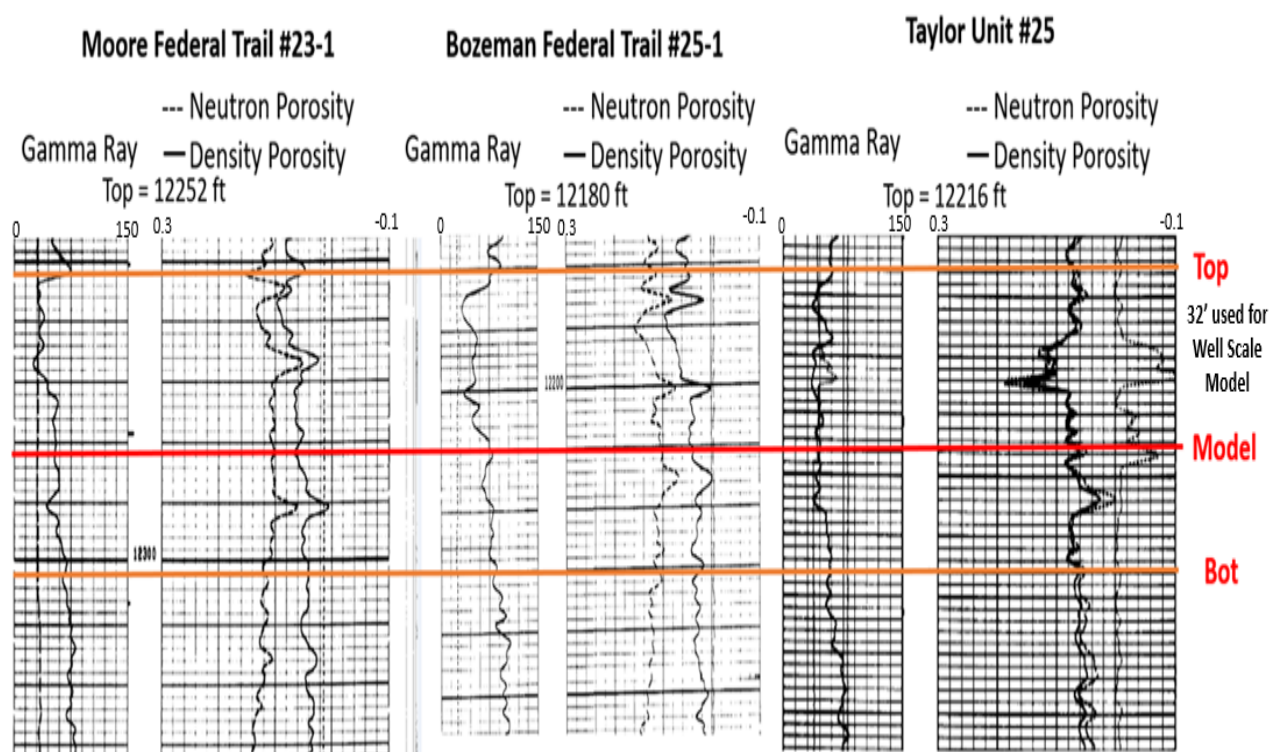


Figure 10: Well log pickings from three vertical offset wells.

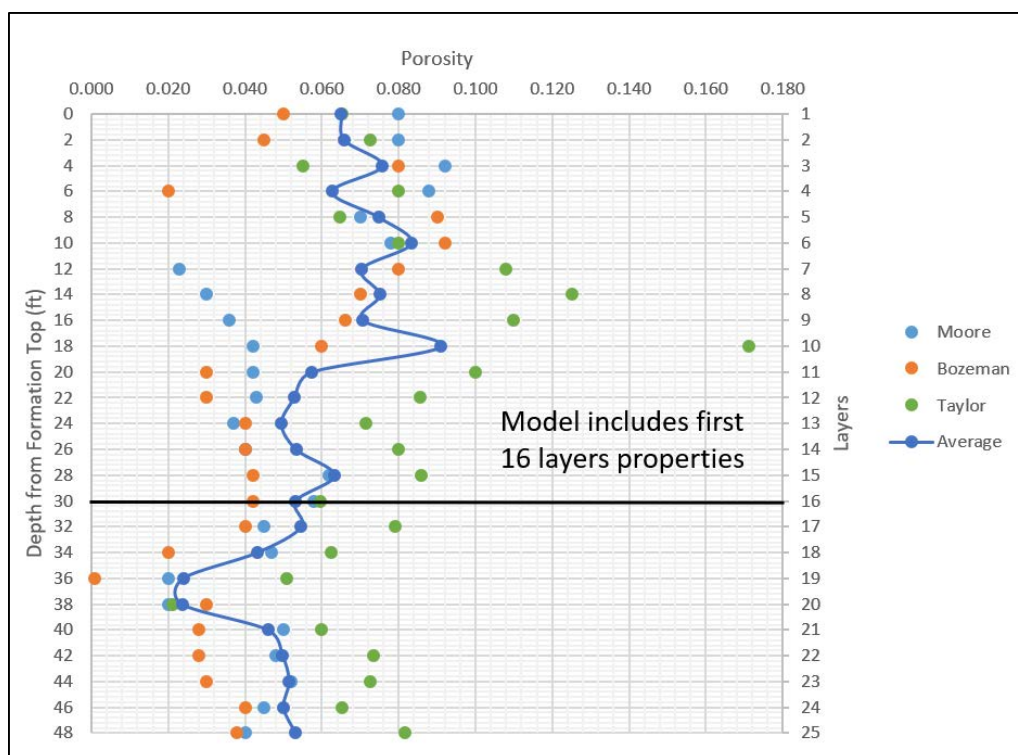


Figure 11: Porosity estimation from three vertical offset wells with 2-foot interval from formation top.

As seen from the porosity distribution on Figure 11, there are the large ranges of porosity values from 0.001 to 0.171, and estimated porosity in each well was not correlated by actual geologic layers. However, by averaging the value at two-foot interval, there were distinct high porosity intervals and low porosity intervals starting at layer 11, which were realistically representative for two distinct sedimentary facies: tidally-influenced facies (good quality reservoir) and wave-influenced facies (poor quality reservoir) (LaFontaine, 2018). For this reason, the average values of porosity were used for the model (Figure 12), which has the porosity values ranging from 0.05 to 0.091. Two distinct sedimentary facies can be seen from Figure 12 from porosity distribution and will be discussed later in outcrop model analysis section.

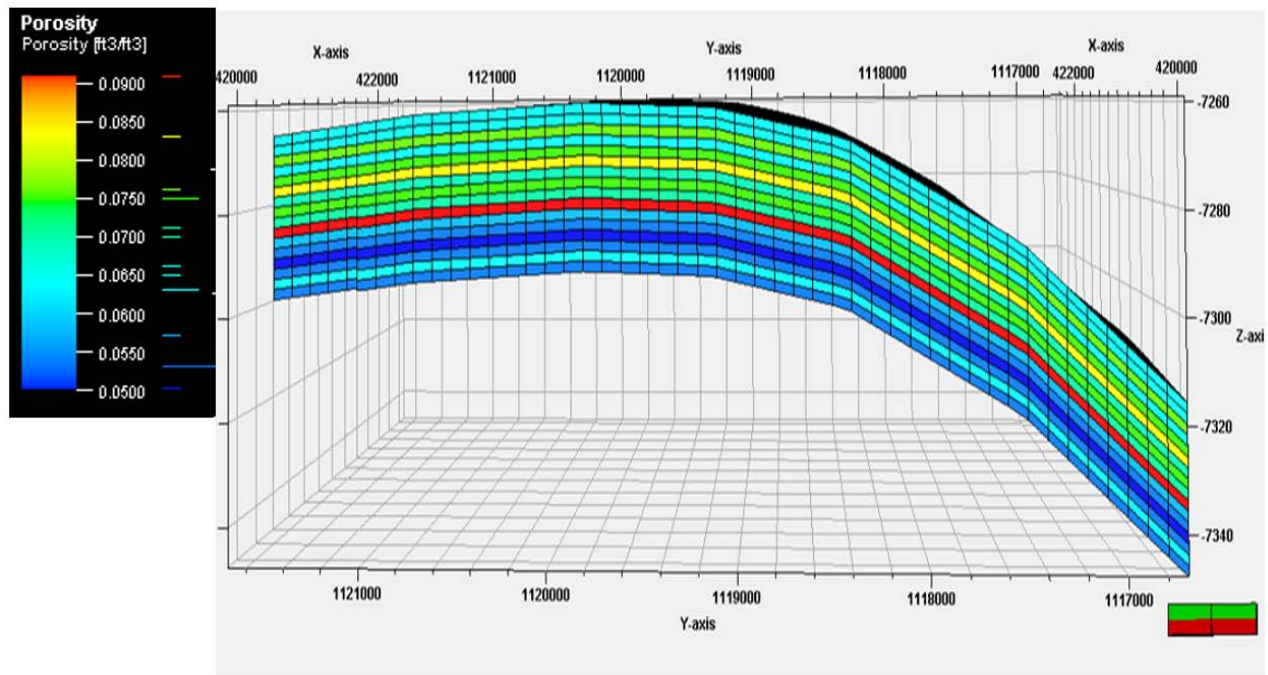


Figure 12: Porosity distribution ranging from 0.05 to 0.091 on Well Scale model. (Arrow illustrates the direction of the model)

3.2.2. Permeability

Permeability was estimated using the core porosity and permeability correlation from the cross plot provided by SM Energy shown in Figure 13. The porosity-permeability cross plot includes two trend lines: blue and black trend line. The blue trend line only shows the average correlation between porosity and permeability, which may not be representative for two distinct sedimentary facies. The black trend line was chosen to provide better estimation of permeability in two distinguished types of rocks presented in core samples with the following equations.

$$\text{if } PHIE \leq 0.039, k = 0.00001 \times e^{190.7 \times PHIE} \quad (8)$$

$$\text{if } PHIE > 0.039, k = 0.000964 \times e^{73.59 \times PHIE} \quad (9)$$

Where:

$PHIE = \text{Porosity (fraction)}$

$k = \text{Permeability (millidarcy)}$

Permeability ranges from 0.001 millidarcy to 200 md (Figure 13). The core samplings used in this plot are reported to be taken from many core samples from the Frontier Formation around the reservoir study area (Figure 2C). The variation of permeability can possibly come from the diagenetic alteration (LaFontaine, 2018) at different places in the formation. In this project, the green zone from the concentration cross plot (Figure 13B) will be the focus as it defines the most common values within the available porosity values (Figure 11) from the core sample analyses.

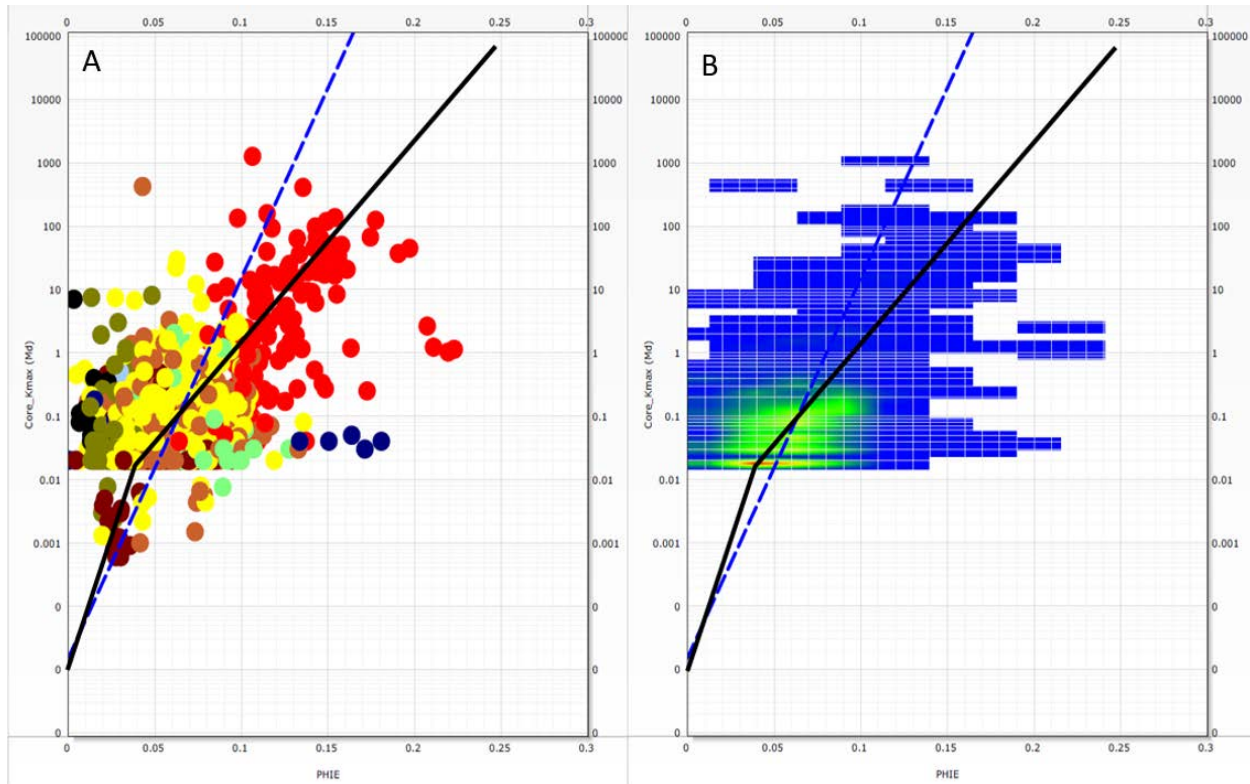


Figure 13: Permeability and porosity cross plot provided by SM Energy. One trend line (dashed) has one slope, and the other (black lines) has two different slopes changing at a porosity of 3.9%. (A) Core samples of WCM from different wells within study area. (B) Concentration cross plot for most common values distribution in core analysis. (PHIE = porosity measured from cores, Core_K_{max} = Permeability measure from cores).

Using Equations 8 and 9, the permeabilities of 50-foot thickness were calculated with the average porosity at each layer and plotted (Figure 14). The values were then input into the reservoir model with the permeability ranging from 0.0382 md to 0.7806 md shown in Figure 15.

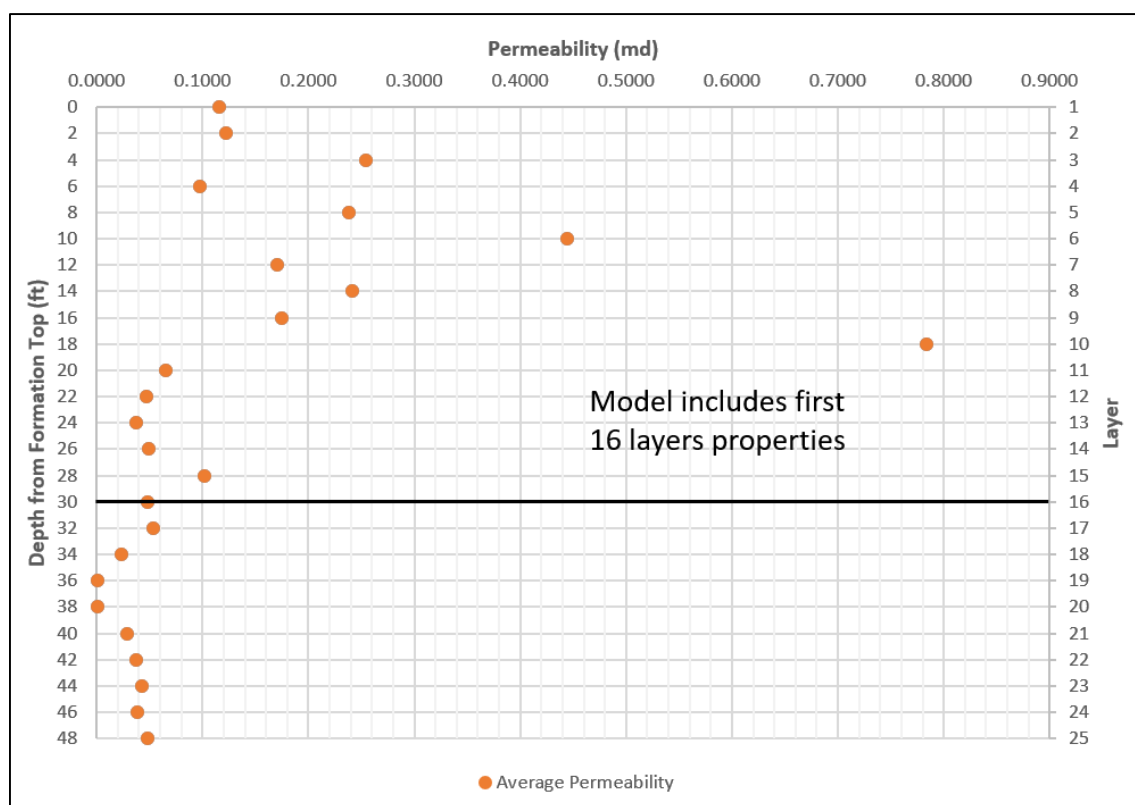


Figure 14: Permeability estimation from porosity-permeability cross plot.

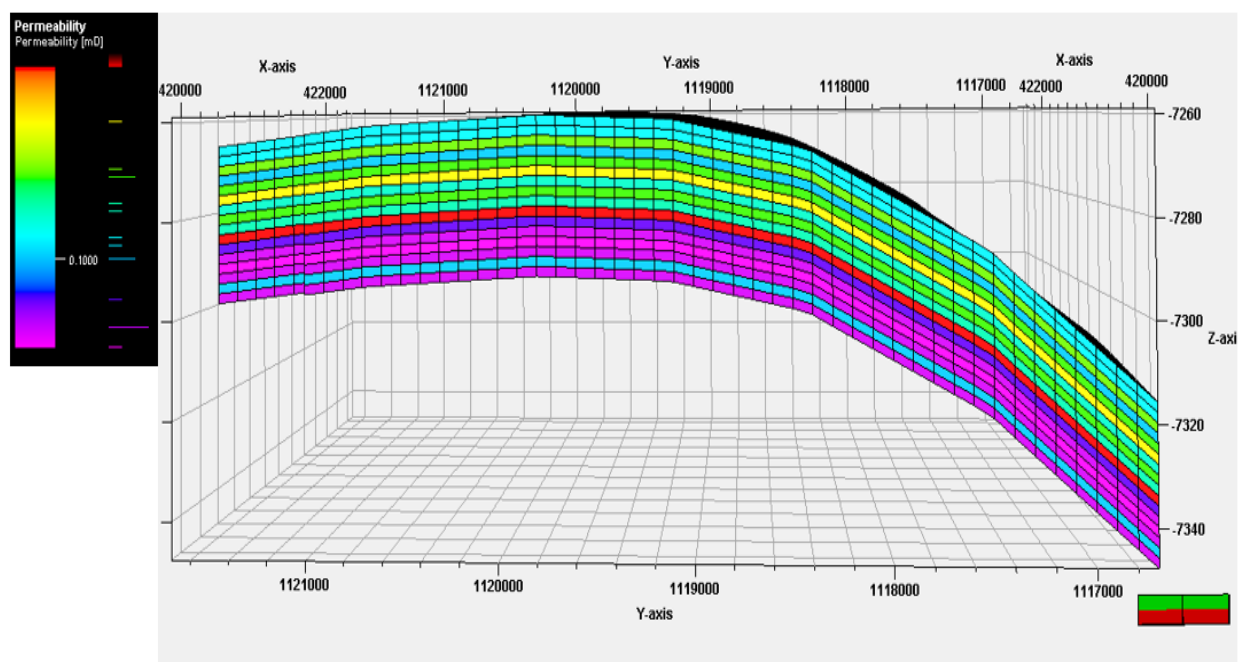


Figure 15: Permeability distribution ranging from 0.0382 md to 0.7806 md on Well Scale model. (Arrow illustrates the direction of the model)

3.2.3. Water Saturation

Water saturations were found based on the three offsets well logs that were interpreted by SM Energy geologists (Figure 16). Logs interpretation shows the reservoir contains water saturations ranging from about 45% to 100%. The Rush State well had a water cut of 35% to 45% after the first year of production. Some other wells in the study area also produce with 50% to 60% water cut (Wyoming Oil and Gas Conservation Commission, 2016). For simplicity, the range of water saturation in this reservoir model is estimated from 45% to 65%. For the model, the water saturation is distributed based on porosity dependence. Lower porosity rock will contain more water while higher porosity rock will contain less water. Based on the well logs, the top of WCM contains more sandstones which has higher porosity compared to the bottom of the observed interval. Using linear interpolation from 45% to 65% water saturation with 5% to 9.1% of porosity, the equation to distribute the water saturation into the model is developed to be:

$$\text{Water saturation} = -4.878 \times \text{Porosity} + 0.894 \quad (10)$$

As a function of porosity, the values of water saturation were then input into the reservoir model as shown in Figure 17.

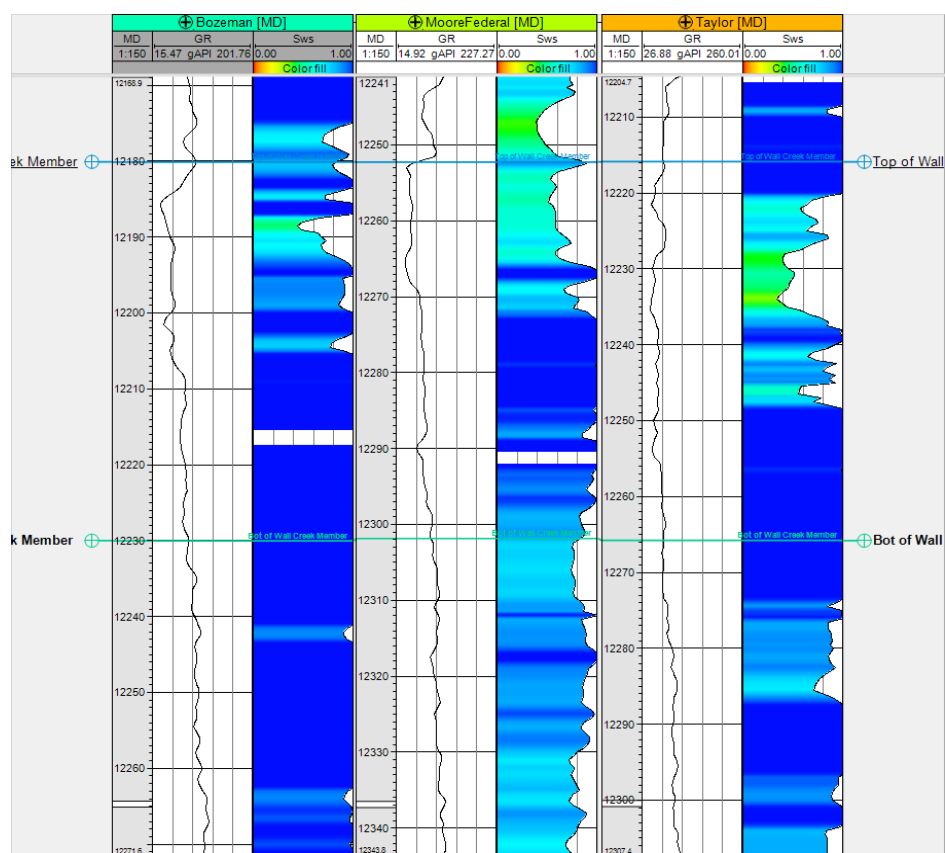


Figure 16: Water saturation logs of three vertical offset wells interpreted by SM Energy geologists.

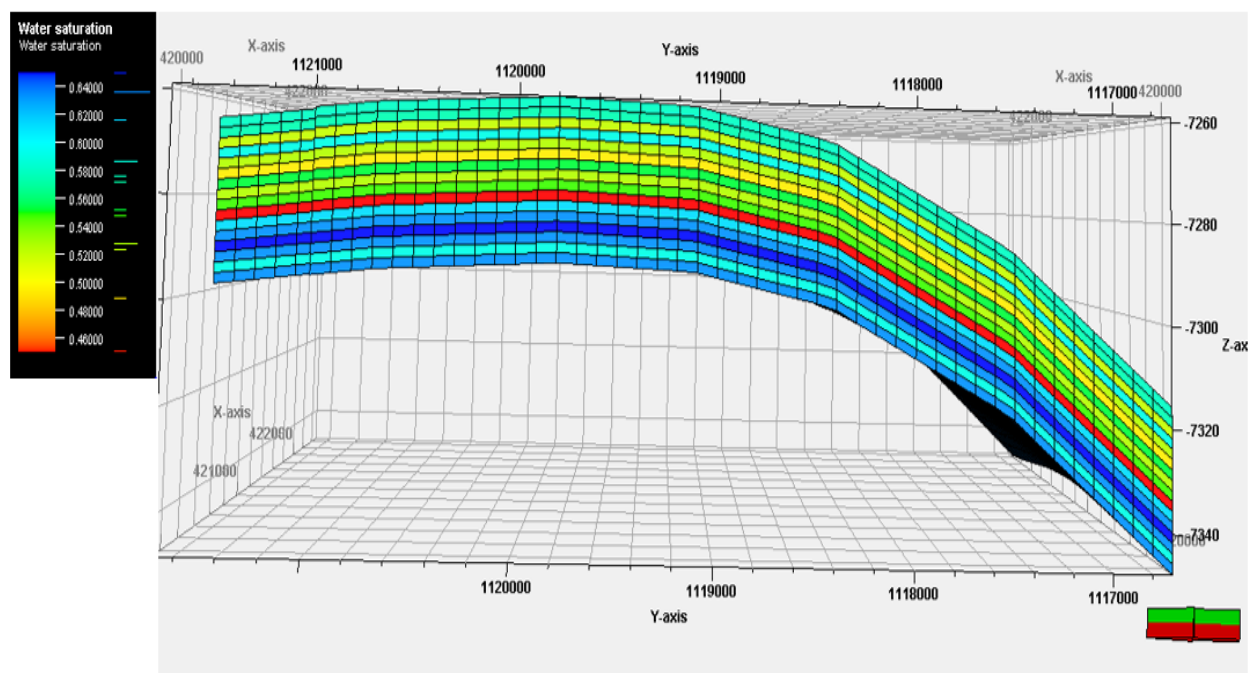


Figure 17: Water saturation model ranging from 45% to 65%. (Arrow illustrates the direction of the model)

3.3. Fluid Properties

The Soave-Redlich-Kwong EOS (Eq. 2) was used as the EOS model to perform PVT matching to create the fluid model for the reservoir. However, EOS model often cannot match the PVT experimental data (Pedersen et al., 1985), so it needs to apply some tunings on the EOS model to fit the specific fluid sample. The solution for EOS tuning is not unique (Liu, 1999). PVTi software was used for EOS tuning that allowed to apply different regression parameters for the Soave-Redlich-Kwong EOS such as Omega A (Ω_a), Omega B (Ω_b), Acentric factor (ω), volumetric shift parameter, binary interaction coefficients and other regression variables. The initial properties of each component (CO_2 , N_2 , H_2S , and C1 to C7+) on the EOS model is shown in Appendix A, Table XV. The final regression results for the properties of each component are shown in Appendix A, Table XVI. Matched fluid properties are shown in Figure 18. The matched parameters include relative volume, gas and oil densities, gas and oil viscosities, formation volume factor of oil and gas, total formation volume factor, gas-oil ratio, and z-factors. The matching shows the smooth blue curves along with the red data points to create the fluid model to describe the fluid properties of WCM. The fluid model was then exported as a black oil model for the Well Scale model to perform the simulation.

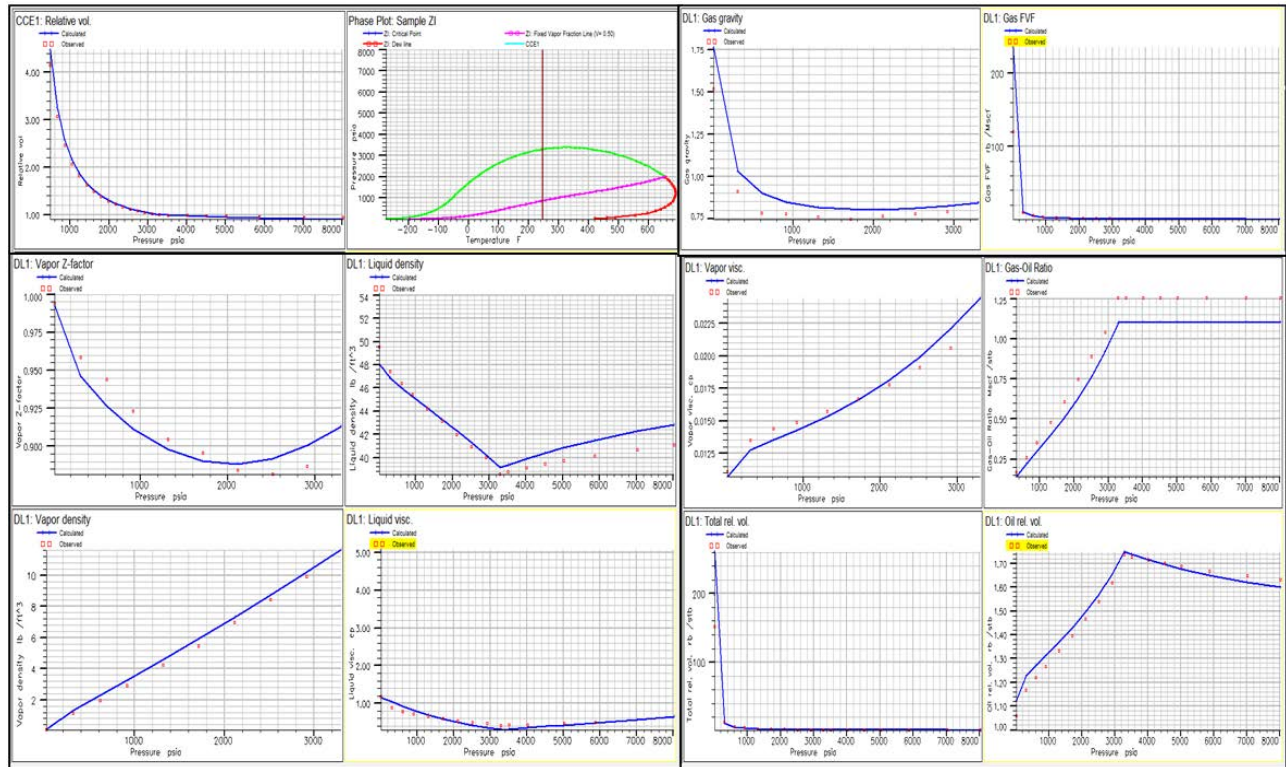


Figure 18: PVT matching results for fluid model. Red dots are PVT data, blue lines are matched model.

3.4. Relative Permeability and Capillary Pressure

Based on historical production observation, few conclusions were made to help the historical production matching process. The oil is produced at very high rate of 560 bbl/day and declines to 80-120 bbl/day after few months. The gas production appears to decline at the similar rate as the gas-oil ratio is typically constant over the production period. Therefore, the only source of gas is the solution gas evolved from oil with the constant gas-oil ratio. For water production, there was an abnormally high rate of about 4,500 bbl/day at the beginning compared to initial oil production rate, which can be due to the fluid used during hydraulic fracturing. After removing the frac fluid, the water rates are mostly constant at 50-70 bbl/day, which indicates the only source of water is the water retained in the reservoir rocks. Reported water cuts in the field ranging from 25% to 45%, it suggests that WCM reservoir rocks contains decent amount of

retained water. The study of tight reservoir of Frontier Formation by Moore (2016) suggests the possible irreducible water saturation for three types of reservoir rocks is: 15-20% for sweet spot sandstones, 50% for tight gas reservoirs, and more than 60% for shale and siltstones. As seen from the well logs for water saturation of three vertical offset wells, the water saturation (45-65%) around Rush States well is higher than in sweet spot sandstones (15-20%). According to the study of LaFontaine (2018), the WCM consists of cross-bedded sandstones with the muddy silt deposits in tidally-influenced facies, which might suggest higher irreducible water saturation of the WCM from the sweet spot sandstones. Thus, for preliminary runs of historical production matching, the parameters for Brook-Corey relations (Eq. 3, 4, and 5) were initially set as Table II. The initial relative permeability curves (shown in Figure 29) were used for the preliminary runs.

Table II: Initial parameter for relative permeability curve

| Parameter | Values | Remarks |
|------------------|---------------|------------------------------------------------|
| S_{or} | 0.23 | Default Petrel setting for sandstone reservoir |
| S_{wir} | 0.35 | Based on observation |
| S_{gr} | 0.05 | Default Petrel setting for sandstone reservoir |
| n_o | 3 | Modified for matching |
| n_w | 5 | Modified for matching |
| n_g | 2.5 | Modified for matching |
| $K_{ro,max}$ | 0.8 | Default Petrel setting for sandstone reservoir |

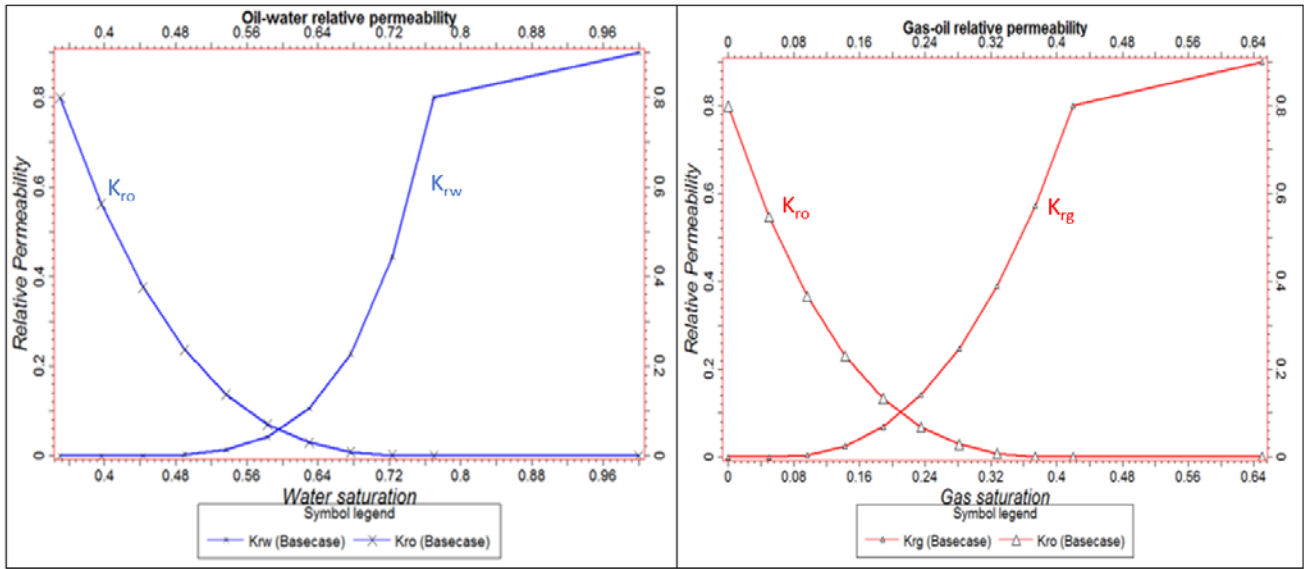


Figure 19: Relative permeability for the preliminary run.

Capillary pressure is the pressure difference across the interface between oil phase and water phase that must be reached to initiate the flow (Dandekar, 2013). Capillary pressure was defined by using the correlation for oil-water (Eq. 11) implemented in Petrel to generate a capillary pressure function (Skjæveland et al., 2000):

$$P_c = \frac{c_w}{\left(\frac{S_w - S_{wR}}{1 - S_{wR}}\right)^{a_w}} + \frac{c_o}{\left(\frac{S_o - S_{oR}}{1 - S_{oR}}\right)^{a_o}} \quad (11)$$

Where:

P_c = capillary pressure (psi)

S_w = water saturation

S_{wR} = residual water saturation

S_o = oil saturation

S_{oR} = residual oil saturation

a_w = pore size distribution index for water – wet system

a_o = pore size distribution index for oil – wet system

c_w = entry pressure for water – wet system

c_o = entry pressure for oil – wet system

Capillary pressure function is generated (Figure 20) by inputting these parameters (Table III) into Petrel. For this model, capillary pressure allowed the water to migrate inside the reservoir into the well as the well produced. The parameters were modified during history matching to achieve the certain rate of water production according the historical production.

Table III: Values to generate a capillary pressure function using correlation for oil-water in Petrel

| Parameters | Values |
|--------------------|--------|
| Max P_c | 40 |
| S_w at $P_c = 0$ | 0.65 |
| a_o | 3.86 |
| a_w | 3.86 |

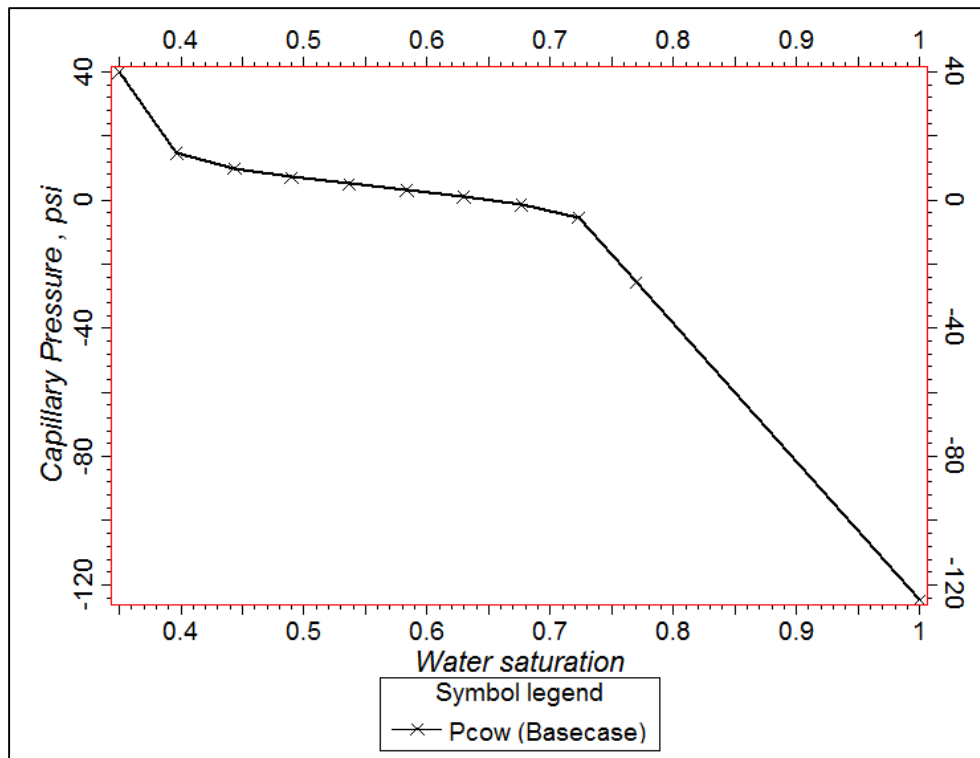


Figure 20: Capillary pressure for the preliminary run.

3.5. Well Completion

Based on the completion report for the Rush State well, the entire horizontal portion of the well was completed with a 4 ½-inch liner inside a 6-inch open hole. The well was hydraulically fractured using sliding sleeves with 15 fracture stages. Well completion was modeled using the Petrel hydraulic fractures model to define fracture conductivity, height, half-length, orientation and location. These were represented in a single rectangular box. Each box defines one fracture by changing the permeability multiplier on each grid cell connects with a fracture based on the input parameters. The hydraulic fractures were initially modeled as 50 feet height and 100 feet half-lengths. For simplicity, the hydraulic fractures penetrated vertically through the formation due to unavailable data. Sensitivity analysis for hydraulic fractures dimensions was performed later for reliability. The location of each fracture was based on the actual depth measured from the well shown in Table IV. The completion model is shown in Figure 21 below with the hydraulic fractures extending out of the reservoir boundary to illustrate full perforation of target zones :

Table IV: Fracture Depth on Well Scale Model

| Fractures | 1 | 2 | 3 | 4 | 5 | 6 | 7 | 8 |
|-------------------|-------|-------|-------|-------|-------|-------|-------|-------|
| Depth (ft) | 12775 | 13009 | 13246 | 13524 | 13752 | 14018 | 14253 | 14533 |
| Fractures | 9 | 10 | 11 | 12 | 13 | 14 | 15 | |
| Depth (ft) | 14768 | 15049 | 15271 | 15543 | 15769 | 16046 | 16286 | |

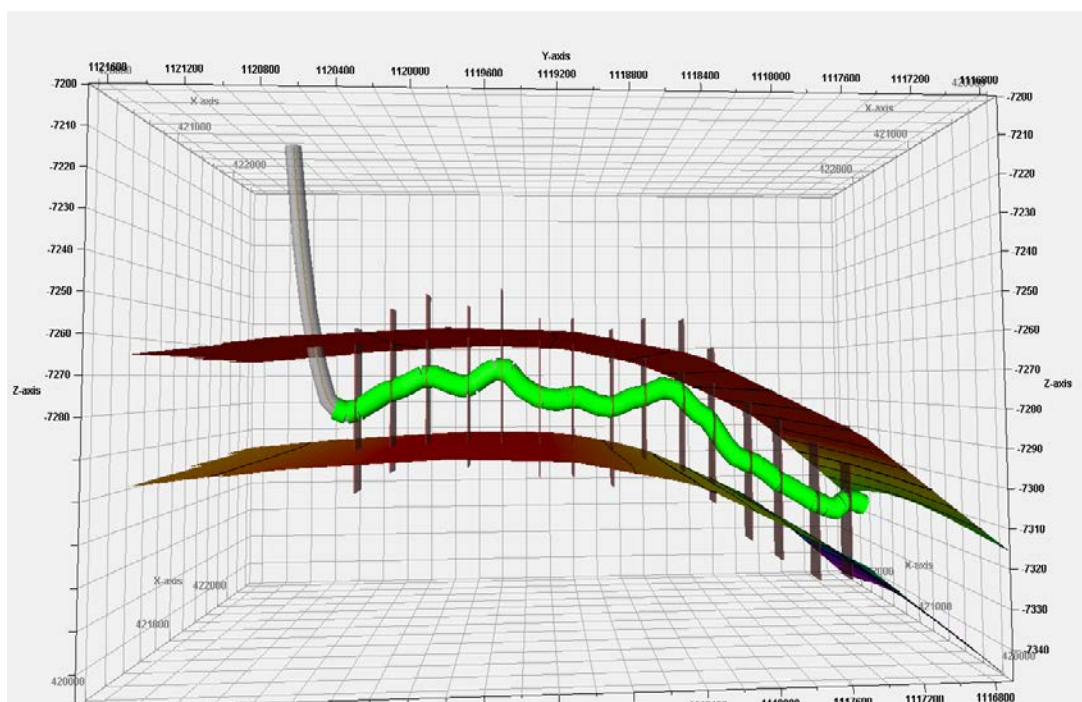


Figure 21: Rush State well completion using the completion report from SM Energy. Entire horizontal portion of 4 1/2 inch liner (grey) inside a 6-inch open hole (green). Each hydraulic fracture is represented by the single red rectangular box that penetrated through formation.

3.6. Preliminary Run and Sensitivity Analysis

3.6.1. Preliminary run for history matching

The preliminary history match was run from May 2014 through September 2016 using the Rush State well production. The model was constrained to the historical oil rates. To validate the model, gas rates, water rates, and bottomhole pressures were matched to the historical production. These three parameters are very important to describe how well the reservoir is modeled with the proper reservoir capacity (porosity, permeability, and pressures support) and fluid behavior (production trend). From SM Energy, the pressure reports show that the bottomhole pressures of the Rush State well fluctuated around 650 psi, and the well production was declined periodically due to no additional pressure support from any source. Figure 22 and 23 shows the preliminary match for historical production; however, some modifications were needed to get a better match. The water production matched well. Although the oil production is

constrained by the model, the oil production was lower than historical production, and the bottom hole pressures were very low compared to the reports. The preliminary run suggests that the model does not have enough pressure support to produce enough fluid from the reservoir, and the gas production is slightly higher than the data suggests.

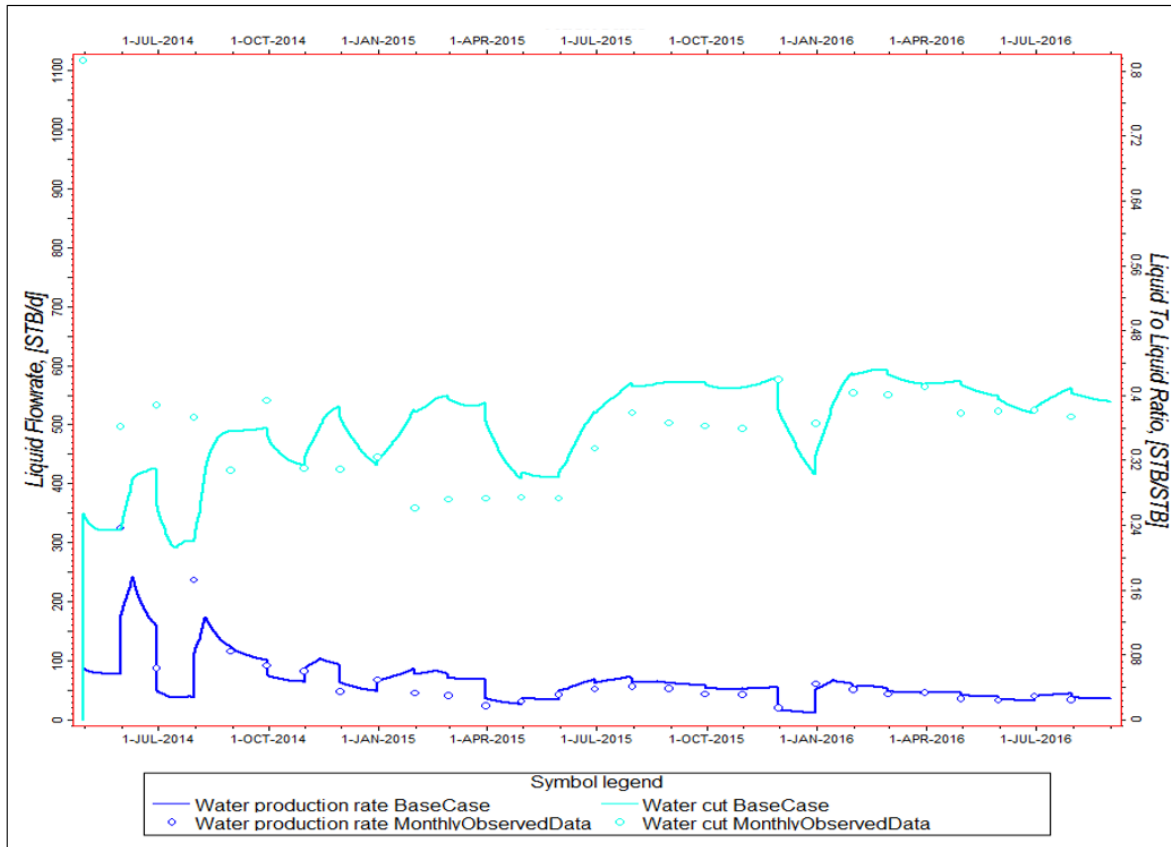


Figure 22: Preliminary results of history matching with reasonable match for water production and water cut

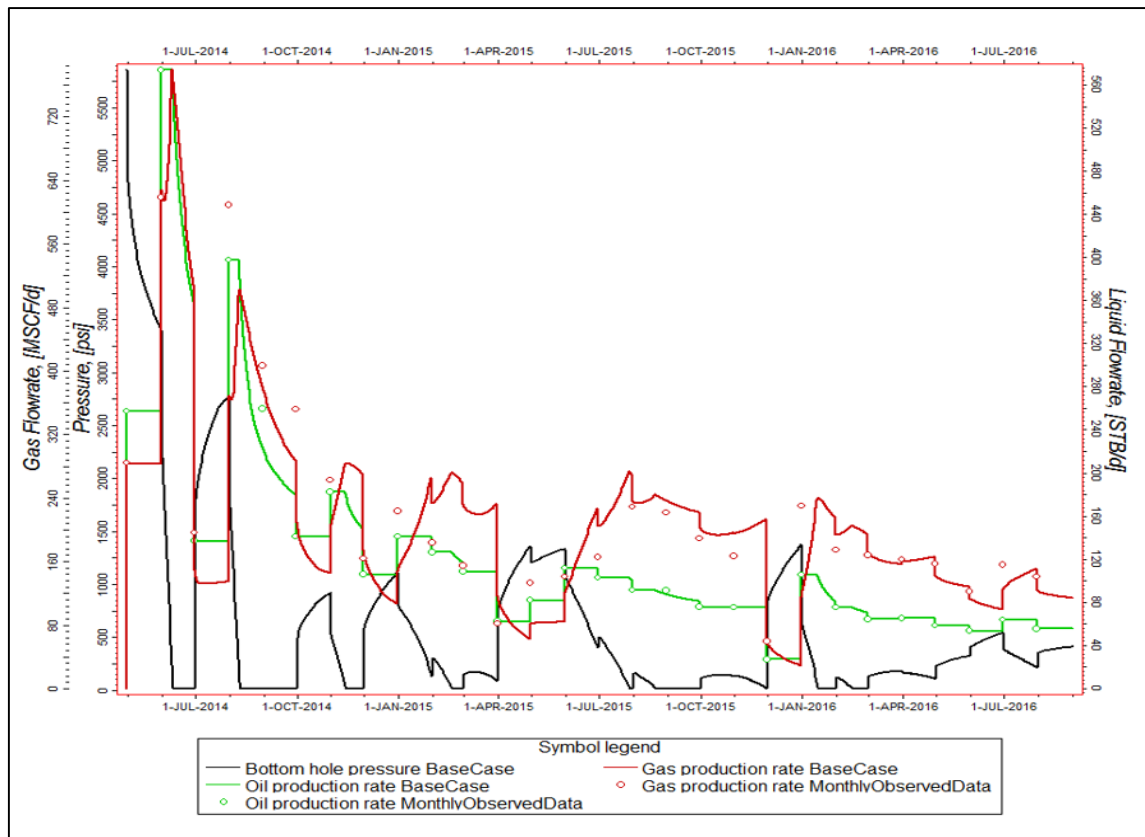


Figure 23: Preliminary results of history matching with reasonable match for oil and gas production and bottomhole pressure.

3.6.2. Sensitivity analysis

Sensitivity analysis were performed to suggest what properties should be changed to alter the reservoir production. The sensitivity analysis was run using the bottom hole pressures from the preliminary run to compare the modification of properties with initial inputs. Preliminary run was denoted as base case that used oil the production constraint as mentioned in previous section. Figure 24 shows the fluid cumulative production of the base case and the sensitivity analysis case matched each other. This verifies that using the bottom hole pressure constraint is valid when modifying other properties to test how fluid production may change. As gas production is directly proportional to oil production by gas-oil ratio, some results of sensitivity analysis will only show oil and/or water production, other results will be shown in Appendix A.

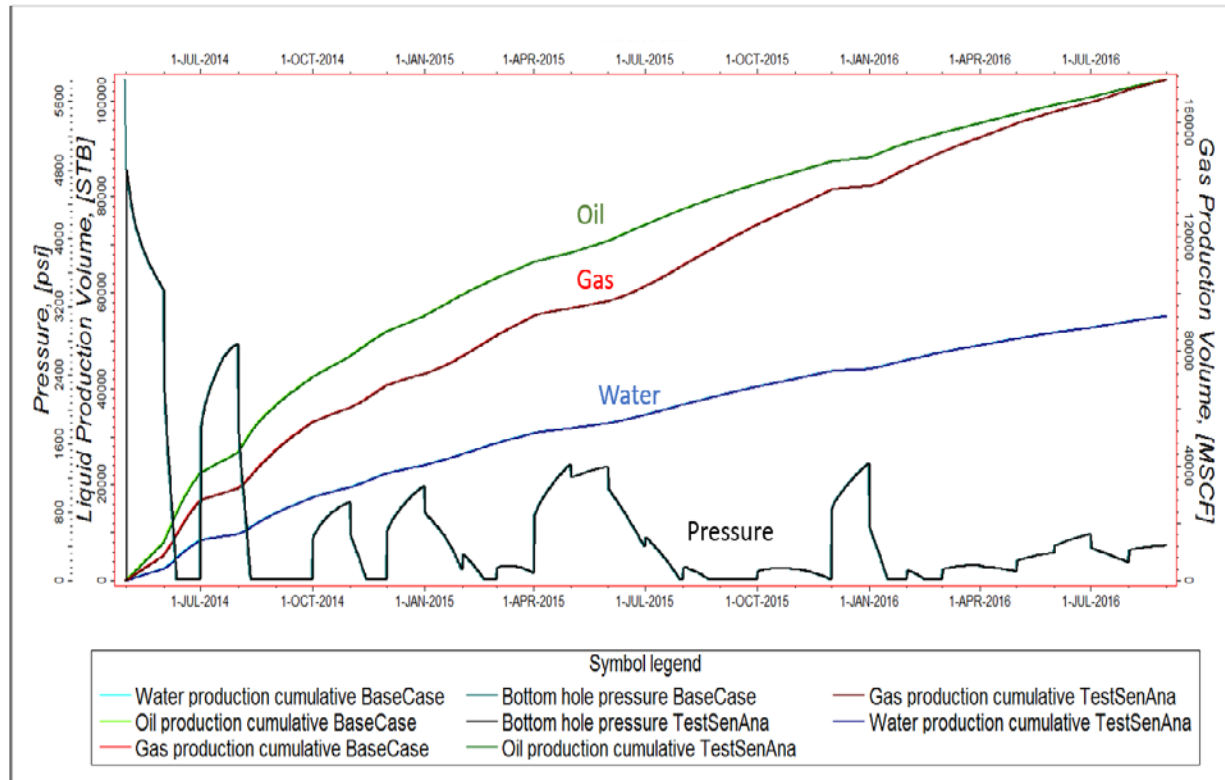


Figure 24: Test run for sensitivity analysis using bottom hole pressure constrained from preliminary run for Rush State data. Oil, gas, and water cumulative production from two cases are matched on top of each other.

The sensitivity analysis was conducted for 24 cases (Table V) along with initial properties input of the based model to observe how the fluid production is going to change:

Table V: Sensitivity analysis cases

| Case Number | Properties | Remark |
|-------------|--------------------------------|--------------------------------------------------------------------------|
| 1 | Porosity | -30% offset from average porosity |
| 2 | | +30% offset from average porosity |
| 3 | Permeability | 10% of average permeability (minimum) |
| 4 | | 600% of average permeability (maximum) |
| 5 – 14 | | Random permeability distribution within minimum and maximum permeability |
| 15 | Hydraulic Fracture Half Length | 50 foot half-length of hydraulic fracture |
| 16 | | 400 foot half-length of hydraulic fracture |
| 17 | Corey oil exponent (n_o) | $n_o = 2$ ($n_o = 3$ for base case) |
| 18 | | $n_o = 4$ ($n_o = 3$ for base case) |
| 19 | Corey water exponent (n_w) | $n_w = 4$ ($n_w = 5$ for base case) |
| 20 | | $n_w = 6$ ($n_w = 5$ for base case) |
| 21 | Corey gas exponent (n_g) | $n_g = 2$ ($n_g = 2.5$ for base case) |
| 22 | | $n_g = 3$ ($n_g = 2.5$ for base case) |
| 23 | $K_{ro,max}$ | $K_{ro,max} = 0.4$ ($K_{ro,max} = 0.8$ for base case) |
| 24 | | $K_{ro,max} = 0.6$ ($K_{ro,max} = 0.8$ for base case) |

3.6.2.1. Porosity

Figure 25 shows the porosity graphs with three differences cases (Base case, case 1, and case 2) with 30% offset from average porosity. The offset percentage was chosen based on the porosity estimated from the well logs with the possible minimum and maximum porosity in this reservoir. Random distribution for porosity was not considered due to the preservation of two distinct sedimentary facies presented in WCM.

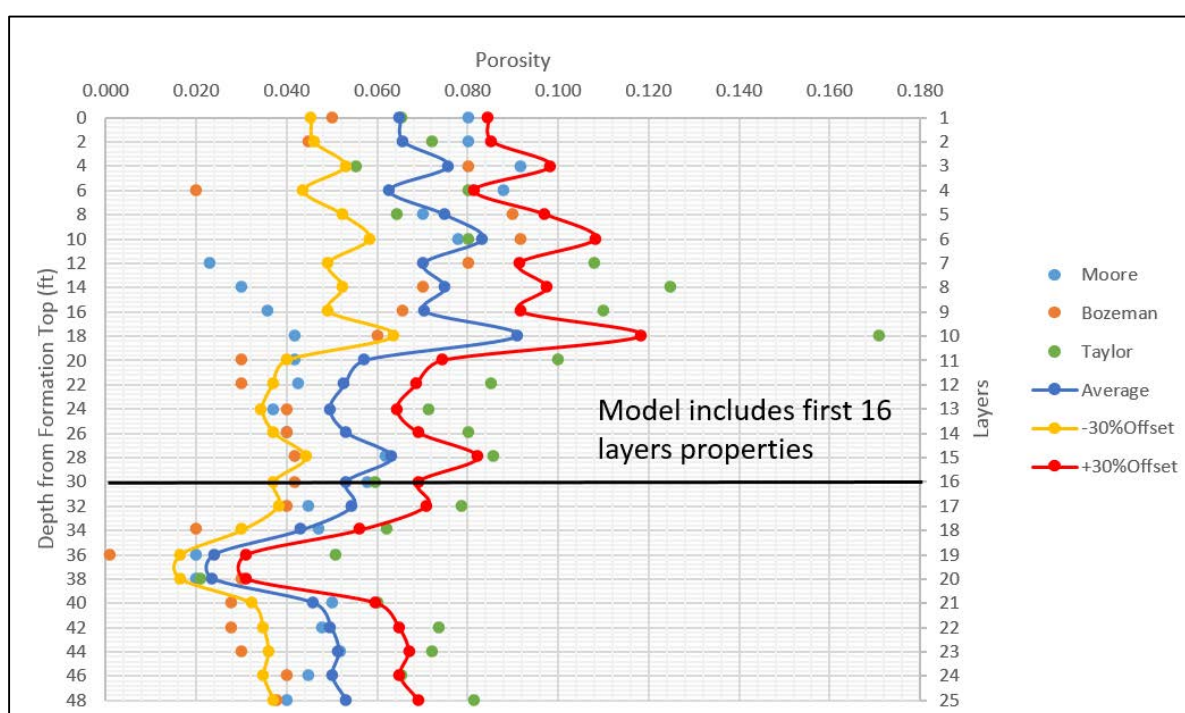


Figure 25: Porosity sensitivity analysis with 30% offset from average porosity with 2-foot interval.

The results shown in Figure 26 and Figure 27 indicate that significant changes in production occur by modifying the porosity with an approximate 250% increase and decrease in production cumulative at the end of historical production when the porosity was changed by 30%. Therefore, production is very sensitive to changes in porosity for history matching.

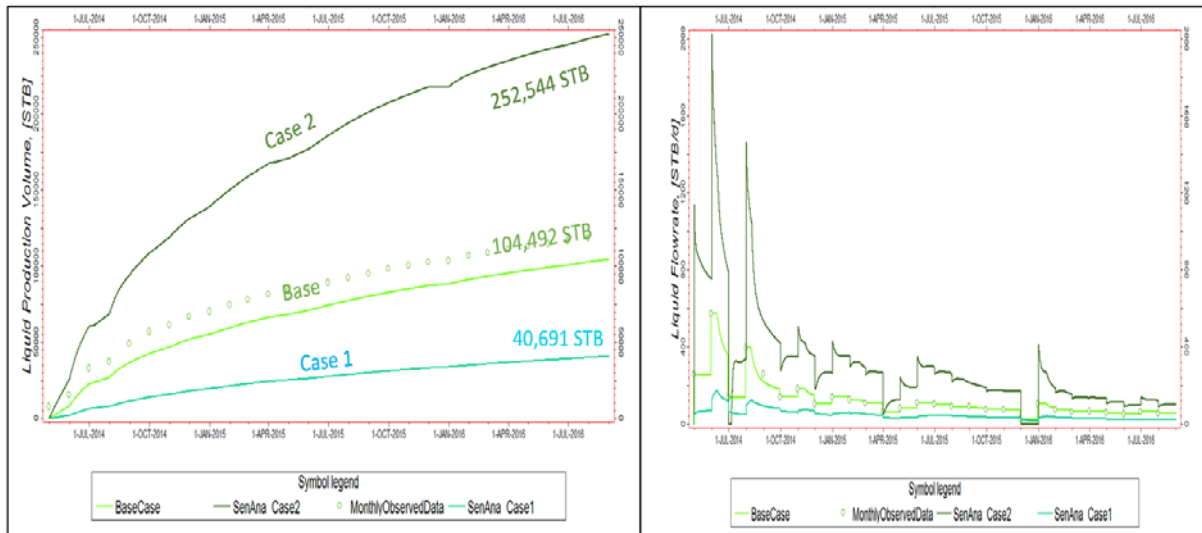


Figure 26: Oil production cumulative and oil production rate for porosity sensitivity analysis.

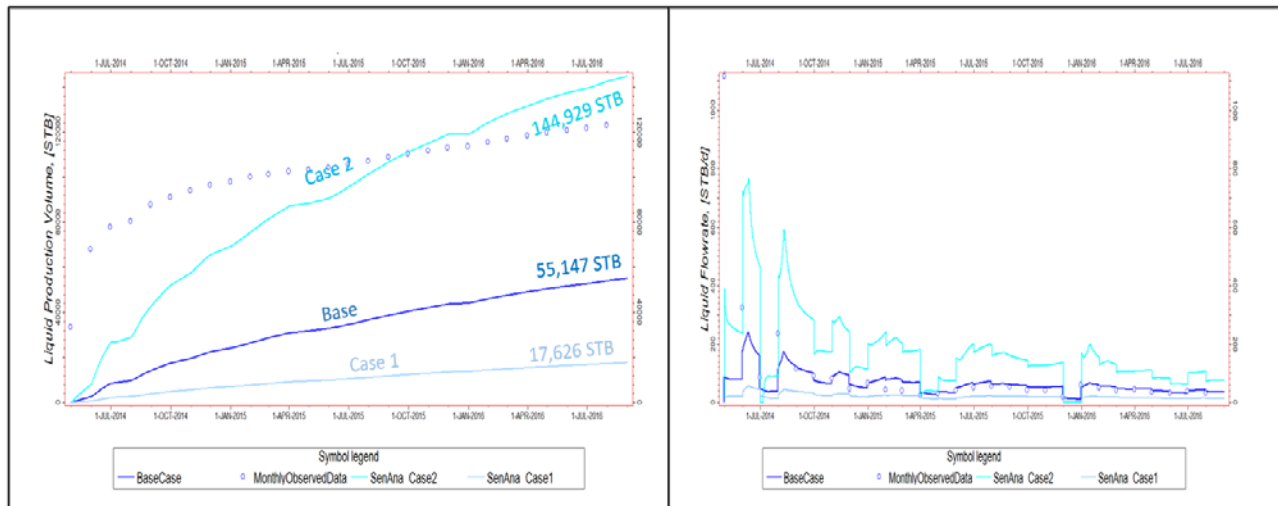


Figure 27: Water production cumulative and water production rate for porosity sensitivity analysis.

3.6.2.2. Permeability

Figure 28A is a graph of permeability and porosity illustrating the range of relationships for sensitivity analysis. The minimum and maximum range for permeability is defined by using the range of green concentration zone of core samples from the cross plot (Figure 28B). Average permeability was multiplied by 0.1 and 6 for minimum and maximum permeabilities, respectively. Randomization was used to distribute the permeability within the minimum and maximum ranges.

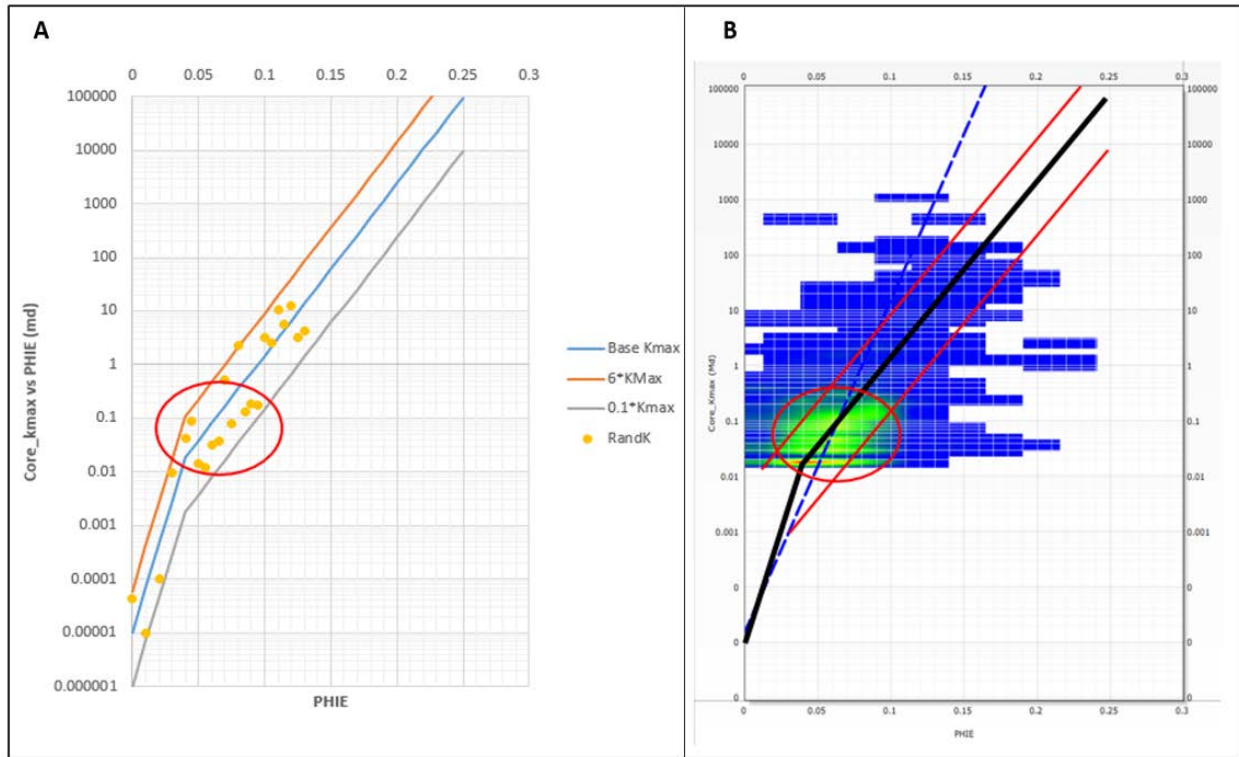


Figure 28: Permeability sensitivity analysis with 12 cases of random distribution, minimum and maximum ranges of permeability. (A) A graph illustrates random permeability values within the minimum and maximum ranges. (B) Concentration porosity-permeability cross plot for core samples.

Minimum and maximum permeabilities were input into the 16 layer model for the average permeability case. Figure 29 shows the top view and side view of the random permeability distribution model. As the results in Figure 30, a random permeability distribution does not cause significant differences to the production; however, the minimum and maximum permeability cases show 30% and 200% differences, respectively.

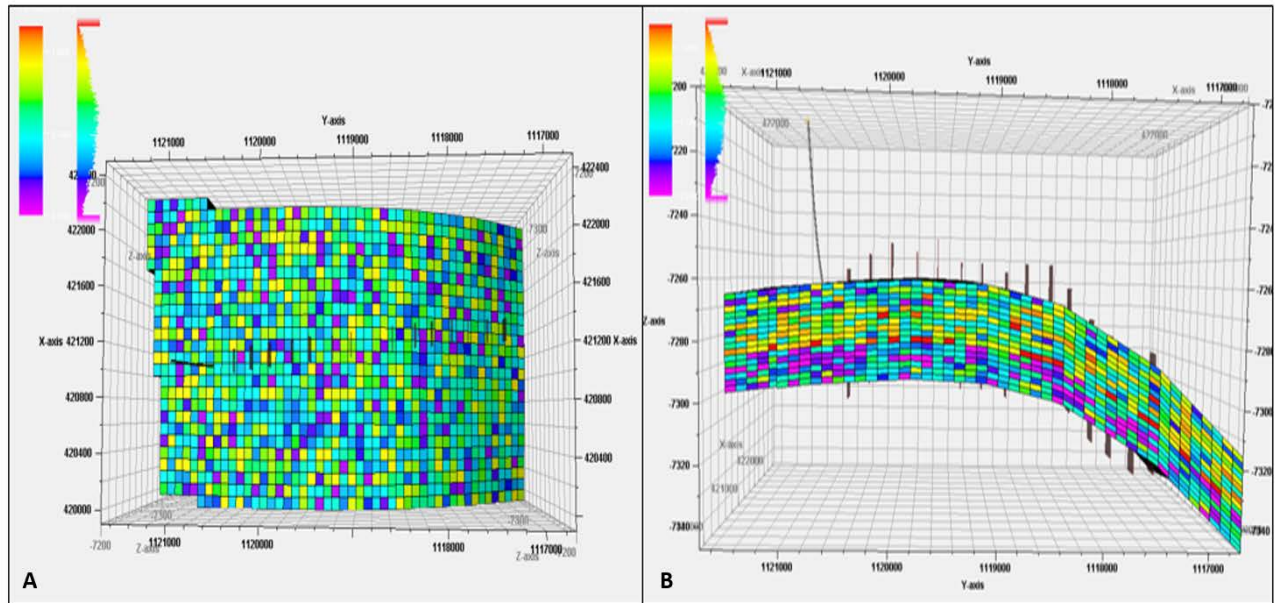


Figure 29: Top view (A) and side view (B) of random permeability distribution model.

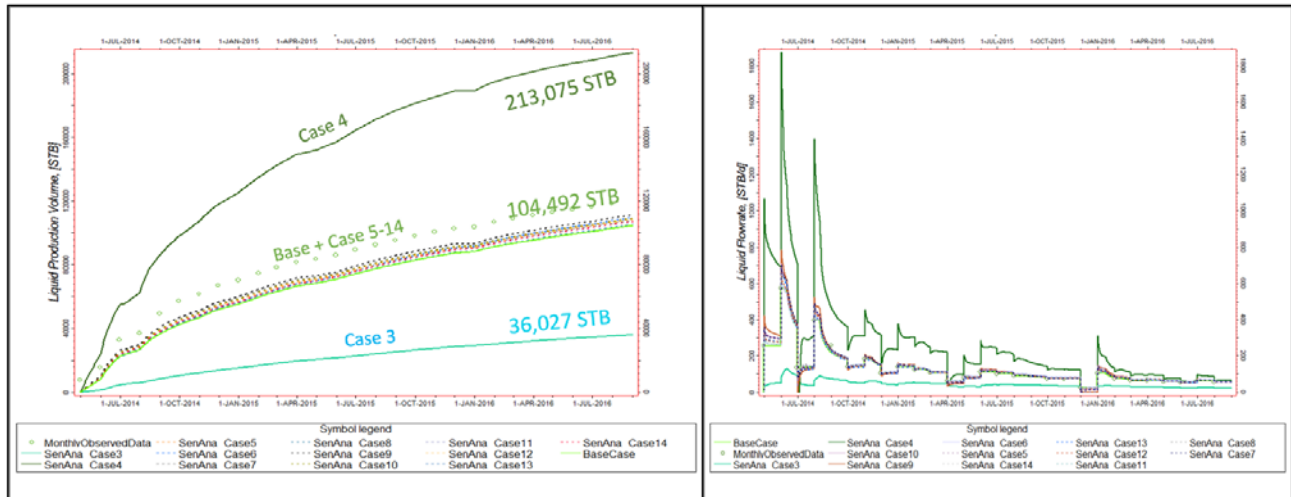


Figure 30: Oil production cumulative and oil production rate for permeability sensitivity analysis

3.6.2.3. Hydraulic Fractures

Modeling of hydraulic fractures was analyzed using different hydraulic fracture half-lengths. The fracture height is not a significant concern due to the 32-foot thickness of the reservoir model. Sensitivity analysis was conducted for hydraulic fractures with 50 foot, 100 foot, and 400 foot half lengths. The three hydraulic fracture models are shown in Figure 31. The results shown in Figure 32 indicate that there is not significant difference in production for 50-

foot or 100-foot half length. 400-foot half length is unreasonable because SM Energy engineers could not support any evidence of that hydraulic fracture half length, but the results show that the difference is only 25% higher than 100-feet half length. Thus, the 100-foot half length is less important than other variables and is a reasonable parameter that can be used to model the hydraulic fractures.

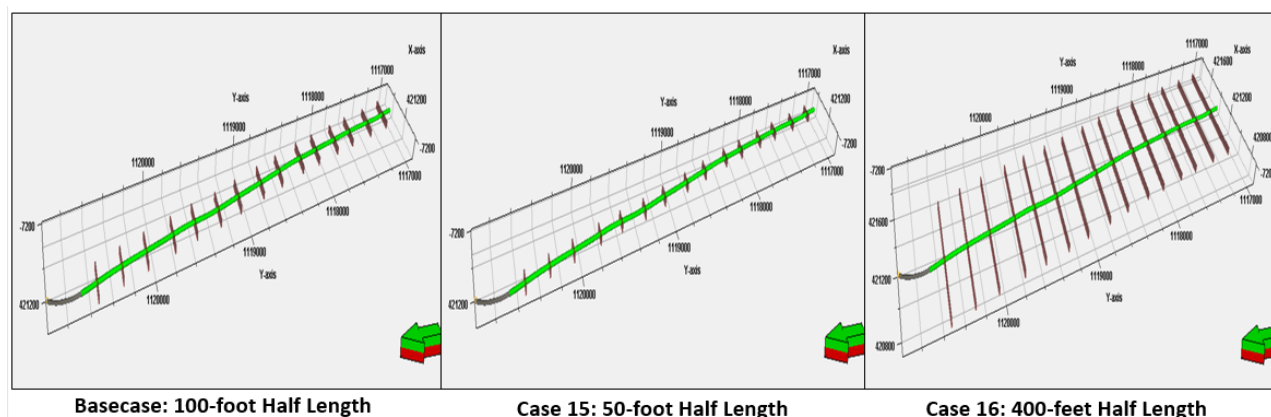


Figure 31: Hydraulic fractures sensitivity analysis. (Arrow illustrates the direction of the model)

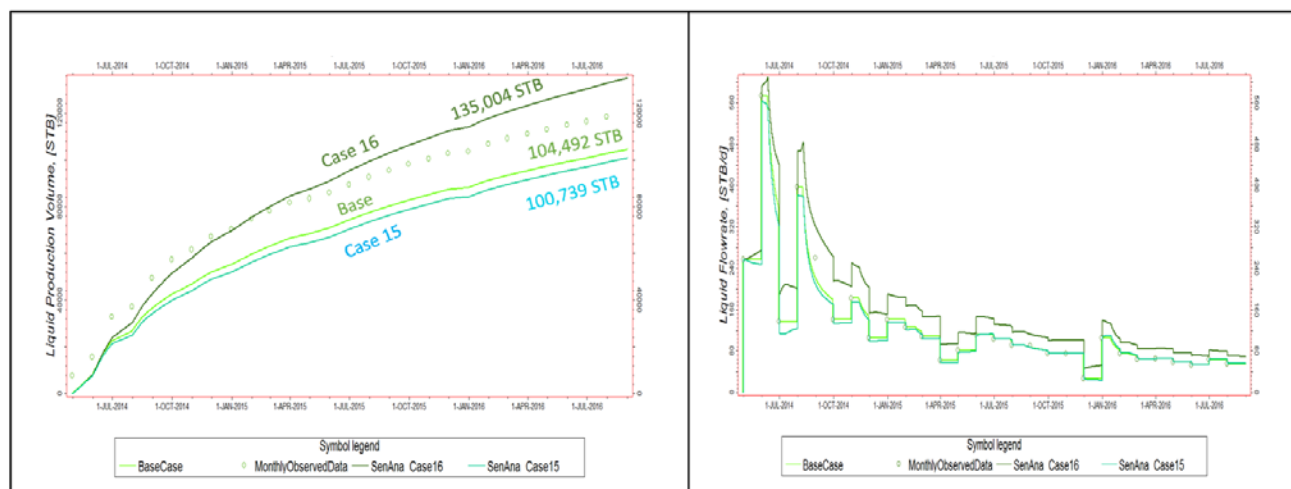


Figure 32: Oil production cumulative and oil production rate for hydraulic fractures sensitivity analysis.

3.6.2.4. Relative Permeability

Relative permeability data were not available for this reservoir; therefore, the relative permeability was established through history matching. Several parameters were used to modify the relative permeability to get most reasonable curves to describe the fluid behavior. Each parameter will define the curvature of relative permeability. Modification of the Corey exponents by increasing or decreasing the values will decrease and increase the curvature of relative permeability curve, respectively. If the relative permeability curve of one fluid has less curvature, it indicates the interfacial tension occurs between fluids is low which allows more favorable migration of that fluid (Amaefule and Handy, 1982; Asar and Handy, 1988). All three types of Corey exponents were tested. The results are shown in Figure 33 to Figure 38. The results included in this section are for the production of the specific type of fluid that the Corey exponent was modified.

Figure 33 shows relative permeability curves for the three different cases where the oil Corey exponent values ranged from 2, 3 (base case), and 4. The cumulative oil production shows about a 25% difference over this range of Corey exponent of oil (Figure 34).

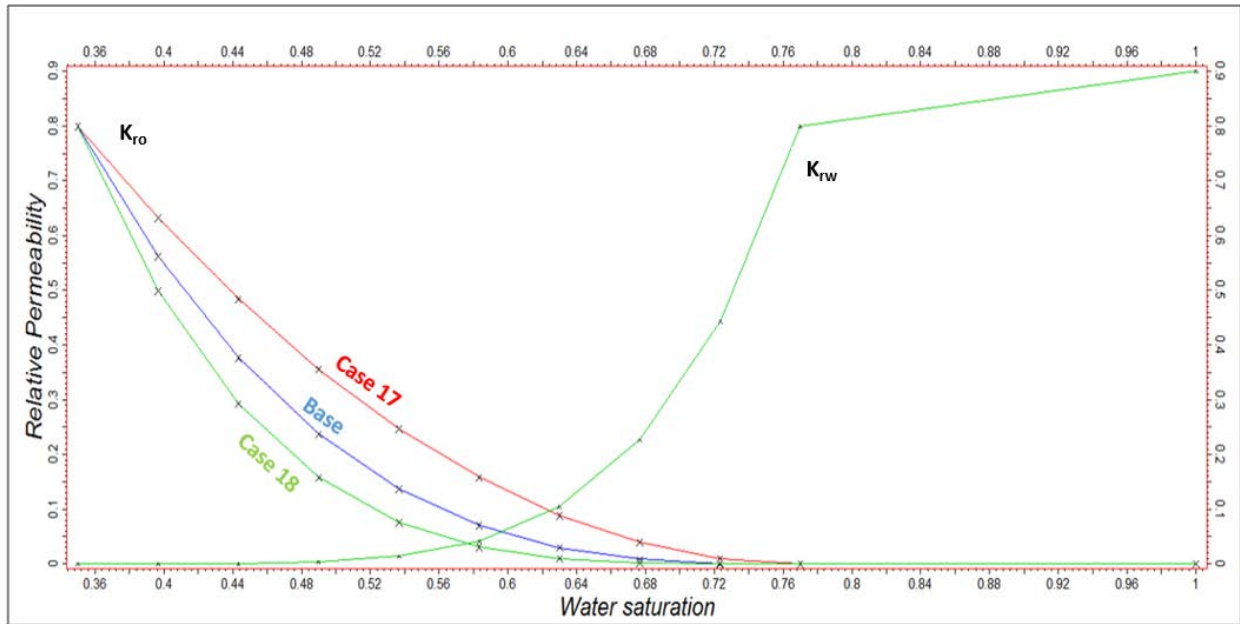


Figure 33: Oil/Water relative permeability curves for oil Corey exponent sensitivity analysis.

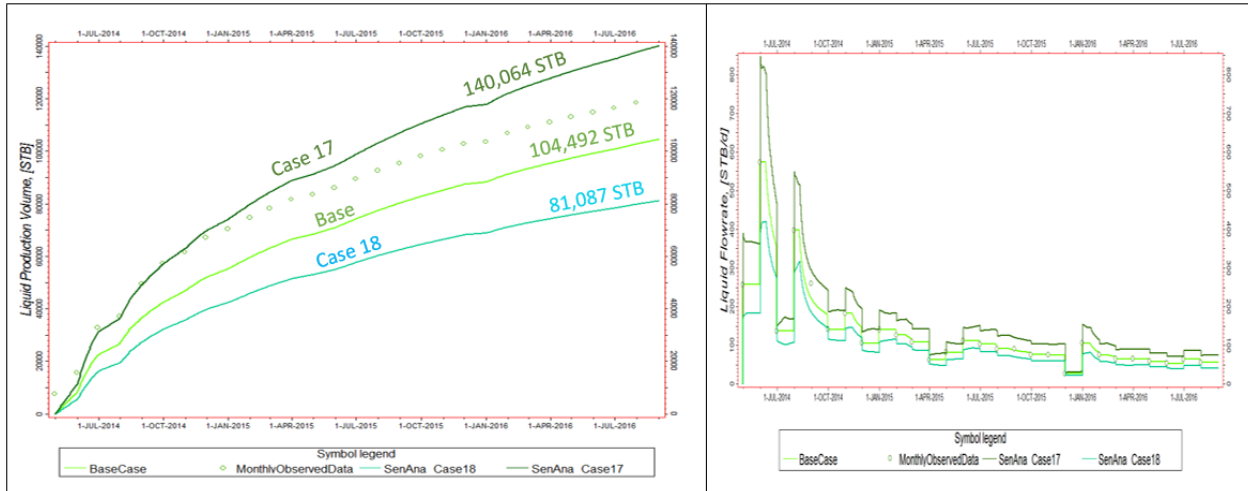


Figure 34: Oil production cumulative and oil production rate for oil Corey exponent sensitivity analysis

Figure 35 shows relative permeability curve for the three different cases where the water Corey exponent values ranged from 4, 5 (base case), and 6. The cumulative water production shows about a 35% difference over this range of Corey exponent of water (Figure 36).

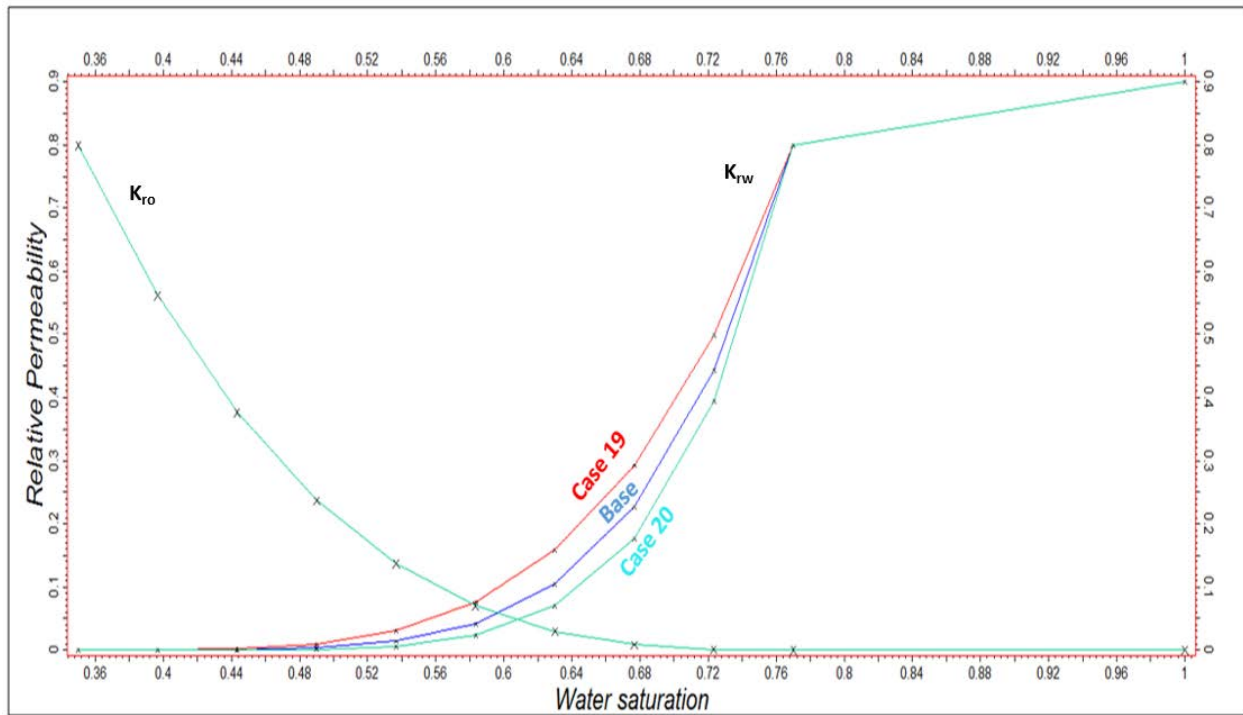


Figure 35: Oil/Water relative permeability curves for water Corey exponent sensitivity analysis.

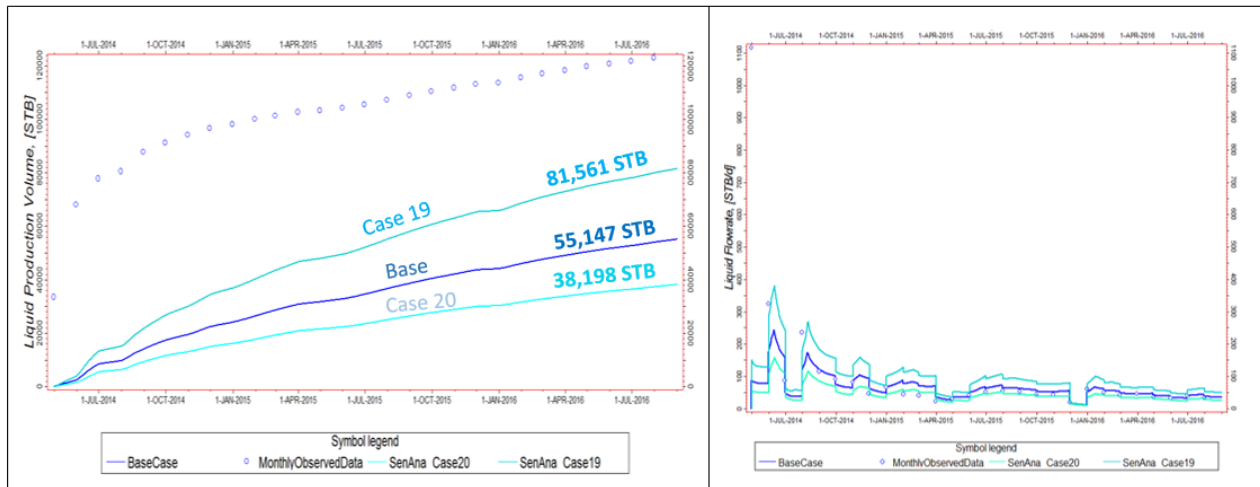


Figure 36: Water production cumulative and water production rate for water Corey exponent sensitivity analysis.

Figure 37 shows relative permeability curve for the three different cases where the gas Corey exponent values ranged from 2, 2.5 (base case), and 3. The cumulative gas production shows about a 15% difference over this range of Corey exponent of gas (Figure 38).

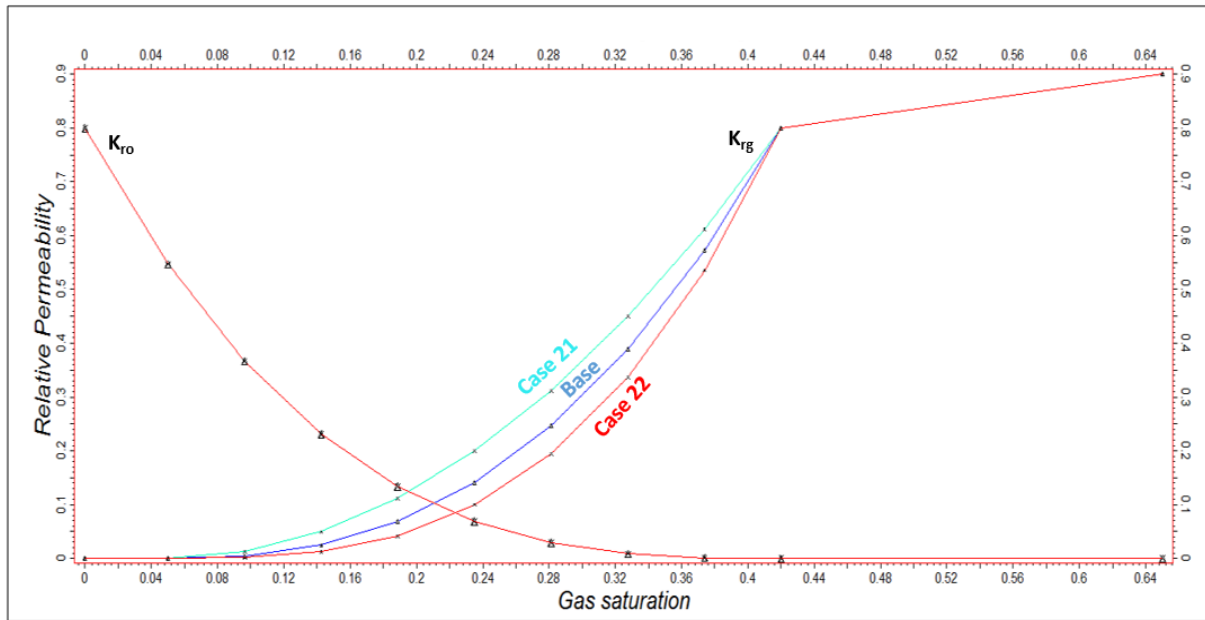


Figure 37: Oil/gas relative permeability curves for gas Corey exponent sensitivity analysis.

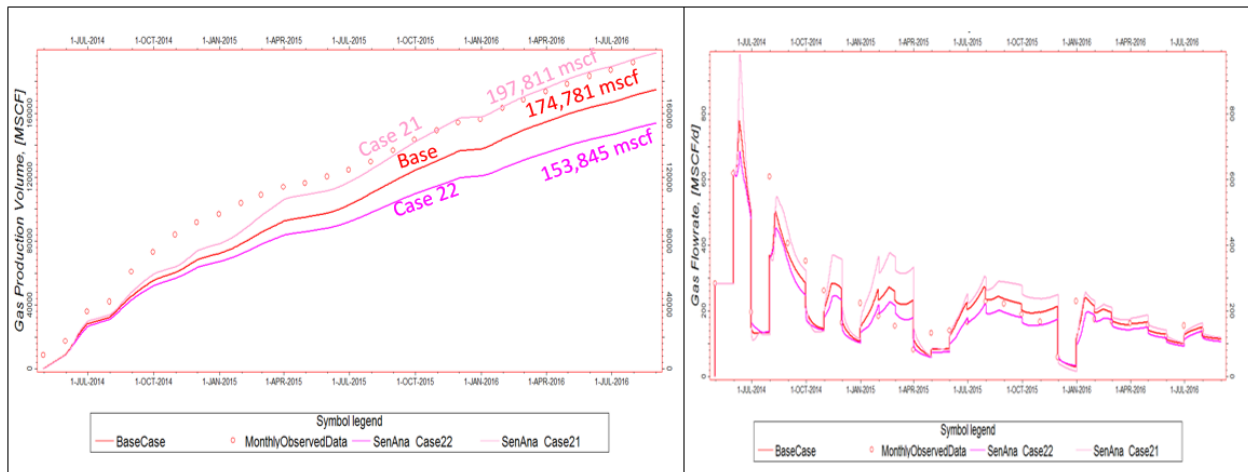


Figure 38: Gas production cumulative and gas production rate for gas Corey exponent sensitivity analysis

Another parameter used in this sensitivity analysis is a relative permeability of oil at highest oil saturation (K_{ro} at S_{omax}). This parameter is used to test how sensitive the end point of relative permeability of oil affects on the overall production. Figure 39 shows different end point of K_{ro} at S_{omax} of 0.4, 0.6, and 0.8 (base case). The results on Figure 40 shows that the differences in production between each incremental of K_{ro} at S_{omax} are only 10%, which is not significant with the big change in K_{ro} at S_{omax} .

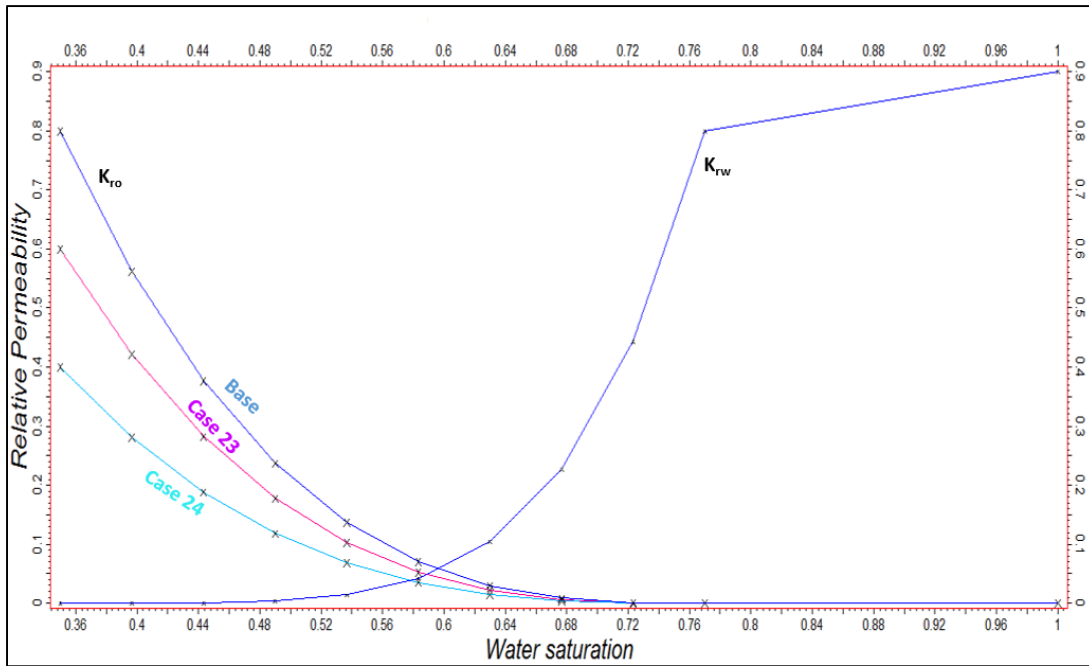


Figure 39: K_{ro} at S_{omax} for oil/water relative permeability curves sensitivity analysis.

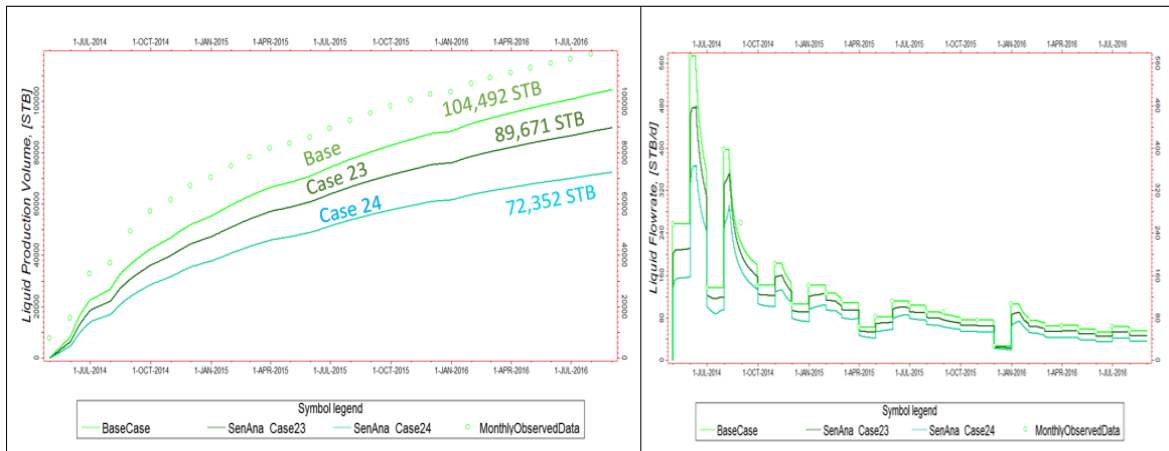


Figure 40: Oil production cumulative and oil production rate for K_{ro} at S_{omax} sensitivity analysis

3.6.2.5. Summary of Sensitivity Analysis

From the results of sensitivity analysis, porosity and permeability have the biggest impact on the total production of all fluids. Any modification of porosity and permeability must be considered with the most care within geological reasons to ensure the reliability of the model. As shown on random permeability distribution results, the current method to input the permeability

by layers is reasonable to define the permeability of the model to avoid any optimistic results that can cause by randomizing the permeability on the model. Sensitivity analysis on hydraulic fractures shows that 100-foot half length is reasonable for simulation purpose. Sensitivity analysis on relative permeability shows that each parameter defined in rock physics is very sensitive to the production of each fluid. The modification of each parameter to create the relative permeability curve for history matching will be the most important step to define a reasonable model for fluid behavior in WCM.

3.7. History Matching

3.7.1. Logarithmic grid refinement application

During history matching, many modifications are performed to match the historical production and bottom hole pressure. However, a model is not able to reproduce both reasonable bottom hole pressures and fluid flow behavior. Observations on each modification have shown that the current hydraulic fracturing model may overestimate the effect of hydraulic fractures on production and pressure. Due to the tight reservoir, the permeability was low compared to a conventional reservoir; therefore, using the equivalent grid sizes might not explain the fluid flow behavior properly. The logarithmic grid refinement (LGR) was then applied into each hydraulic fractures to model the fluid flow into each fracture and into the well (Doleshal, 2017). The LGR parameters consisted of 25 grid cells in I direction with average cell size of 100 feet and ten LGR divisions with minimum distance of 2 feet in J direction shown in Figure 41.

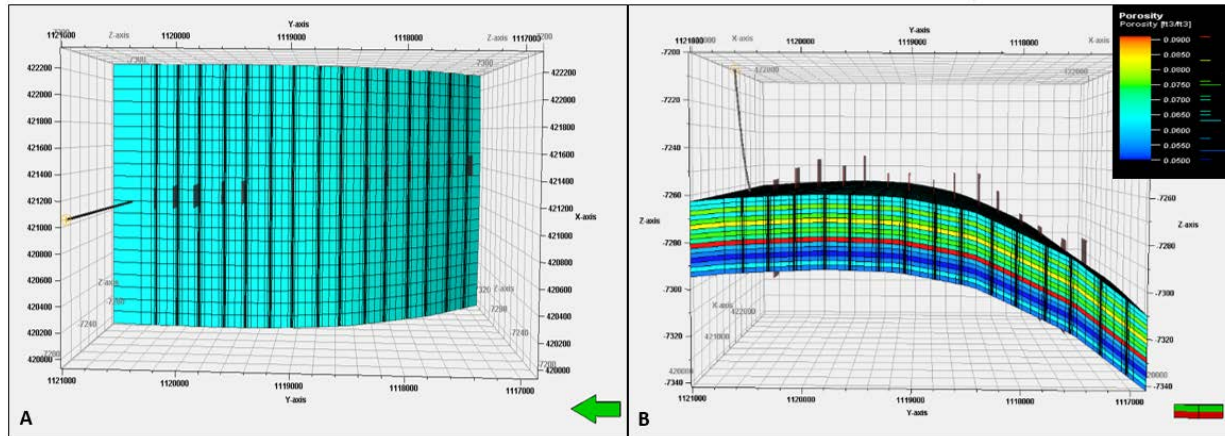


Figure 41: Top (A) and side (B) view of the Petrel reservoir model for a single horizontal well showing LGR application. (Arrow illustrates the direction of the model)

3.7.2. Modification of reservoir properties

After the application of LGR on hydraulic fractures, modification of rock physics is performed to describe the fluid flow behavior from the reservoir into the well through better defined hydraulic fractures. Flow rate patterns of each fluid and bottom hole pressures are two features that have been mostly focused on during the matching. Table VI shows the input parameters for each fluid, and Figure 42 shows the final modification of relative permeability curves, and

Table VI: Modified parameter for relative permeability curve

| Parameter | Values |
|----------------|--------|
| S_{or} | 0.20 |
| S_{wir} | 0.35 |
| S_{gr} | 0.05 |
| n_o to water | 2.40 |
| n_o to gas | 3.00 |
| n_w | 6.00 |
| n_g | 2.65 |
| $K_{ro,max}$ | 0.80 |

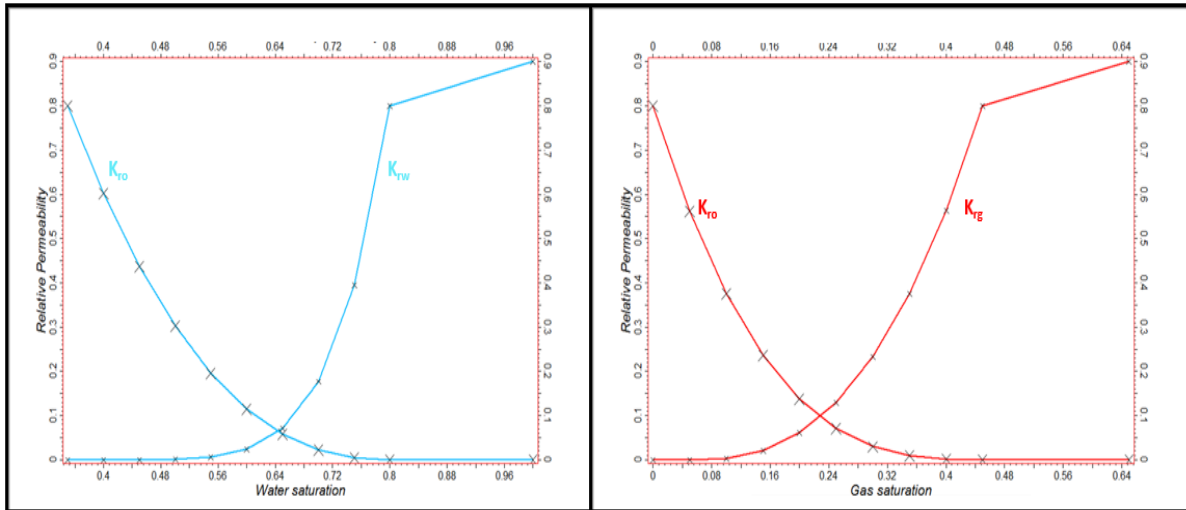


Figure 42: Modified relative permeability for the historical production matching.

After matching the flow rate pattern of each fluid, the bottom hole pressures are still not within a range of 600-700 psi as reported. Due to the sensitive of permeability on a model, the reduction of only 4% in permeability values help to ensure the bottom hole pressures are within range without affecting significantly to the overall production. Greater reduction of permeability may affect the entire modification of rock physics. Figure 43 shows the values of each permeability used in each layer after the modification.

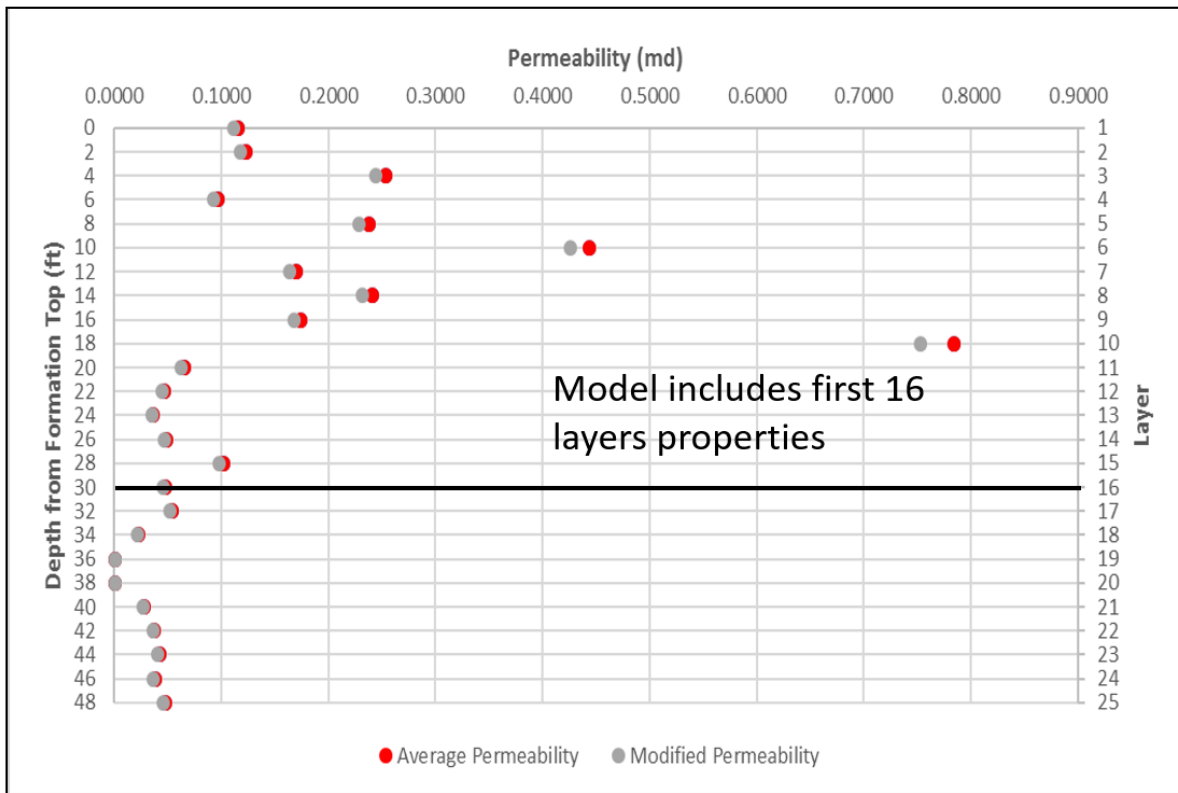


Figure 43: Modified permeability for history matching.

3.7.3. History matching results

After the addition of LGR and modification of reservoir properties, history matching was rerun on production data from May 2014 to September 2016. The well is constrained to the oil rates, and the matching parameters are water and gas production and estimated bottomhole pressure inside the well. As the results, the model has matched the historical production data. Matched bottomhole pressure confirmed the proper input of reservoir properties to illustrate the subsurface condition of the reservoir. Water and gas production matched the historical data, which confirmed that the relative permeability and fluid properties had properly described the fluid flow pattern from the reservoir into the well through the hydraulic fractures as shown in Figure 44 and 45.

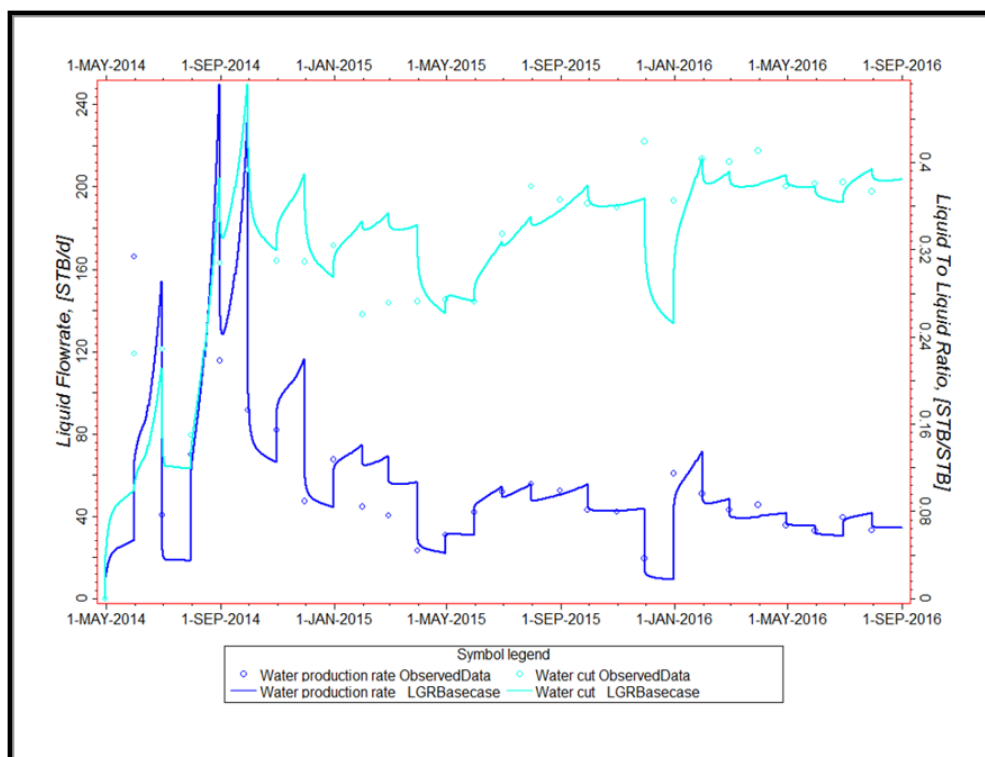


Figure 44: History matching results for with reasonable match for water production and water cut.

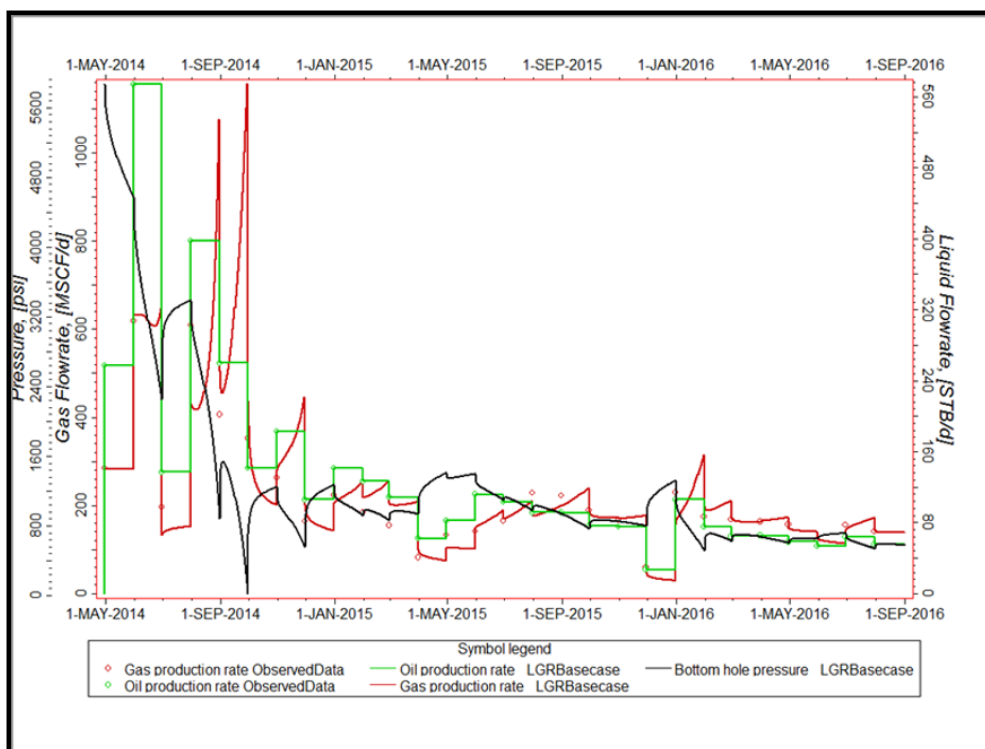


Figure 45: History matching results for with reasonable match for oil and gas production and bottom hole pressure.

3.8. Field Analysis

Well spacing analysis and fracture spacing analysis were performed to optimize the spacing distances between the wells and between each fracture. The same model boundary (5000 feet by 2500 feet) was used for this analysis with the similar model parameter for each well. Figure 46 shows five cases of the fracture spacing analysis with different number of fracture stages and fracture spacing. Figure 47 and 48 shows the results of cumulative oil production and production rate for each case.

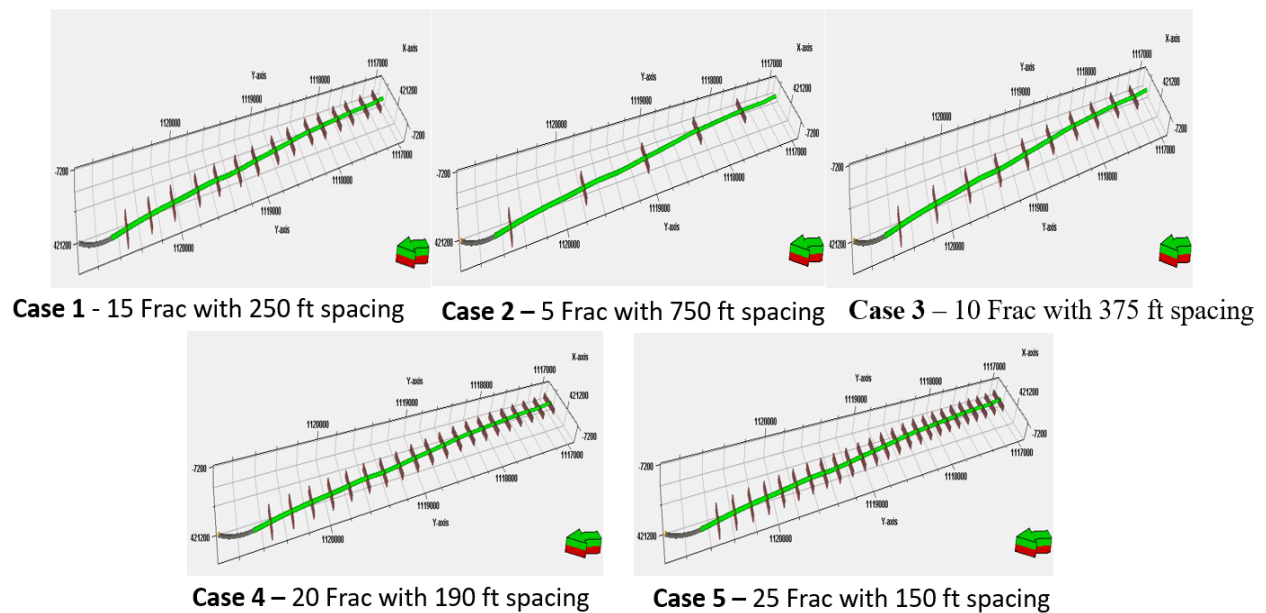


Figure 46: Fracture spacing analysis with 5 cases for different number of fracture stages and fracture spacing. (Arrow illustrates the direction of the model)

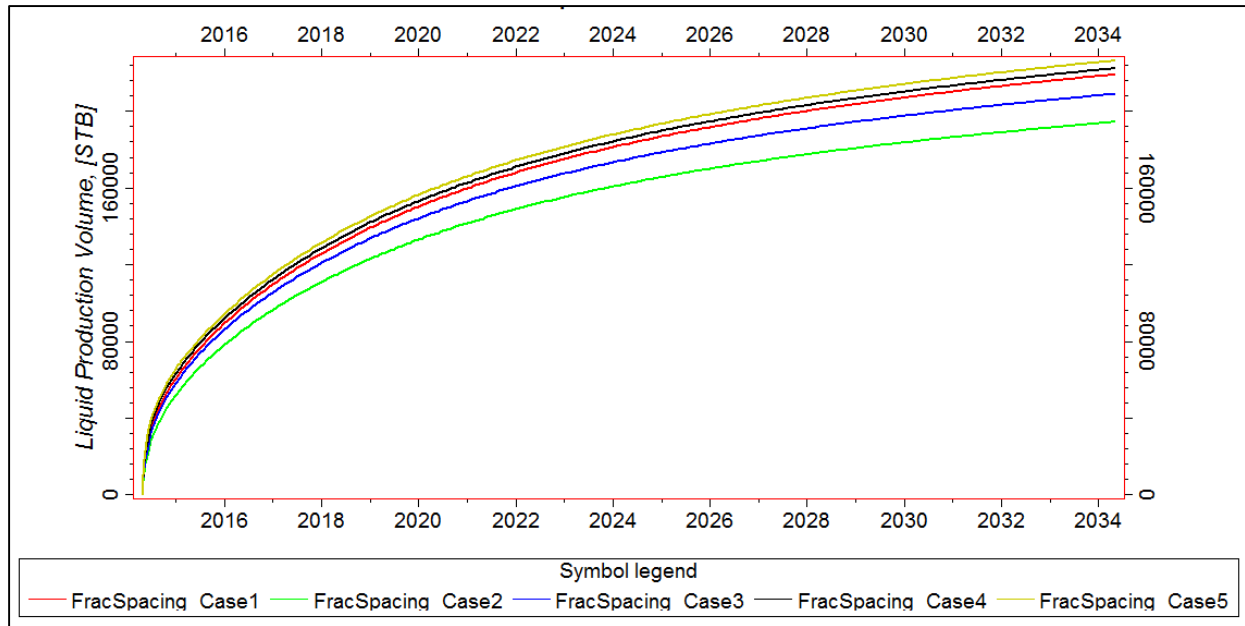


Figure 47: Fracture spacing analysis results for oil cumulative production.

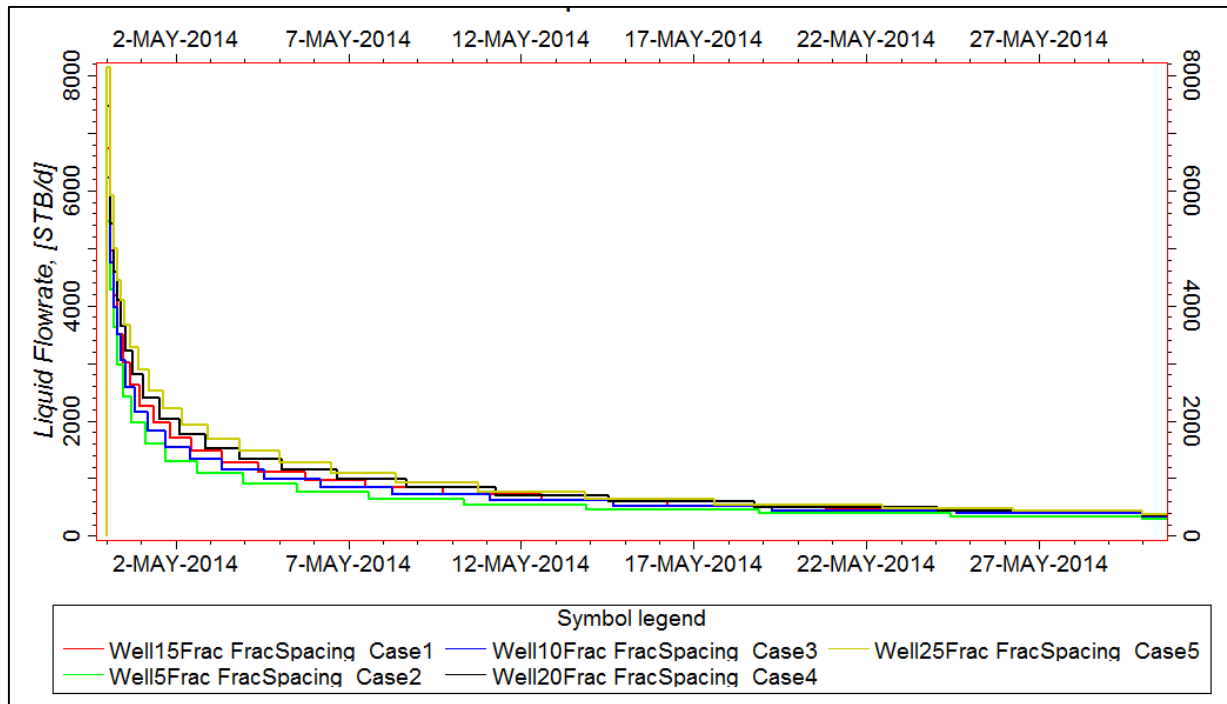


Figure 48: Fracture spacing analysis results for oil production rate.

The fracture spacing analysis shows that more stages of hydraulic fracture improve the total production (Figure 47) at the early years, but production rate of the well also decline much faster (Figure 48). Decreasing the fracture spacing by increasing number of fracture stages may

show the favorable production results; however, an economic analysis needs to be applied to find the optimal spacing. For the remainder of the current work, 250 feet spacing will be used.

Figure 49 show five cases of well spacing analysis with different numbers of well in the reservoir. Figure 50 and 51 show the results of cumulative oil production and the production rate of a middle well.

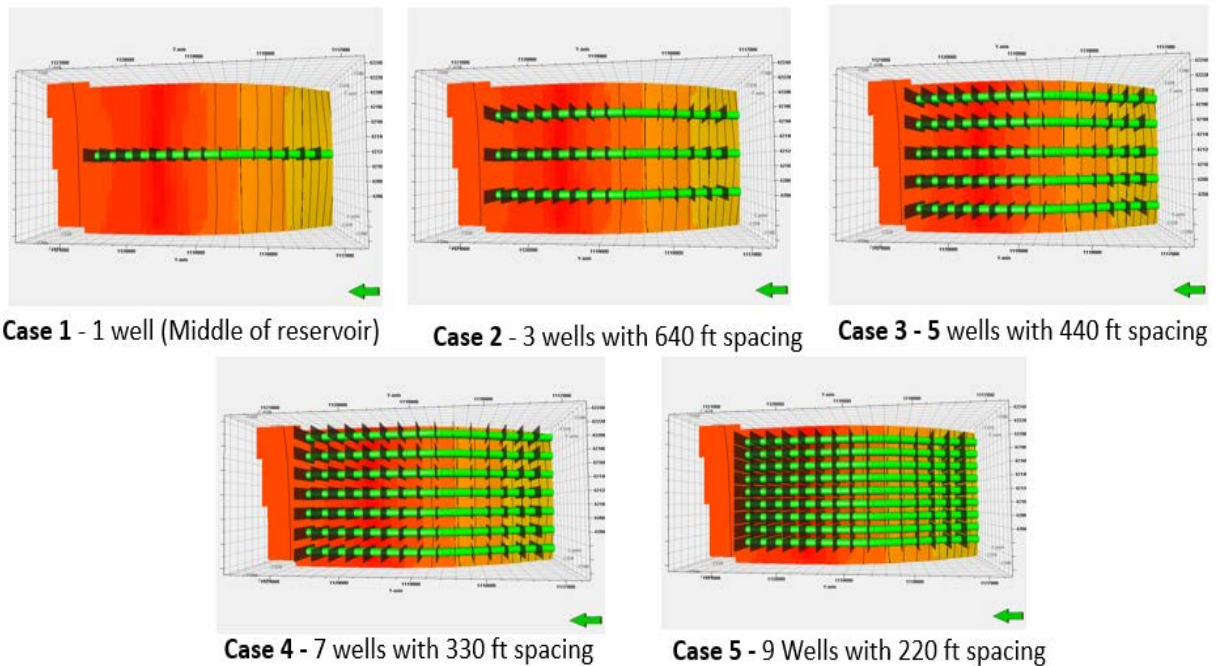


Figure 49: Well spacing analysis with 5 cases for different number of wells and well spacing in a same reservoir.

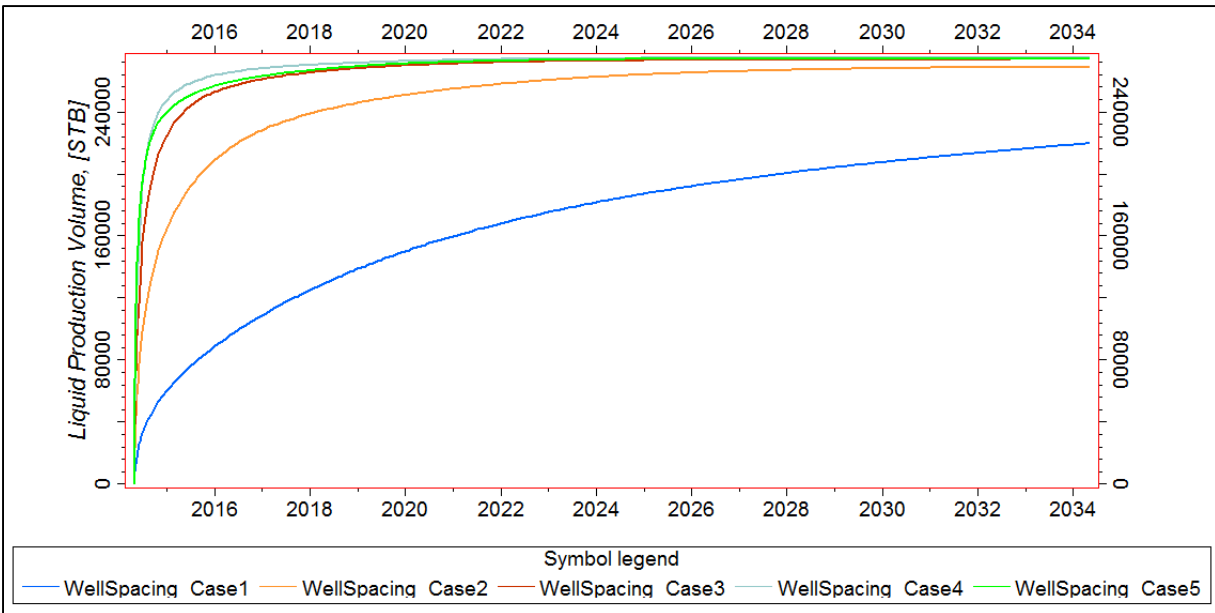


Figure 50: Well spacing analysis results for oil cumulative production.

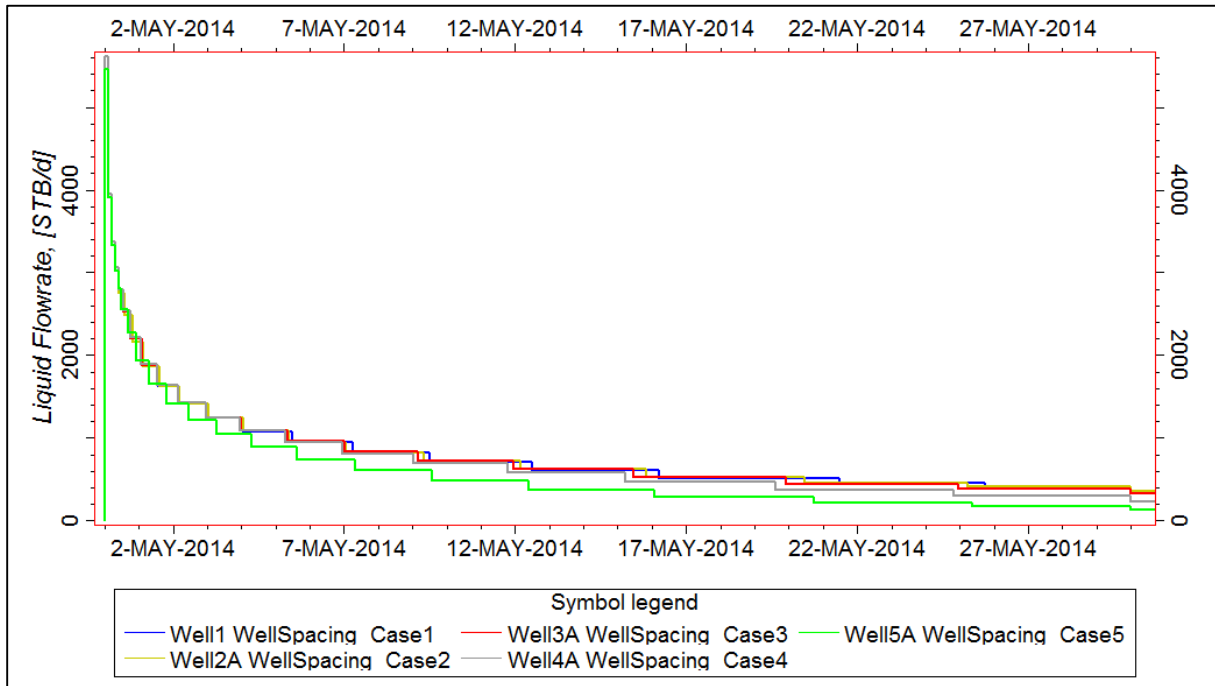


Figure 51: Well spacing analysis results for oil production rate of a middle well in each case (right)

As seen from Figure 50, there is a big improvement by developing more wells in the half section field; however, more than 5 wells does not appear to show any improvement (Case 4 and Case 5). The production rate of a middle well show that well interference has greatly affected the

production rate significantly in Cases 4 and 5 (Figure 51). Therefore, the optimal well spacing that can be used in this study would be 440 feet spacing between the wells. Again, a full economic analysis with well costs would be needed to determine the best well spacing, but that is beyond the scope of this work.

3.9. Summary of Well Scale Model

Well Scale model uses a single horizontal well to create a model to verify the reliability of reservoir properties used for WCM. Modification of each property results in a good history matching for historical production and bottom hole pressure. This confirms the reliability of each input properties and the method to model a Wall Creek Member reservoir. These properties are then integrated into the Integrated Outcrop model to analyze the effect of geologic features on fluid flow behavior. Field analysis also provides optimum values for fracture spacing of 250 feet and well spacing of 440 feet between each well.

4. Integration of the Outcrop Observation and Subsurface Properties

According to the outcrop study (LaFontaine, 2018), the WCM consists of a complex succession of stacked parasequences including basal river-dominated delta, a storm-wave dominated shoreface, and a tidally influenced delta. All facies in the parasequences are defined by sedimentologic analysis to represent the architectures controlled by deposited environment and then upscaled to integrate into the full outcrop model. More information about the geologic interpretation can be found from a study by LaFontaine (2018). In the current paper, the progress of upscaling and the results analysis will be shown to incorporate with the geologic study to better understand how architectural control impact fluid flow behaviors.

4.1. High-Resolution Models

The High-Resolution models (Model 2) are created to describe the characteristics of each facies that are present in the WCM. Each model contains different orientations and transmissibility multipliers of mud drapes, which represents the important features in each facies. The model was created to represent a single grid block (30 feet to 100 feet) in the outcrop model. Figure 51 shows one example of the High-Resolution models including the mud drapes that are used to analyze how the abundances and dimensions of mud drapes affect permeability in the reservoir. The black blocks represent the mud drapes observed from the outcrop study (Figure 52). The High-Resolution model is approximately 75 feet by 45 feet by 5 feet. The included cell thickness is only a few centimeter thick to capture how the thin-beds affect fluid flow that are not normally captured in coarse models. Other facies models are shown in Appendix B.

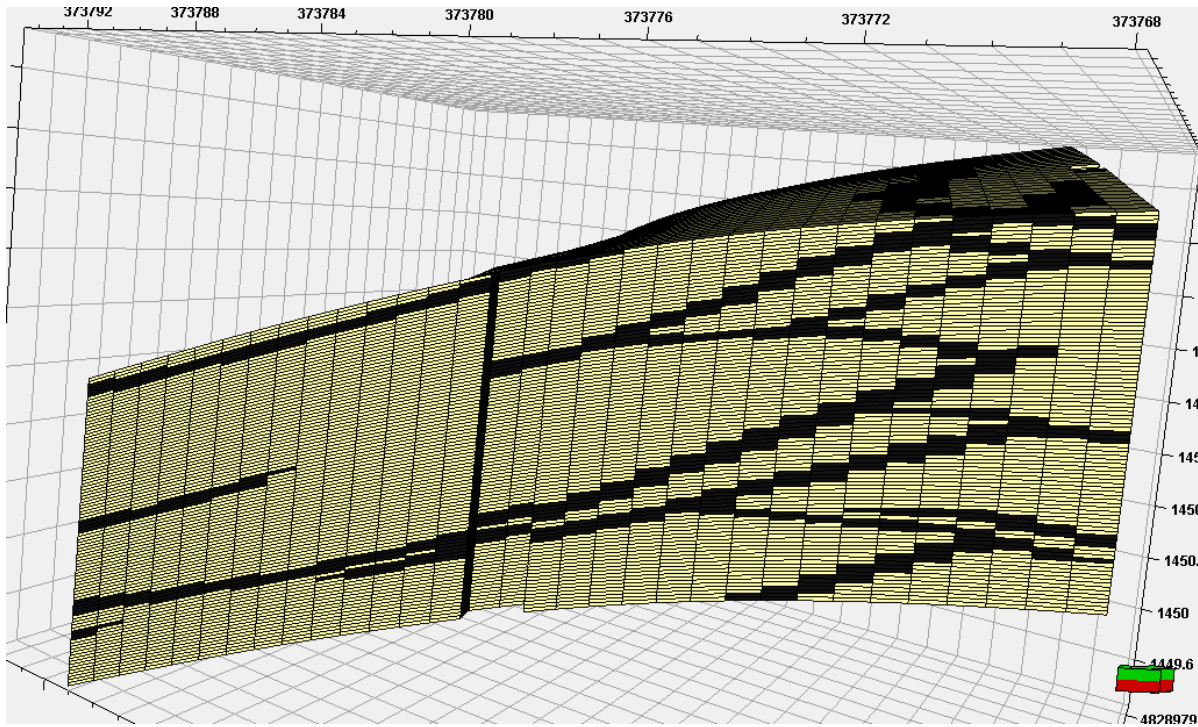


Figure 52: An example of defined geologic model for 5 feet thick tidal bar top. (Arrow illustrates the direction of the model)

Within the lower 50 feet to 65 feet of the WCM along the outcrop, several facies were identified and measured with great detail to capture the fine scale features such as the mud drapes (LaFontaine, 2018). Six facies were found to be present from the outcrop and from the core samples taken from the SM Energy wells. These facies are noted in Table VII. Four of the facies, which are tidal bar top and tidal bar base, shoreface parasequences, and thin interbedded sandstone with siltstone/mudstone facies, are modeled at high resolution to observe the impact of mud drape presence in each facies. Other facies are not affected significantly by mud drapes in this study area.

Table VII: Characteristics of facies observed from the Tisdale Anticline outcrop (LaFontaine, 2018)

| Petrel Facies | Characteristics |
|---------------------------------------------|------------------------------------------------------------------------------------------------------------------------------------------------------------------------------------------------------------------------------------------------------------------------------------------------------------------------------------------------------------------------------------|
| Tidal bar top | Upper fine to lower medium grain, cross-bedded sandstone with common mud draped foresets and bedded boundaries. |
| Tidal bar base | Wavy to lenticular bedded, alternating thin sand and mud/muddy silt deposits, with rare, thick mud beds up to ~10 cm thick, interbedded with upper fine to lower medium grain, cross-bedded sandstone with common mud draped foresets and bedded boundaries. |
| Shoreface parasequences | Upward transition between thin, interbedded sandstone and siltstone to the parallel laminated storm deposits. |
| Cross-bedded sandstone | Fine to upper fine-grained, planar and trough-cross bedded sandstone with rare mud draped foresets and rare mud clasts. |
| Planar lamination, scouring facies | Consists of three similar facies: Swaley cross-stratified sandstone, hummocky cross-bedded sandstone, low-angle planar laminated sandstone. They all consists of tan to red, very fine to fine grained well sorted sandstone. |
| Thin, interbedded sand with silt/mud facies | Consists of two similar facies with different depositional environment grouped into one facies. One facies contains tan to reddish, fine-grained sandstones with massive to planer lamination that sometimes grades upward into ripple-lamination. Other facies consists of thin, discontinuous fine-grained sand beds interbedded with siltstone and mudstone drapes at cm-scale. |

Flow-based upscaling allows us to use the fine scale models to estimate the directional permeability of the model grid blocks. Then, all the High-Resolution models are combined into one outcrop model that includes all the stratigraphic system of the WCM.

4.2. Flow Based Upscaling

Outcrop study indicated the presence of mud drapes can affect significantly the fluid flow (Zupanic, 2017; LaFontaine, 2018), but they cannot be captured by common methods such as logs or seismic. This study allows the abundance and dimension of mud drapes to be measured in each facies and to define them in the geologic models. For this project, we are capturing this fine-scale (cm-scale) geologic information from the outcrop into the given model, but the resolution is too fine for the flow model to be able to run. Thus, flow-based upscaling (Durlofsky, 2005) will be used to describe the permeability on the coarse grid. Petrel software was used to perform the simulation to estimate the permeability in three directions. The simulation allowed the fluid flow through part of reservoir in only one direction. For example, if

the fluid flow is in X direction, the boundaries in Y and Z direction will be closed (Figure 53).

This will only be done for the section of reservoir that is being upscaled. Darcy's law will be applied to calculate the average permeability for each simulation to calculate the permeability in each direction. The fluid used for flow-based upscaling is fresh water with the following properties:

Table VIII: Properties of fresh water for flow-based upscaling

| Properties of fresh water | Values | Units |
|---------------------------|--------|-------------------------|
| Salinity | 0.0000 | ppm |
| Formation volume factor | 1.0358 | res bbl/standard barrel |
| Viscosity | 0.2421 | cp |

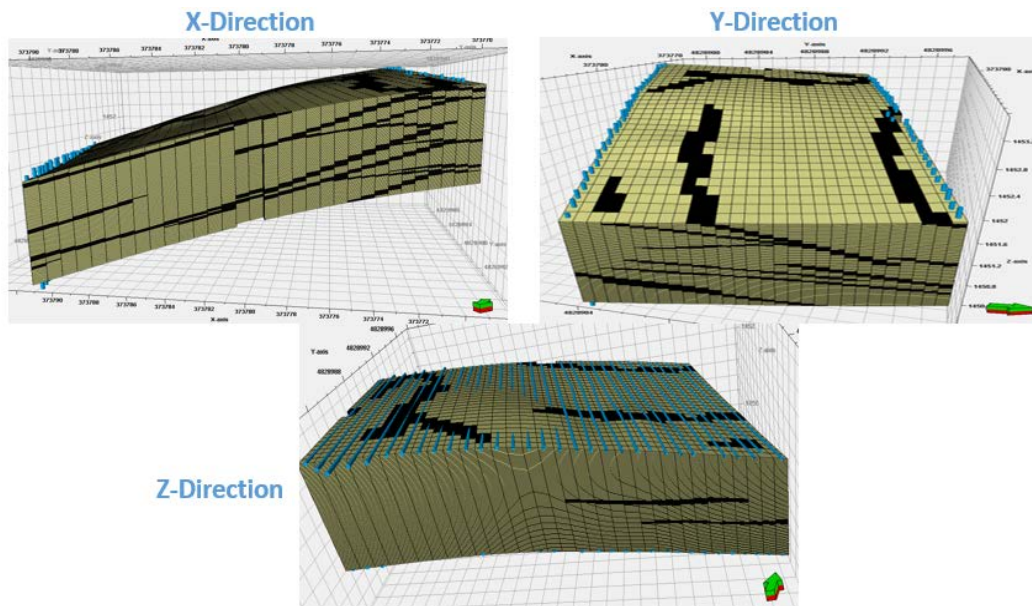


Figure 53: Examples of flow-based upscaling in three directions for tidal bar top model. (Arrow illustrates the direction of the model)

Four different high-resolution models are upscaled to estimate percent reduction of permeability (see Appendix B for models and results). These models correlate to the four facies with mud drapes described in Table VII

- Model 2A: Thin, interbedded sandstones with siltstone/mudstone: 36 feet by 48 feet by 3 feet (175,861 cells)

- Model 2B: Shoreface parasequence: 52 feet by 50 feet by 8 feet (205,375 cells)
- Model 2C: Tidal bar base: 74 feet by 47 feet by 10 feet (87,000 cells)
- Model 2D: Tidal bar top: 75 feet by 45 feet by 6 feet (89,600 cells)

Each of the high-resolution models contains about 87,000 to 205,000 cells that are upscaled into one single cell to estimate the permeability reduction due to the presence of mud drapes in three directions. Transmissibility multiplier are used to define the percentage of conductivity that allow the fluid flow through (Manzocchi et al., 1999). The values for transmissibility multiplier range from 0 (no fluid can flow through) to 1 (all fluid can flow through). Transmissibility multipliers are applied to mud drape grid blocks to analyze the restriction of mud drapes to the flow in different scenarios. Figure 54 shows one example of how the transmissibility multipliers affect the permeability reduction on the tidal bar top facies.

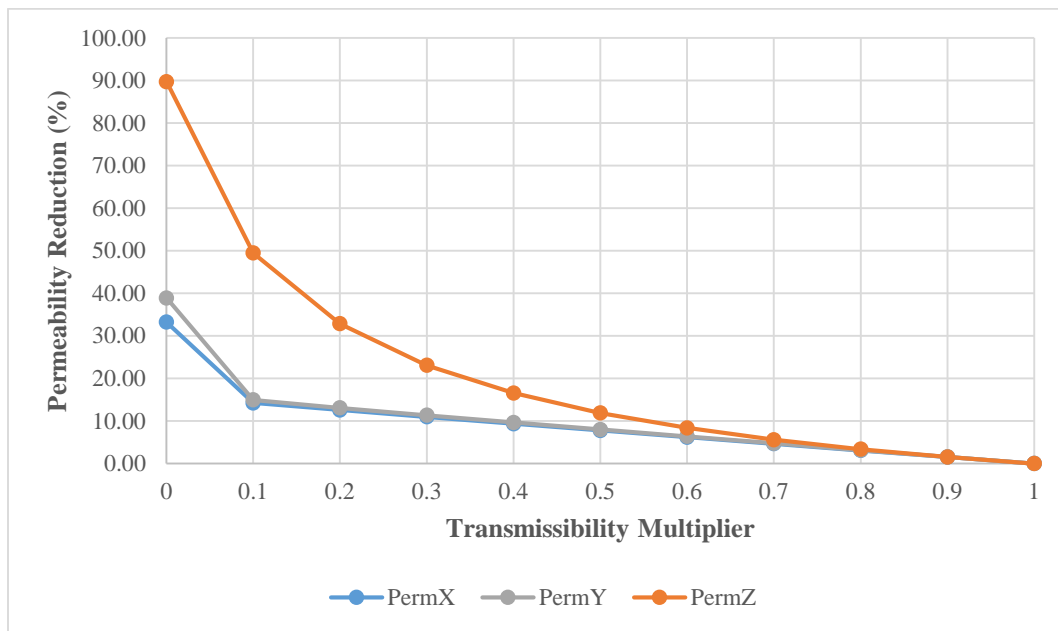


Figure 54: Example of permeability reduction of tidal bar top with T_m from 0 to 1

Table IX shows the percentage of permeability reduction for each facies at transmissibility multipliers of 0 and 0.5 (T_m). The reduction in horizontal permeability ranges

from 9% to 39% where the vertical permeability is reduced from 66% to 100% for $T_m = 0$. When $T_m = 0.5$, the reduction is much less. The reduction in horizontal permeability ranges from 2.09% to 8.01% where the vertical permeability is reduced from 5.89% to 11.90% for $T_m = 0.5$. Because the mud drapes are deposited horizontally, they have more impact on vertical permeability. The results are used for facies characterization that are included in the Integrated Outcrop model to account for the effect of mud drapes on the fluid flow behavior.

Table IX: Results of flow-based upscaling for each facies of WCM.

| Facies | Percentage of Permeability Reduction ($T_m = 0$) | | | Percentage of Permeability Reduction ($T_m = 0.5$) | | |
|-------------------------------------|----------------------------------------------------|-------------|-------------|------------------------------------------------------|-------------|-------------|
| | X-Direction | Y-Direction | Z-Direction | X-Direction | Y-Direction | Z-Direction |
| Upper Tidal Bar | 33.19 | 38.91 | 89.73 | 7.79 | 8.01 | 11.89 |
| Lower Tidal Bar | 15.48 | 13.66 | 66.05 | 4.39 | 4.63 | 5.89 |
| Shoreface Parasequences | 23.96 | 26.29 | 100 | 7.40 | 7.58 | 11.90 |
| Thin, interbedded sand and silt/mud | 9.75 | 8.73 | 97.88 | 3.75 | 2.09 | 6.18 |

4.3. Integrated Outcrop Model

The Integrated Outcrop model (Model 3) incorporates all field observations including detailed architectures of the Wall Creek outcrop and upscaled model results. The model size is about 2300 ft by 1600 ft by 60 ft, which is an approximate size of the outcrop that was used to capture all the characteristics of the Wall Creek architectures. Each of the facies found from observation is included in the model with its porosity and permeability observed from the equivalent facies in core data. Table X shows the color codes used to describe each type of facies in the model.

Table X: Color description of each facies for the Integrated Outcrop model.

| Color code | Upscaled Facies Description |
|------------|---------------------------------------------|
| Orange | Tidal bar top |
| Grey | Tidal bar base |
| Teal | Shoreface Parasequences |
| Red | Cross-bedded sandstone |
| Green | Parallel-laminated storm deposits |
| Yellow | Thin, interbedded sand with silt/mud facies |

Four different Integrated Outcrop models are discussed in this section and are used for the WCM analysis:

- Model 3A (Figure 55): Geologic structural model – a 5° dipping model
- Model 3B (Figure 56): Proxy structural model – a 5° dipping model with simplification of facies distribution
- Model 3C (Figure 57A): Geologic stratigraphic model – a flattened model
- Model 3D (Figure 57B): Proxy stratigraphic model – a flattened model with simplification of facies distribution

All Integrated Outcrop models have similar features from the outcrop at Tisdale Anticline. Using control points of each facies taken from the outcrop and measuring the content of each facies rock, the model captures the dimension and orientation of each grid block that represents the distributions of every facies as shown by different colors.

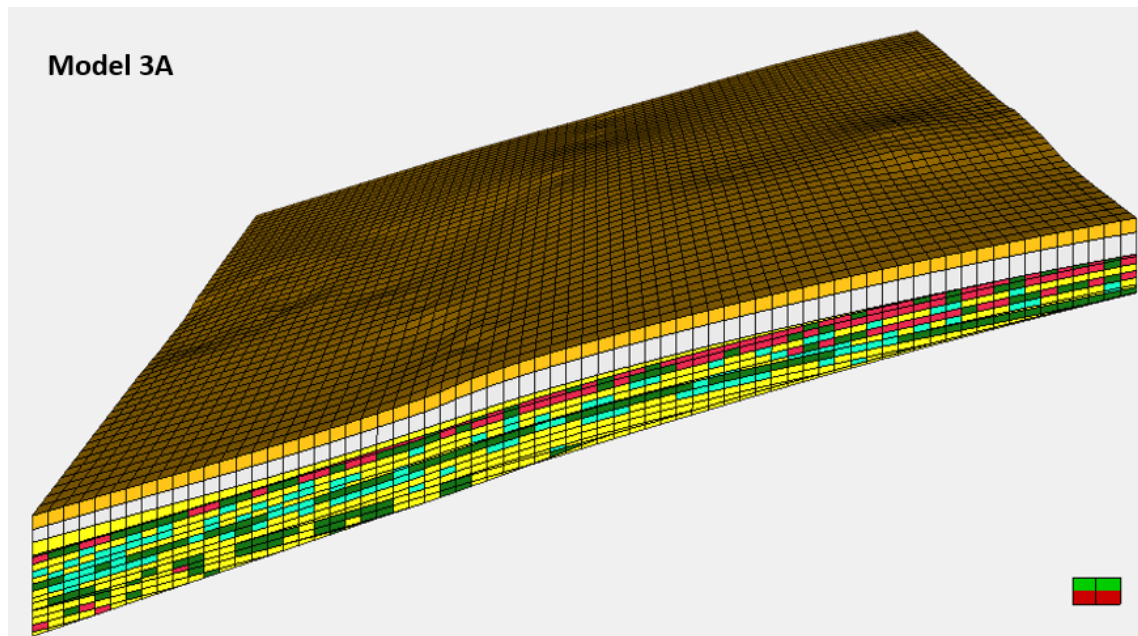


Figure 55: Integrated Outcrop model (Model 3A) including architectural stratigraphy of WCM based on the measured points taken at the outcrop. (Arrow illustrates the direction of model)

While Figure 55 indicates the details that can be included when outcrop study is available, most reservoir models are built only using well log and core information. Figure 56 represents a proxy structural model (Model 3B) that simplifies the architectures of the outcrop, which only models the facies based on the percentage of facies distribution. This model is similar to what engineers often build if they do not have the outcrop information

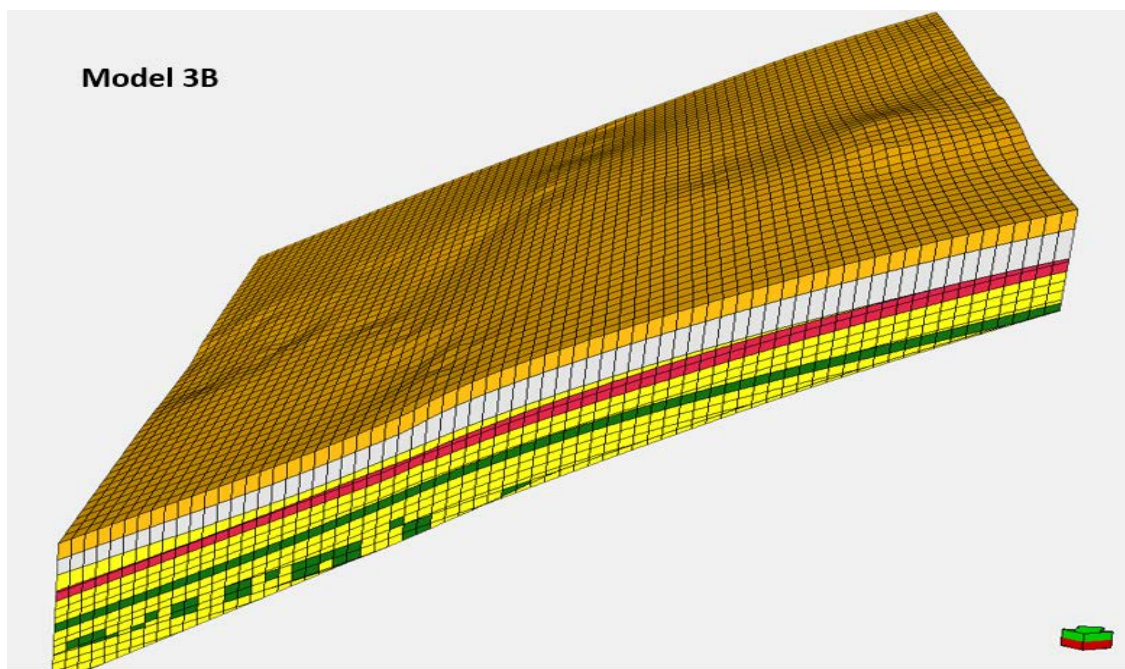


Figure 56: Proxy structural model (Model 3B) including the simplification of facies distribution of the outcrop. (Arrow illustrates the direction of model)

Both models from Figure 55 and Figure 56 were built based on the actual coordinated points measured from the outcrop. The model structure is dipping at approximately 5 degrees. They are designated as structural models. Figure 57 shows other two models that were created with flattened stratigraphic structure to be designated as stratigraphic models.

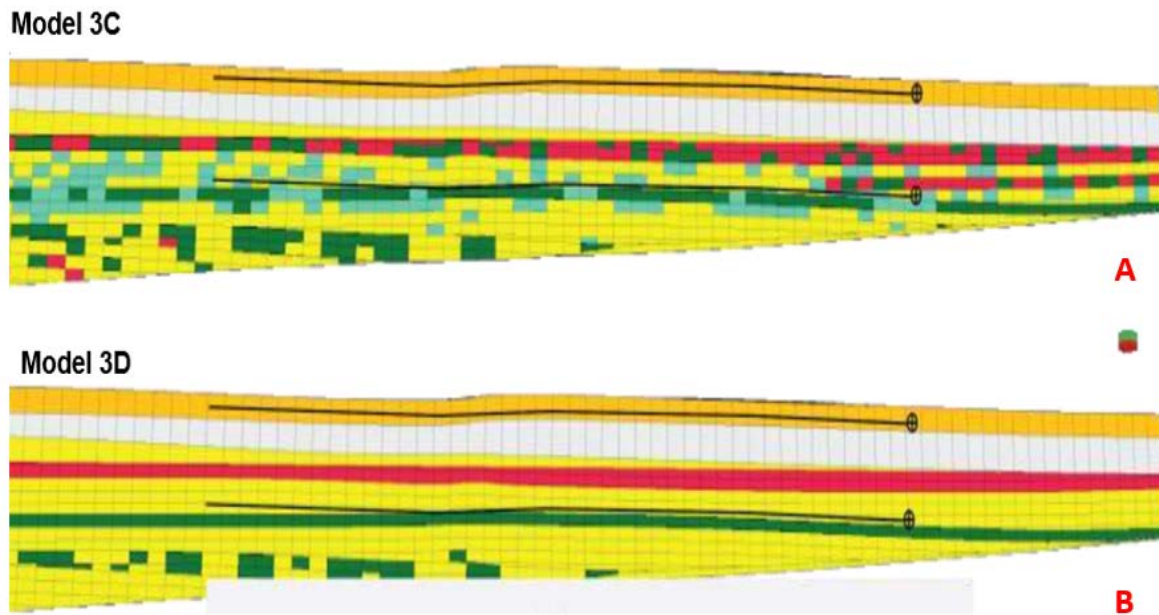


Figure 57: Integrated Outcrop models with flattened structure: (A) geologic stratigraphic model (Model 3C) and (B) proxy stratigraphic model (model 3D). (Arrow illustrates the direction of model)

The WCM consists of two packages of facies: tidally-influenced facies and wave-influenced facies. These two facies can be further distinguished by the actual reservoir quality using permeability values interpreted from the core data of the well Buttermilk State 3976-15-22-1FH (LaFontaine, 2018). By looking at Figure 58 and well logs of three vertical offset well (Figure 10), there are certainly the boundary line between tidally-influenced facies with cleaner sand – low gamma rays and wave-influenced facies at 18 feet thick from the top of formation. These observations match the outcrop study that defines the top two tidal bars layers as a high-quality zone. Therefore, the results of interpretation for permeability and porosity from wells logs were averaged for outcrop model input properties. The water distribution was also distributed based on porosity dependence.

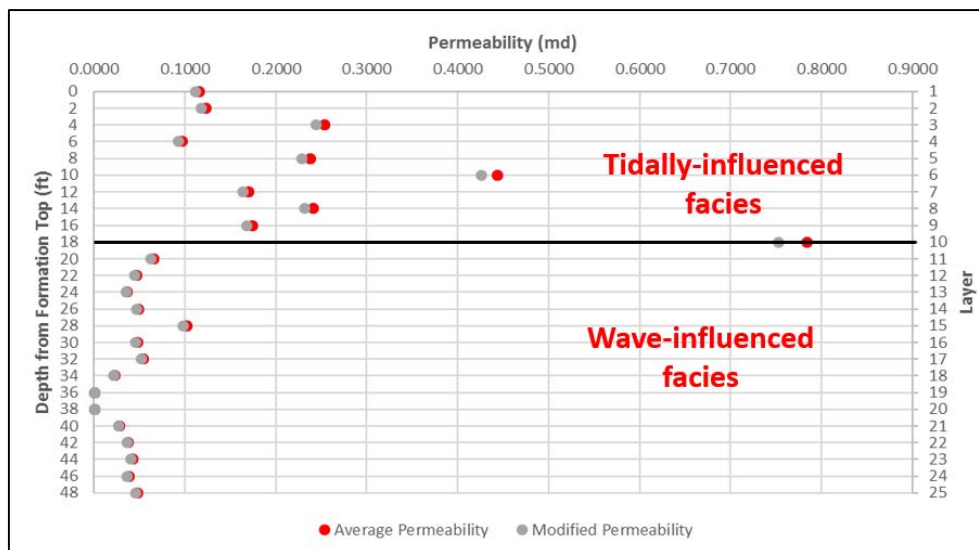


Figure 58: Permeability graph with boundary line between two distinct sedimentary facies.

4.4. Sensitivity Analysis of Integrated Outcrop Models

4.4.1. Structural models vs Stratigraphic models

To perform the analysis with all possible scenarios using the Integrated Outcrop models, the following procedures are created to analyze the effect that geologic features have on fluid flow behavior in WCM. The fluid used in these analyses are fresh water (no salinity). The pressure of model is set at 5866 psi according to the actual reservoir pressure of Rush State well model at 7260 feet below sea level. The flowing bottomhole pressure is set at 100 psi to create the drawdown pressure of 5766 psi for the well performance. For each of the four Model 3: (geologic structural (A), proxy structural (B), geologic stratigraphic (C), proxy stratigraphic (D)), seven different wells configurations are created (3 vertical and 4 lateral). Figure 59 shows the location of all wells (red is vertical well, green is horizontal well), but only one well is present in any individual run.

- 3 Vertical Wells:
 - o Top apex of geomodel (Southwest),

- Direct center of geomodel
- Bottom apex of geomodel (Northeast).
- 4 Lateral wells:
 - West-East trending, through middle of model at tidal bar top (orange).
 - West-East trending, through middle of model at continuous green/teal horizon.
 - North-South trending, through middle of model at tidal bar top (orange).
 - North-South trending, through middle of model at continuous green/teal horizon.

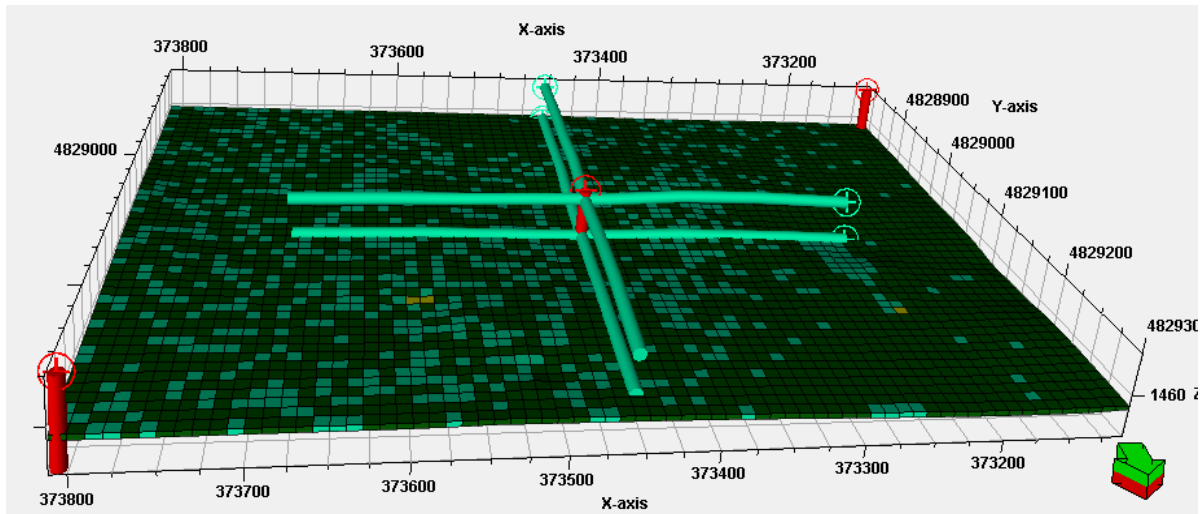


Figure 59: Well placement for outcrop analysis – Vertical wells (red) and Horizontal wells (teal) (Arrow illustrate the direction of the model).

Total of 84 cases are run with 42 cases for structural models (Model 3A and 3B) (28 geologic and 14 proxy) and 42 cases for stratigraphic models (Model 3C and 3D) (28 geologic and 14 proxy) with the scenarios below. Geologic models will be performed with $T_m = 0$ (3A-0 and 3C-0) and $T_m = 0.5$ (3A-0.5 and 3C-0.5), while proxy models will use the direct values from the core data (3B-1 and 3D-1).

- 3 Vertical wells:
 - Perforating tidal bar top only (orange)

- Perforating entire interval
- 4 Lateral wells:
 - Completion with no fractures
 - Completion with hydraulic fractures: 50 feet fracture height, 100 feet half length, 250 feet fracture spacing, 7 stages.

Two following tables show the input of the properties taken from Buttermilk State well (LaFontaine, 2018), which are used for the structural versus stratigraphic analysis.

Table XI: Porosity/Permeability input for geologic structural and stratigraphic models (Model 3A-0 and 3C-0) with $T_m = 0$

| Petrel Facies | Kx | Ky | Kz | Φ |
|---------------|--------|--------|-----------|--------|
| Yellow | 0.0014 | 0.0014 | 0.0000257 | 3.29% |
| Green | 0.0009 | 0.0009 | 0 | 3.82% |
| Teal | 0.001 | 0.001 | 0 | 3.79% |
| Red | 0.002 | 0.0018 | 0.0003 | 4.91% |
| Grey | 0.0017 | 0.0018 | 0.0004 | 4.74% |
| Orange | 0.002 | 0.0018 | 0.0003 | 4.91% |

Table XII: Porosity/Permeability input for geologic structural and stratigraphic models (Model 3A-0.5 and 3C-0.5) with $T_m = 0.5$

| Petrel Facies | Kx | Ky | Kz | Φ |
|---------------|---------|---------|---------|--------|
| Yellow | 0.0015 | 0.0015 | 0.0011 | 3.29% |
| Green | 0.0012 | 0.0012 | 0.0015 | 3.82% |
| Teal | 0.0012 | 0.0012 | 0.0018 | 3.79% |
| Red | 0.0028 | 0.0028 | 0.00237 | 4.91% |
| Grey | 0.0019 | 0.0019 | 0.0019 | 4.74% |
| Orange | 0.00276 | 0.00276 | 0.00237 | 4.91% |

Table XIII: Porosity/Permeability input for proxy models (Model 3B-1 and 3D-1)

| Petrel Facies | Kx | Ky | Kz | Φ |
|---------------|--------|--------|--------|--------|
| Yellow | 0.0015 | 0.0015 | 0.0015 | 3.29% |
| Green | 0.002 | 0.002 | 0.002 | 4.51% |
| Teal | - | - | - | - |
| Red | 0.003 | 0.003 | 0.003 | 4.91% |
| Grey | 0.002 | 0.002 | 0.002 | 4.74% |
| Orange | 0.003 | 0.003 | 0.003 | 4.91% |

The results from simulation can be seen in Appendix C as a simulated data for each case. The data were then analyzed with LaFontaine (2018) to come to the following summary for structural models versus stratigraphic models. The detailed analyses can be seen from the LaFontaine study (2018). The summary of these analyses are categorized into:

- Pore-scale heterogeneities: Transmissibility multipliers are linked to a range of lithologies to define the permeability values for the fine-grained sediments. Applying one value of transmissibility multiplier into all facies of the reservoir model is not reasonable due to the variation of fine-grained sediments. The current study suggests that the mud-rich heterolithic deposits such as tidal bar facies and thin, interbedded sandstone and mudstone/siltstone facies should be characterized by T_m with a value equal or close to 0. Shoreface deposits otherwise have a widespread of mud drapes which suggest the higher T_m values (i.e $T_m = 0.5$).

- Bed-scale architectural anisotropies: Wave-influenced facies in the fine scale model such as Models 2A and 2B have great reduction on vertical permeability and less reduction on horizontal permeability due to the widespread mud drapes. Tidally influenced facies such as Models 2C and 2D shows that the mud drapes abundances and connectivity have great impact on the fluid migration pathways. Model 2D suggests that the fluid flows in depositional strike rather than depositional dips ($K_x > K_y$, Table II) due to mud drapes orientations; while Model 2C rejects this hypothesis. However, greater abundances of mud drapes are present in Model 2D than Model 2C (15.41% > 8.59%), which may suggest the hypothesis would be correct if the mud drapes abundances are significant enough. These tidal shale networks have greater reduction in horizontal permeability due to upward changes in mud drape geometry than wave-influenced facies. This is also seen in vertical wells between geologic models (Model 3A and 3C) and proxy models (Model 3B and 3D). The laterally continuous parasequence-scale facies

architecture (green/teal) horizons that block upward flow can be observed using the vertical well with tidal bar top perforation and vertical well with all perforation. The results show the production contrasts are much greater in a well that is exclusively completed in the upper zone.

- Reservoir scale controls on fluid migration: Comparison between structural models and stratigraphic models shows that stratigraphy is more influence on reservoir production (LaFontained, 2018). With $T_m = 0$, vertical permeability within the architectural controls of facies have significant impact on the production. This is proved by the application of hydraulic fractures, which improve the migration of fluid vertically. With $T_m = 0.5$, there is minor change in production for all types of models, which depends mostly on the intra-parasequence facies distribution in each model. The lateral well trending between North-South and West-East results show that North-South well may encounter more homogenous architecture, which is preferable for less complicated drilling or completion; however, when hydraulic fractures are introduced, the factors of architecture may reduce greatly.

- Drawbacks of modeling methodologies: (1) The link of transmissibility multiplier with lithology is uncertainty. (2) Bed-scale modeling to incorporate mud drape dimensions help to accurately capture the fluid flow behavior. (3) Other heterogeneities such as natural fractures and diagenetic alterations are not accounted for but may have certain effects on flow. (4) The outcrop may or may not capture entirely the extend of faults and fractures present in the Powder River Basin subsurface.

4.4.2. Field Development Analysis

Field development analysis use the reservoir properties from the Well Scale model (Model 1) such as matched PVT fluid model (Figure 18) and modified relative permeability (Figure 42) to describe the fluid flow behavior in the WCM. Also, for the Field Development

Analysis, porosity, permeability and water saturation are taken from the Well Scale model instead of the Buttermilk well. Table XIV shows the color codes used to describe each type of facies in the model and the permeability, porosity, and water saturation initially assigned to each facies.

Table XIV: Color description and initial assigned permeability of the Integrated Outcrop model.

| Color code | Upscaled Facies Description | Permeability (md) | Porosity (fraction) | Water Saturation (fraction) |
|-------------------|---------------------------------------------|--------------------------|----------------------------|------------------------------------|
| Orange | Tidal bar top | 0.159 | 0.069 | 0.557 |
| Grey | Tidal bar base | 0.348 | 0.078 | 0.514 |
| Teal | Shoreface Parasequences | 0.001 | 0.024 | 1.000 |
| Red | Cross-bedded sandstone | 0.054 | 0.055 | 0.626 |
| Green | Parallel-laminated storm deposits | 0.054 | 0.055 | 0.626 |
| Yellow | Thin, interbedded sand with silt/mud facies | 0.038 | 0.050 | 0.650 |

Three different Integrated Outcrop models are created for Field Development Analysis using the different reservoir properties in Table XIV. Note: This analysis uses only the structural models (3A and 3B). The flattened models are not used.

- Model 3Aa: Base case for geologic structural model
- Model 3Ab: Reduced case for geologic structural model applying the permeability reduction with $T_m = 0$ (Table IX)
- Model 3Bc: Proxy (Px) case for proxy structural model.

Three analyses were performed to test the important of the architectural controls and facies characterization on the fluid flow behavior and well performances. The first analysis tested the effect of architectural controls and facies characterization on the fluid production. The second analysis tested how the hydraulic fractures may affect the fluid flow behavior such as oil and water. The third analysis showed the well spacing study applied to the outcrop models.

A horizontal well was modeled to have similar parameters as the Rush State well including hydraulic fractures properties and spacing. Because the Integrated Outcrop model is

about half the size in length of the Well Scale model, the number of fracture are decreased to eight fractures with optimal 250 feet spacing (Figure 60). The well was drilled into the high-quality zones of tidal bar that is a favorable target zone of the WCM. The fractures height was modeled to penetrate vertically most of the reservoir. Fluid properties and rock physics estimated from the well scale model were used to define the reservoir properties for the outcrop model.

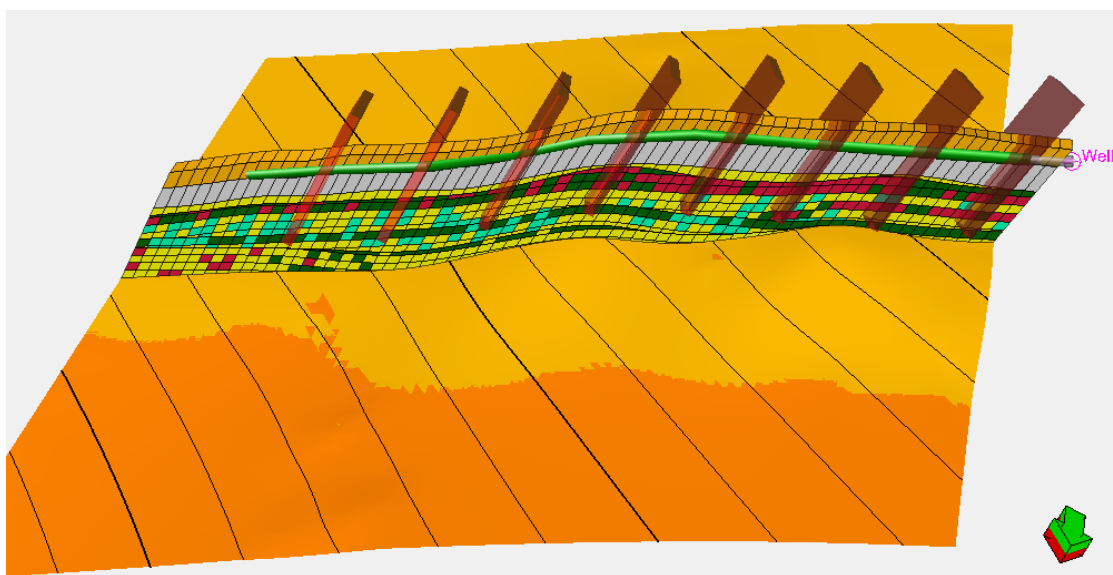


Figure 60: A horizontal well was modeled at the middle of the reservoir that penetrated the first two tidal bar layers of the geologic model. (Arrow illustrates the direction of the model)

First analysis shows three cases of a horizontal well in three different scenarios that are the production of the well in Model 3Aa, 3Ab, and 3Bc. Figure 61 shows the cumulative oil production of a well in each case. Proxy case (Model 3Bc) shows the highest production, and the geologic models (Model 3Aa and 3Ab) show the reduction in production when architectural controls and then facies characterization are applied. As the well was placed in tidal bar facies, most of the production came from these facies, but some came from the migration of fluid vertically from wave-influenced facies. Therefore, by applying the reduction of permeability, wave-influenced facies appeared to restrict the fluid migration from lower zones to upper zones that reduced the total oil production of the well.

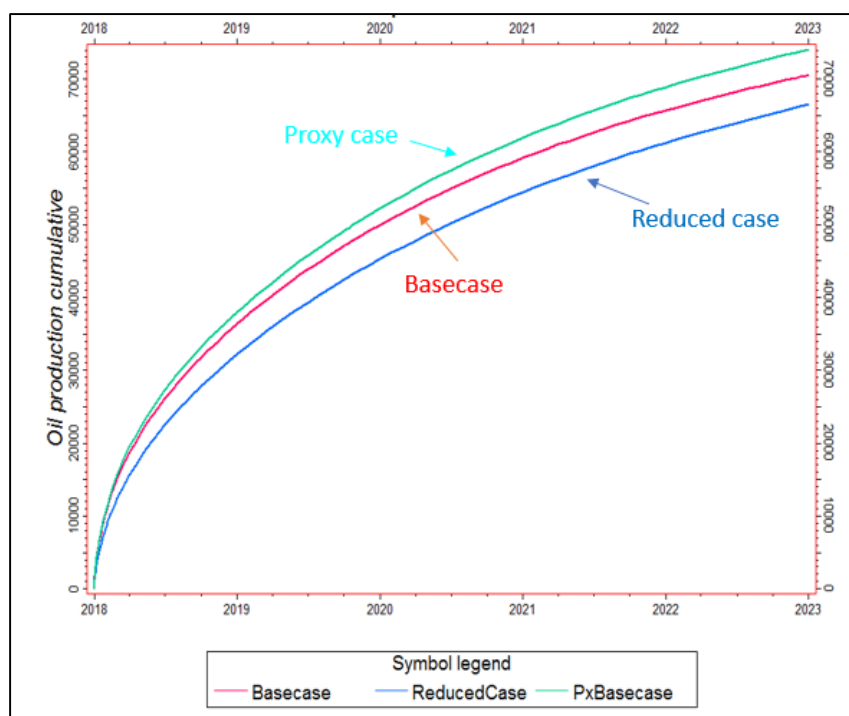


Figure 61: Cumulative oil production of three model scenarios.

The second analysis shows four cases using the Models 3Aa and 3Ab to test how the hydraulic fracture heights impact the water production. As the reservoir has increased water saturation for the lower zones, most of the wells in the Powder River Basin produce high water cut because the completion might penetrate the lower zone containing very high water saturation. In this analysis, the well was remodeled with lower fracture height to keep the well producing only from top two layers as shown in Figure 62. Figure 63 shows the results of cumulative oil and water production. As the oil production mostly comes from top two layers, reducing hydraulic fractures height does not impact significantly the overall oil production. However, the water production was reduced about 5 to 10 percent with reduced fracture height. This is significant because water production can be a problem in the WCM, and limiting fracture heights may help to prevent water production.

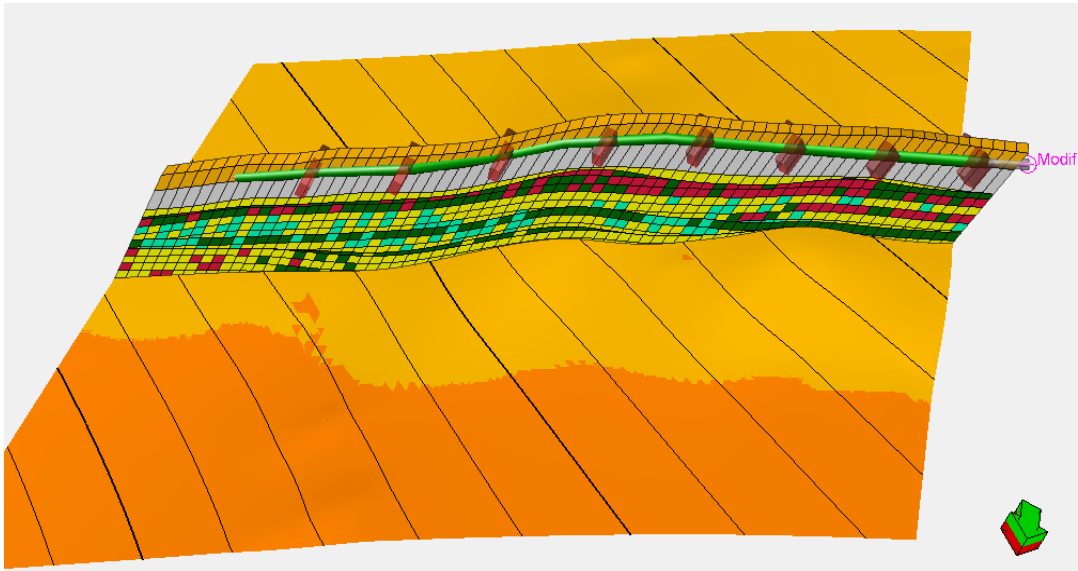


Figure 62: Modified fracture height well penetrate only into the first two layers of interested zones. (Arrow illustrates the direction of model)

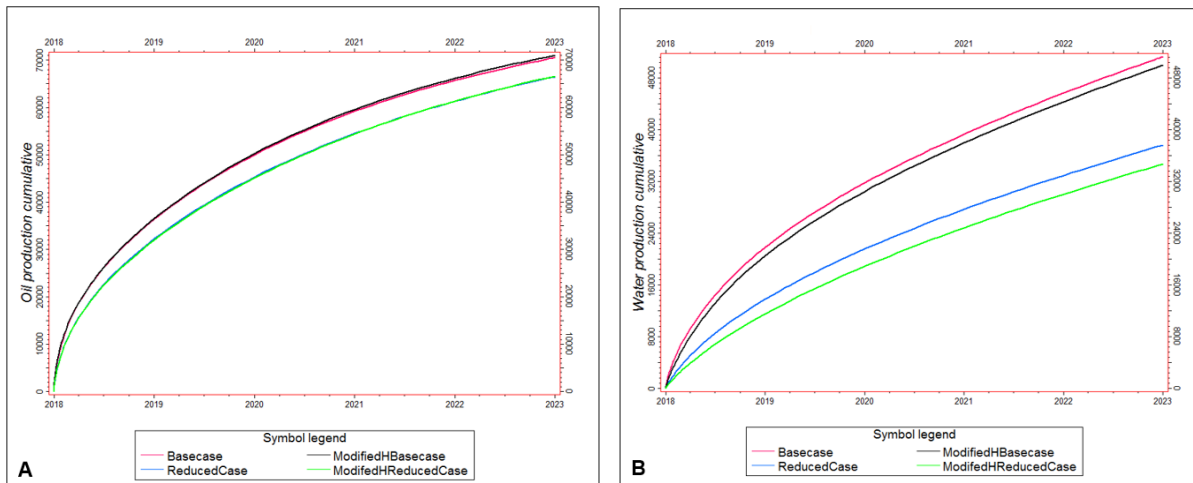


Figure 63: (A) Cumulative oil production and (B) cumulative water production of four scenarios in fracture height analysis on production using Integrated Outcrop model with and without permeability reduction. ((ModifiedHBasecase and ModifiedHReducedCase are the cases with reduced fracture height for model 3a and 3b)).

The final analysis shows the well spacing study that applies three horizontal wells with 440 feet spacing into each of the model (Figure 64). Figure 65 shows the results of cumulative oil production on each case. The proxy case (Model 3Bc) shows the highest production in overall, and the reduced case (Model 3Ab) shows lowest production. Field development applying three wells with 440 feet spacing helps to improve the production by recovering most of the fluid

in the study section. Figure 65 shows that cumulative oil production only increases from 700,000 STB to 1,000,000 STB with two additional wells, so it may not be economic to drill the other two wells.

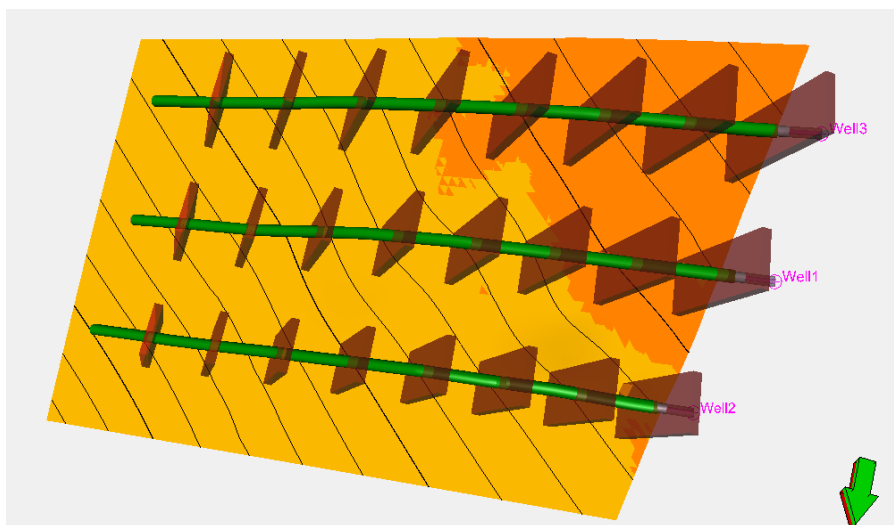


Figure 64: Three horizontal wells with 440 feet spacing for well spacing analysis. (Arrow illustrates the direction of model).

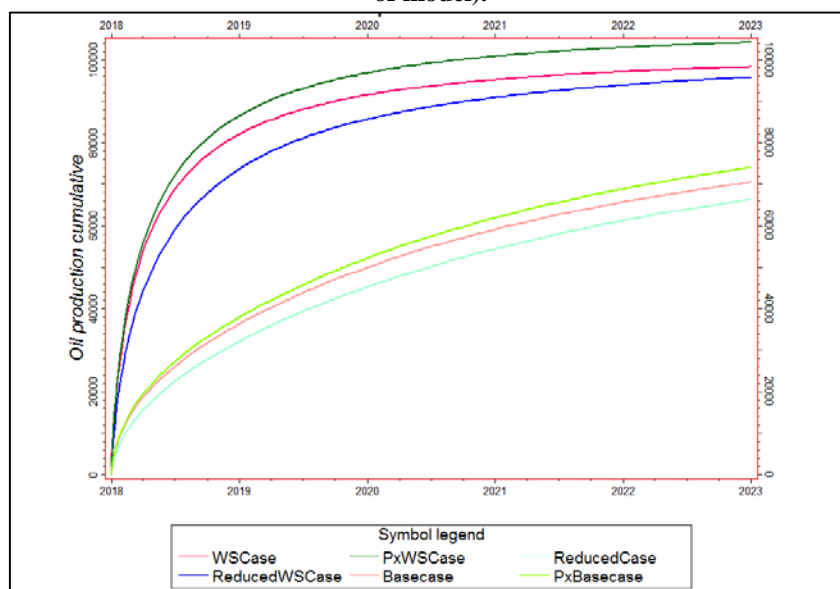


Figure 65: Well spacing analysis compares the effect of stratigraphic system on field development. Upper three lines simulate three wells production. Lower three lines simulate one well production. (WS = Well spacing case)

5. Discussion and Conclusion

Engineers often simplify the subsurface model to manage and predict the capability of the reservoir for well performance, or they use well logs with interpretation from the core data and seismic to describe the subsurface in macro-scale. The study has shown the workflow of creating a subsurface model with greater details by applying the interpretation from outcrop observations using flow-based upscaling. One of the outcome of this study is the percentage of permeability reduction applied for each facies of the Wall Creek Member of Frontier Formation (WCM) at different transmissibility multipliers. Horizontal permeability may not have much impact on the overall production, but vertical permeability reduction caused by geologic features can significantly affect the reservoir performance. Analysis by LaFontaine (2018) has suggested that understanding the link of transmissibility multiplier with lithogy and diagenetic alterations would help to define the effective permeability of each facies better and more accurate.

The importance of integrating outcrop observations into subsurface model is demonstrated by three different Integrated Outcrop models in field development analysis to describe the WCM from the simplest model to the most detailed model. A proxy model (Model 3Bc) was a simplest model with random distribution of facies that engineers can capture from the core data or even the well logs to differentiate each facies. The geologic model (Model 3Aa) was created by correlating the control points of each facies on the Tisdale Anticline outcrop to create the architectural controls for each facies and represent those facies onto the model. The geologic model with reduced permeability (Model 3Ab) has also taken further steps by using flow-based upscaling the very detailed geologic features (high-resolution model) of each facies to determine its effective permeability in three directions. This model 3Ab has included all the architectural system from the outcrop and characterization of each facies to provide the best possible

stratigraphic system of the subsurface model of the WCM. From the field development analysis, the results showed that the proxy model (Model 3Bc) can often overestimate the actual recovery of the fluid by not accounting the fluid flow behavior due to architectural controls as well as the migration of fluid in vertical direction. The results from model 3Ab suggests some major points that should be considered for field development. Many wells producing from WCM has encountered lower production due to low quality rock. Better interpretation can help in developing a well plan to avoid such cases. For well planning, due to the unique reservoir of the WCM, the horizontal well should try to penetrate only into the tidal bar facies if possible while drilling the WCM to avoid the lower zones with very high water saturation. Natural fractures were often encountered while drilling the wells that may lead to upward migration of water. Well completion involving hydraulic fractures should be careful to not penetrate too deep into lower zones, as the model has simulated the increases of water saturation due to hydraulic fractures when the oil production is not improved. Full field development for the WCM should account for the stratigraphic system, so that the actual recovery will not be overestimated.

6. Recommendation

The study has demonstrated that quantification of reservoir heterogeneities (at a scale of cm) could be important to evaluate the reservoir performance. The outcrop of the formation or any analog with similar depositional environment to the subsurface reservoirs become an exceptional tool to study these heterogeneities. This study provides an excellent example of the workflow to attain the stratigraphic study from the outcrop and integrate them into the subsurface model.

Further study on lithology and diagenetic alteration, as well as natural fractures, can provide better upscaling results to apply onto the model. Beside that, for the Wall Creek Member, the percentage of permeability reduction of each facies estimated in this study can be applied to any current subsurface model on the field to reduce the uncertainty for production forecast related to geologic understandings of the field. Fluid properties and relative permeability curves generated from this study can also be used for any kind of reservoir analysis or well performances on the WCM.

7. References Cited

Amaefule, J. O. and Handy, L. L. (1982). *The effects of interfacial tensions on relative oil/water permeabilities of consolidated porous media*. SPE Journal, Vol. 22, No. 3, P. 371-381. SPE-9783-PA.

Anna, L. O., Klett, T.R., Le, P. A., & Anderson, C.P. (2010). *Total petroleum systems and geologic assessment of oil and gas resources in the Powder River basin province, Wyoming and Montana*. Reston, VA: U.S. Dept. of the Interior, U.S. Geological Survey.

Asar, H. and Handy, L. L. (1998). *Influence of interfacial tension on gas/oil relative permeability in a gas-condensate system*. SPE Reservoir Engineering, Vol. 3, No. 1, P. 257-264. SPE-11740-PA.

Bhattacharya, J. P. and Willis, B. J. (2001). *Lowstand deltas in the Frontier Formation, Powder River basin, Wyoming: Implications for sequence stratigraphic models*. AAPG Datapages. Vol. 85, P. 261-294.

Brook, R. H. and Corey, A. T. (1964). *Hydraulic properties of porous media*. Hydrology Papers, No.3, Colorado State University, Fort Collins, Colorado.

Byers, C. W. and Larson, D.W. (1979). *Paleo-environments of Mowry Shale (Lower Cretaceous), western and central Wyoming*. AAPG Bulletin, Vol. 63, No. 3, P. 354-375.

Coats, K. H., Thomas, L. K., and Pierson, R. G. (1998). *Compositional and Black Oil Reservoir Simulation*. SPE Reservoir Evaluation & Engineering. Vol. 1, No. 4, P. 372-379. SPE-50990-PA.

Dandekar, A. Y. (2013). *Petroleum Reservoir Rock and Fluid Properties*. Boca Raton, Florida: CRC Press.

Doleshal B. (2017). *Evaluation of methods to model hydraulic fractures in flow simulation*. Graduate Theses & Non-Theses. 145.

https://digitalcommons.mtech.edu/grad_rsch/145/

Durlofsky, L. J. (2005). *Upscaling and gridding of fine scale geological models for flow simulation*. Paper presented at the 8th International Forum on Reservoir Simulation Iles Borromees, Stresa, Italy, June 20-24, 2005.

Hartmann, D. J. and Beaumont, E. A. (1991). *Exploring for Oil and Gas Trap*. Retrieved from <http://archives.datapages.com>.

LaFontaine, N. (2018). *Facies architecture and controls on reservoir behavior in the Turonian Wall Creek member of the Frontier Formation in the Powder River Basin, Wyoming*. Graduate Student Theses, Dissertations, & Professional Papers.

Liu, K. 1999. *Fully Automatic Procedure for Efficient Reservoir Fluid Characterization*. SPE 56744. Presented at SPE Annual Technical Conference and Exhibition, Houston, USA, 3-6 October, 1999.

King, M. J. and Mansfield, M. (1999). *Flow simulation of geologic models*. SPE Reservoir Evaluation & Engineering. Vol. 2, No. 4, P. 351-367. SPE-57469-PA.

Manzocchi, T., Walsh, J., Nell, P., and Yielding, G. (1999). *Fault transmissibility multipliers for flow simulation models*. Petroleum Geoscience. Vol. 3, No. 1, P. 53-63.

Merewether, E.A. (1996). *Stratigraphy and tectonic implications of Upper Cretaceous rocks in the Powder River Basin, Northeastern Wyoming and Southeastern Montana*. USGS Bulletin 1917-T.

Moore, W. R., Zee Ma, Y., Pirie, I., and Zhang Y. (2016). *Tight gas reservoirs, Part 2: Petrophysical analysis and reservoir modeling*. Unconventional Oil and Gas Resources Handbook. <http://dx.doi.org/10.1016/B978-0-12-802238-2.00015-8> (accessed 27 October, 2017).

Muskat, M. and Botset, H. G. (1931). *Flow of gas through porous material*. Journal of Applied Physics. Vol. 1, No. 1, P. 27-47.

Nixon, R. P. (1973). *Oil source beds in Cretaceous Mowry Shale of northwestern interior United States*. AAPG Bulletin. Vol. 57, No. 1, P. 136-161.

Paterson, L., Painter, S., Zhang, X., and Pinczewski, V. *Simulating residual saturation and relative permeability in heterogenous formations*. SPE paper 36523, presented at 1996 SPE Annual Technical Conference Exhibition, Denver, Colorado.

Pedersen, K.S., Thomassen, P., and Fredenslund, A. (1985). *On the Dangers of “Tuning” Equation of State Parameters*. SPE 14487

Perrot, P. (1998). *A to Z of Thermodynamics*. Oxford University Press.

Qi, D. and Hesketh, T. (2007). *An analysis of upscaling techniques for reservoir simulation*. Petroleum Science and Technology, Vol. 23, No. 7-8, P. 827-842.
<https://doi.org/10.1081/LFT-200033132>

Rice, D.D. and Keighin, C.W. (1989). *Configuration of shelf sandstone oil reservoir, Upper Cretaceous (Turonian) Turner Sandy Member of Carlile Shale, Powder River Basin, Wyoming*. AAPG abstract. Vol. 73, No. 3, P. 405.

Samier, P. (1990). *A finite-element method for calculating transmissibilities*. Proc. 1990 European Conference on Mathematics of Oil Recovery, Arles, France, 11-14 September.

Schuster, N.A. and Riboud, J. (1971). *Well loggings techniques*. World Petroleum Congress.

Skjaeveland, S.M. et al. (2000). *Capillary pressure correlation for mixed-wet reservoirs*. SPE reservoir Evaluation & Engineering., Vol. 3, No. 1.

Soave, G. (1972). *Equilibrium constants from a modified Redlich-Kwong equation of state*. Chemical Engineering Science. Vol. 27, Issues 6, P. 1197-1203.

Warren, J. E. and Price, H. S. (1961). *Flow in heterogeneous porous media*. Society of Petroleum Engineers. doi:10.2118/1579-G (accessed 20 October, 2017)

Wegemann, C. H. (1918). *The Salt Creek oil field Wyoming*. USGS Bulletin 670.

Wyoming Oil and Gas Conservation Commission (2016). Accessed September 25, 2016 from <http://wogcc.state.wy.us/>.

Zupanic, J., Hofmann, M. H., and Hennes, A. (2016). *Stratigraphic architecture and facies distribution within the Wall Creek member of the Frontier Formation, Western Powder River Basin, Wyoming*. AAPG Datapages/Search and Discovery Article #90259 at 2016 AAPG Annual Convention and Exhibition, Calgary, Alberta, Canada, June 19-22, 2016

Zupanic, J. (2017). *Lateral heterogeneity and architectural analysis of the Wall Creek member off the Upper Cretaceous (Turonian) Frontier Formation*. Graduate Student Theses, Dissertations, & Professional Papers. 11033. <https://scholarworks.umt.edu/etd/11033>.

8. Appendix A: Well Scale Model

Table XV: Initial properties for fluid components before matching

| Components | Mol Weight | Crit Pres | Crit Temp | Ω_a | Ω_b | ω | Parachors |
|------------------|----------------------------|-----------|----------------------------|---------------|------------|------------------------|-----------|
| | | (psia) | (°F) | | | | |
| N ₂ | 28.01 | 492.31 | -232.51 | 0.43 | 0.09 | 0.04 | 41.00 |
| CO ₂ | 44.01 | 1071.30 | 88.79 | 0.43 | 0.09 | 0.23 | 78.00 |
| H ₂ S | 34.08 | 1296.20 | 212.81 | 0.43 | 0.09 | 0.10 | 80.00 |
| C1 | 16.04 | 667.78 | -116.59 | 0.43 | 0.09 | 0.01 | 77.00 |
| C2 | 30.07 | 708.34 | 90.10 | 0.43 | 0.09 | 0.10 | 108.00 |
| C3 | 44.10 | 615.76 | 205.97 | 0.43 | 0.09 | 0.15 | 150.30 |
| IC4 | 58.12 | 529.05 | 274.91 | 0.43 | 0.09 | 0.18 | 181.50 |
| NC4 | 58.12 | 550.66 | 305.69 | 0.43 | 0.09 | 0.20 | 189.90 |
| IC5 | 72.15 | 491.58 | 369.05 | 0.43 | 0.09 | 0.23 | 225.00 |
| NC5 | 72.15 | 488.79 | 385.61 | 0.43 | 0.09 | 0.25 | 231.50 |
| C6 | 84.00 | 436.62 | 453.83 | 0.43 | 0.09 | 0.30 | 271.00 |
| C7+ | 208.50 | 251.40 | 847.18 | 0.43 | 0.09 | 0.68 | 540.97 |
| Components | V Crit | Z Crit | V Crit (Visc) | Z Crit (Visc) | Boil Temp | Ref Dens | Ref Temp |
| | (ft ³ /lb-mole) | | (ft ³ /lb-mole) | | (°F) | (lb /ft ³) | (°F) |
| N ₂ | 1.44 | 0.29 | 1.44 | 0.29 | -320.35 | 50.19 | -319.09 |
| CO ₂ | 1.51 | 0.27 | 1.51 | 0.27 | -109.21 | 48.51 | 67.73 |
| H ₂ S | 1.57 | 0.28 | 1.57 | 0.28 | -75.37 | 61.99 | -75.19 |
| C1 | 1.57 | 0.28 | 1.57 | 0.28 | -258.79 | 26.53 | -258.61 |
| C2 | 2.37 | 0.28 | 2.37 | 0.28 | -127.39 | 34.21 | -130.27 |
| C3 | 3.20 | 0.28 | 3.20 | 0.28 | -43.69 | 36.33 | -43.87 |
| IC4 | 4.21 | 0.28 | 4.21 | 0.28 | 10.67 | 34.77 | 67.73 |
| NC4 | 4.08 | 0.27 | 4.08 | 0.27 | 31.19 | 36.15 | 67.73 |
| IC5 | 4.93 | 0.27 | 4.93 | 0.27 | 82.13 | 38.71 | 67.73 |
| NC5 | 4.98 | 0.27 | 4.98 | 0.27 | 96.89 | 39.08 | 67.73 |
| C6 | 5.62 | 0.25 | 5.62 | 0.25 | 147.02 | 42.76 | 60.53 |
| C7+ | 13.14 | 0.24 | 13.14 | 0.24 | 530.19 | 52.01 | 60.00 |

Table XVI: Properties for fluid components after matching using Soave-Redlich-Kwong EOS

| Components | Mol Weight | Crit Pres | Crit Temp | Ω_a | Ω_b | ω | Parachors |
|------------------|----------------------------|-----------|----------------------------|---------------|------------|------------------------|-----------|
| | | (psia) | (°F) | | | | |
| N ₂ | 28.01 | 492.31 | -232.51 | 0.43 | 0.09 | 0.04 | 41.00 |
| CO ₂ | 44.01 | 1071.30 | 88.79 | 0.43 | 0.09 | 0.23 | 78.00 |
| H ₂ S | 34.08 | 1296.20 | 212.81 | 0.43 | 0.09 | 0.10 | 80.00 |
| C1 | 16.04 | 667.78 | -116.59 | 0.50 | 0.10 | 0.01 | 77.00 |
| C2 | 30.07 | 708.34 | 90.10 | 0.54 | 0.09 | 0.10 | 108.00 |
| C3 | 44.10 | 615.76 | 205.97 | 0.30 | 0.09 | 0.15 | 150.30 |
| IC4 | 58.12 | 529.05 | 274.91 | 0.30 | 0.09 | 0.18 | 181.50 |
| NC4 | 58.12 | 550.66 | 305.69 | 0.30 | 0.09 | 0.20 | 189.90 |
| IC5 | 72.15 | 491.58 | 369.05 | 0.33 | 0.08 | 0.23 | 225.00 |
| NC5 | 72.15 | 488.79 | 385.61 | 0.33 | 0.08 | 0.25 | 231.50 |
| C6 | 84.00 | 436.62 | 453.83 | 0.37 | 0.06 | 0.30 | 271.00 |
| C7+ | 208.50 | 360.78 | 823.86 | 0.43 | 0.09 | 0.55 | 540.97 |
| Components | V Crit | Z Crit | V Crit (Visc) | Z Crit (Visc) | Boil Temp | Ref Density | Ref Temp |
| | (ft ³ /lb-mole) | | (ft ³ /lb-mole) | | (°F) | (lb /ft ³) | (°F) |
| N ₂ | 1.44 | 0.29 | 1.44 | 0.29 | -320.35 | 50.19 | -319.09 |
| CO ₂ | 1.51 | 0.27 | 1.51 | 0.27 | -109.21 | 48.51 | 67.73 |
| H ₂ S | 1.57 | 0.28 | 1.57 | 0.28 | -75.37 | 61.99 | -75.19 |
| C1 | 1.57 | 0.28 | 1.57 | 0.28 | -258.79 | 26.53 | -258.61 |
| C2 | 2.37 | 0.28 | 2.37 | 0.28 | -127.39 | 34.21 | -130.27 |
| C3 | 3.20 | 0.28 | 3.91 | 0.34 | -43.69 | 36.33 | -43.87 |
| IC4 | 4.21 | 0.28 | 5.15 | 0.35 | 10.67 | 34.77 | 67.73 |
| NC4 | 4.08 | 0.27 | 4.99 | 0.33 | 31.19 | 36.15 | 67.73 |
| IC5 | 4.93 | 0.27 | 6.03 | 0.33 | 82.13 | 38.71 | 67.73 |
| NC5 | 4.98 | 0.27 | 6.09 | 0.33 | 96.89 | 39.08 | 67.73 |
| C6 | 5.62 | 0.25 | 6.87 | 0.31 | 147.02 | 42.76 | 60.53 |
| C7+ | 13.05 | 0.34 | 13.69 | 0.36 | 535.45 | 52.61 | 60.00 |

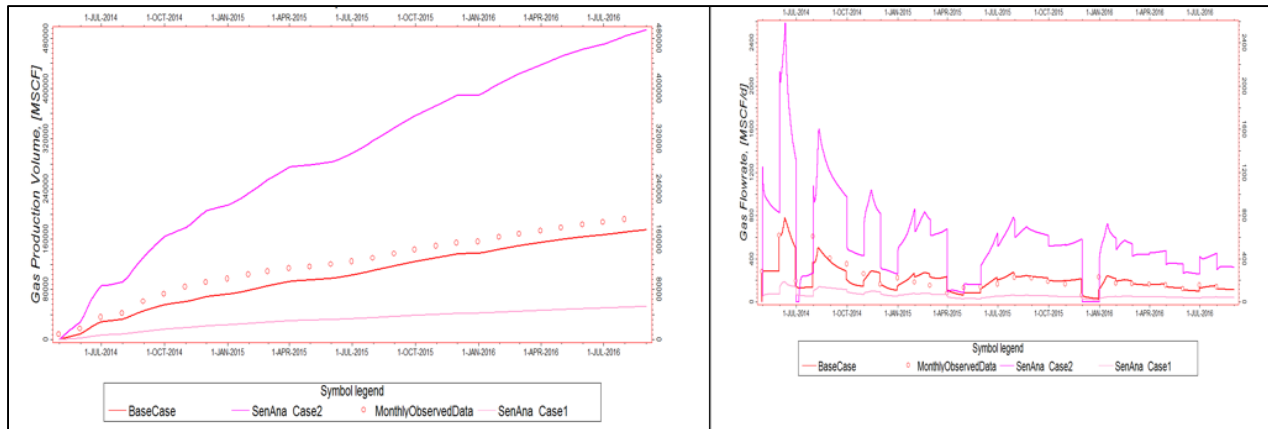


Figure 66: Gas production cumulative and gas production rate for porosity sensitivity analysis.

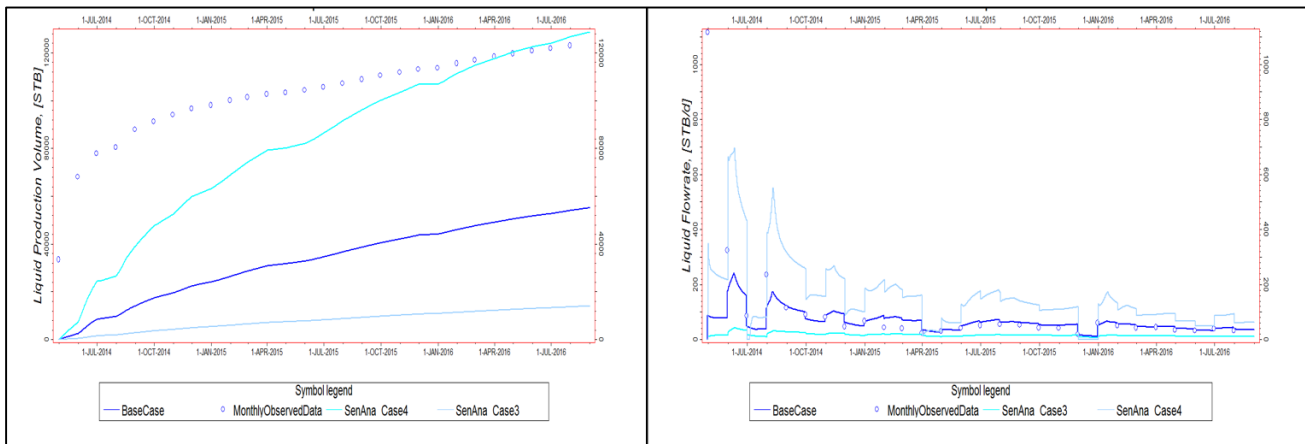


Figure 67: Water production cumulative and water production rate for minimum and maximum permeability sensitivity analysis.

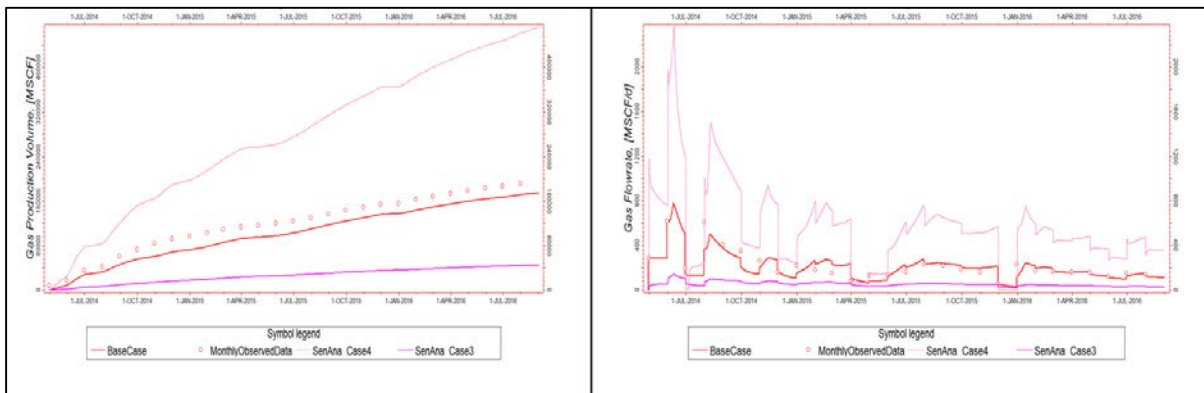


Figure 68: Gas production cumulative and gas production rate for minimum and maximum permeability sensitivity analysis.

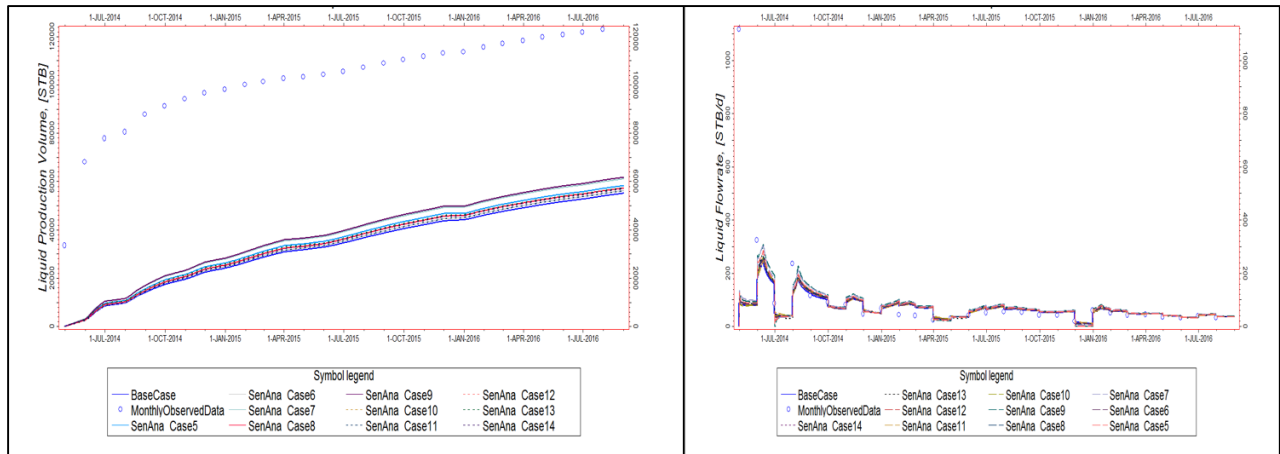


Figure 69: Water production cumulative and water production rate for random permeability sensitivity analysis.

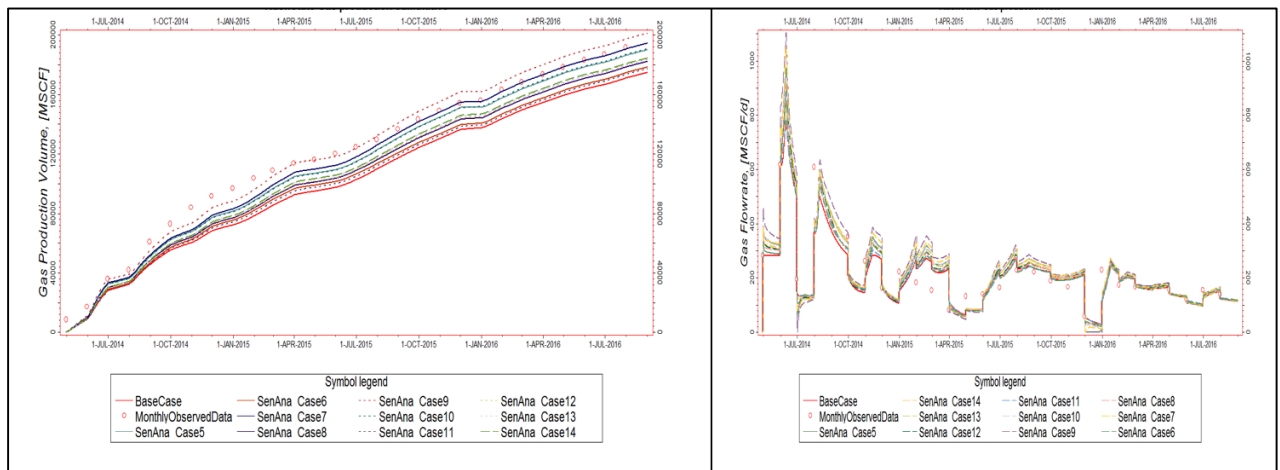


Figure 70: Gas production cumulative and gas production rate for random permeability sensitivity analysis.

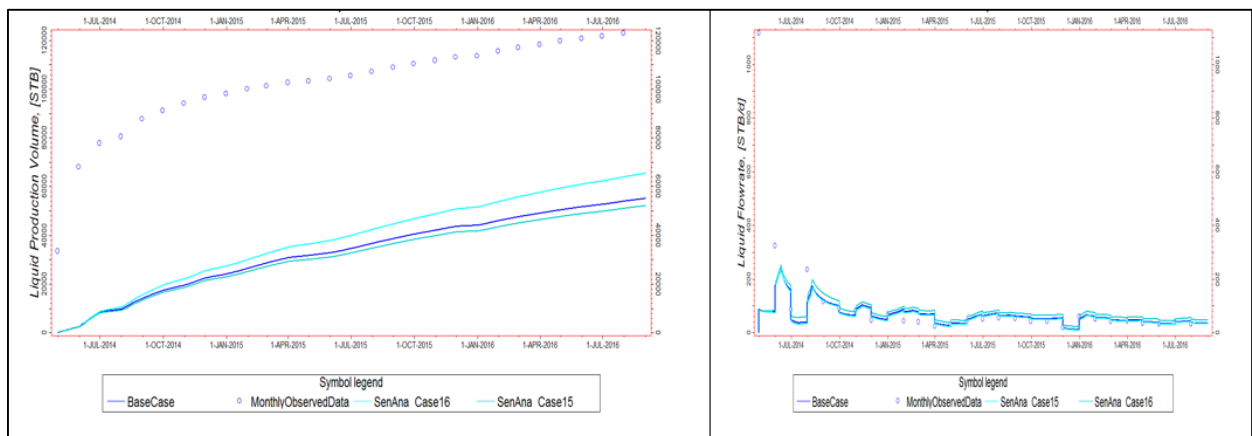


Figure 71: Water production cumulative and water production rate for hydraulic fractures sensitivity analysis.

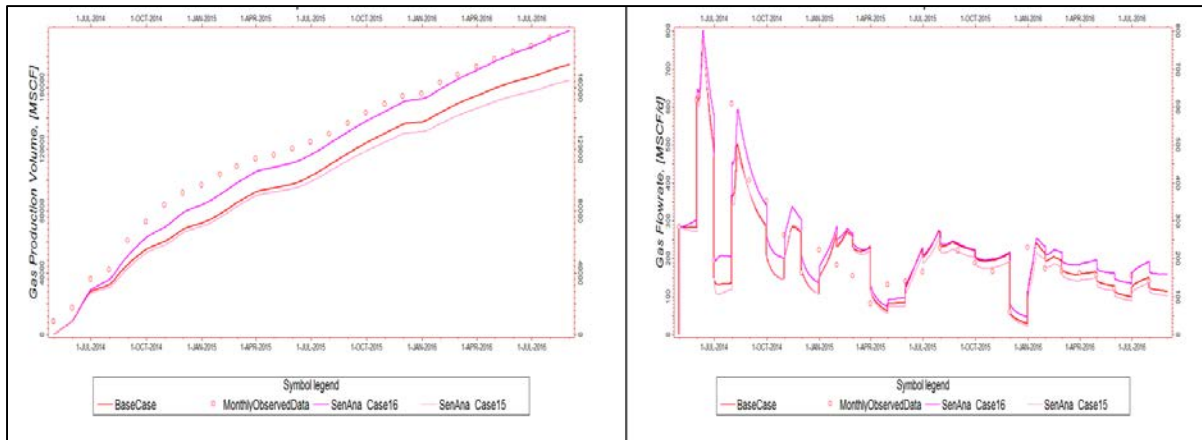


Figure 72: Gas production cumulative and gas production rate for hydraulic fractures sensitivity analysis.

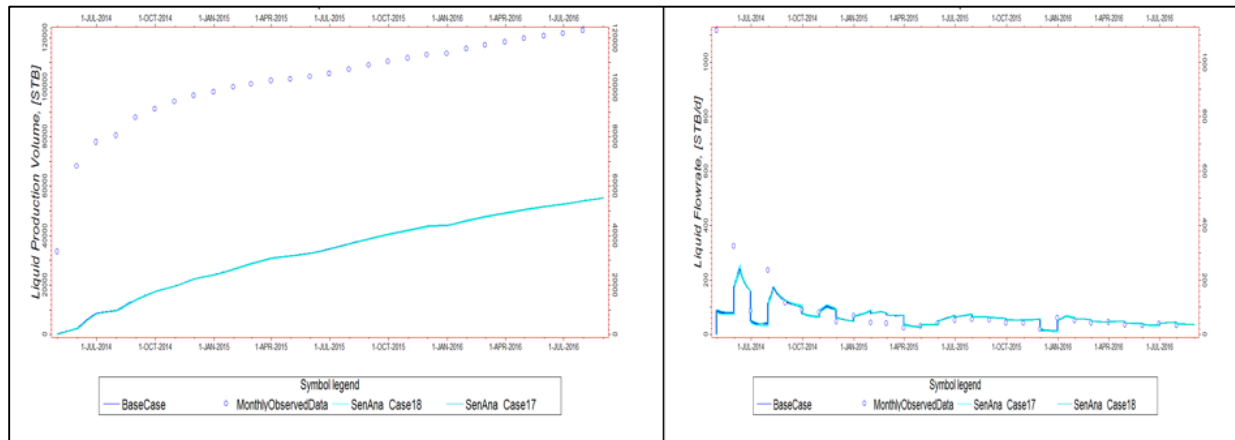


Figure 73: Water production cumulative and water production rate for oil Corey exponent sensitivity analysis.

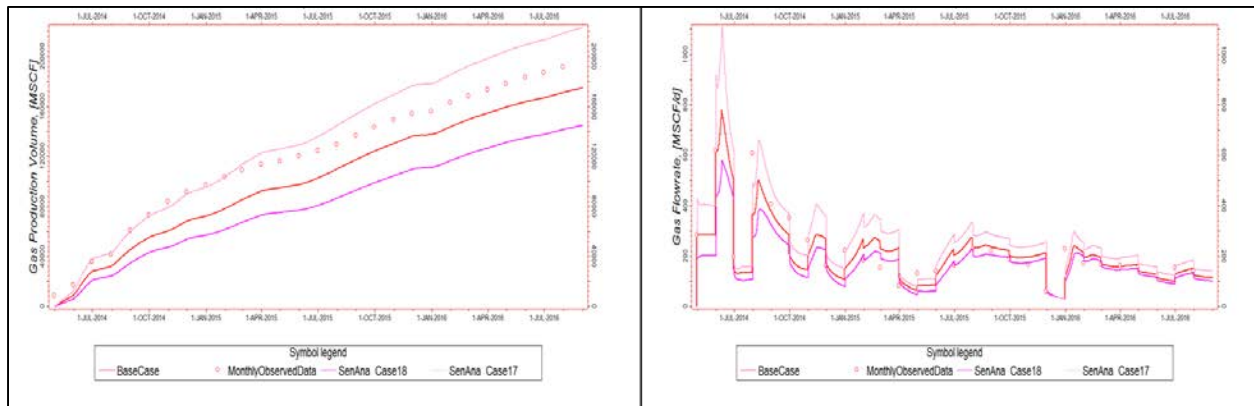


Figure 74: Gas production cumulative and gas production rate for oil Corey exponent sensitivity analysis.

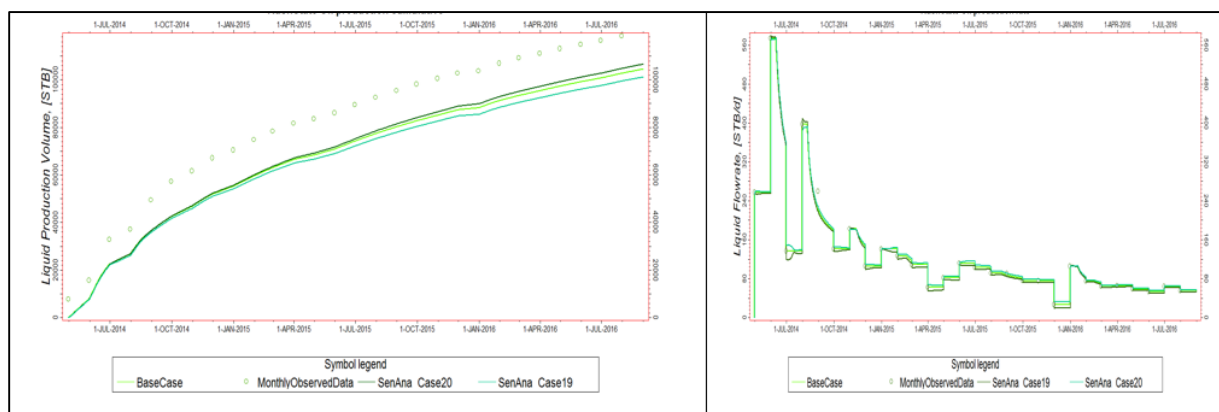


Figure 75: Oil production cumulative and oil production rate for water Corey exponent sensitivity analysis.

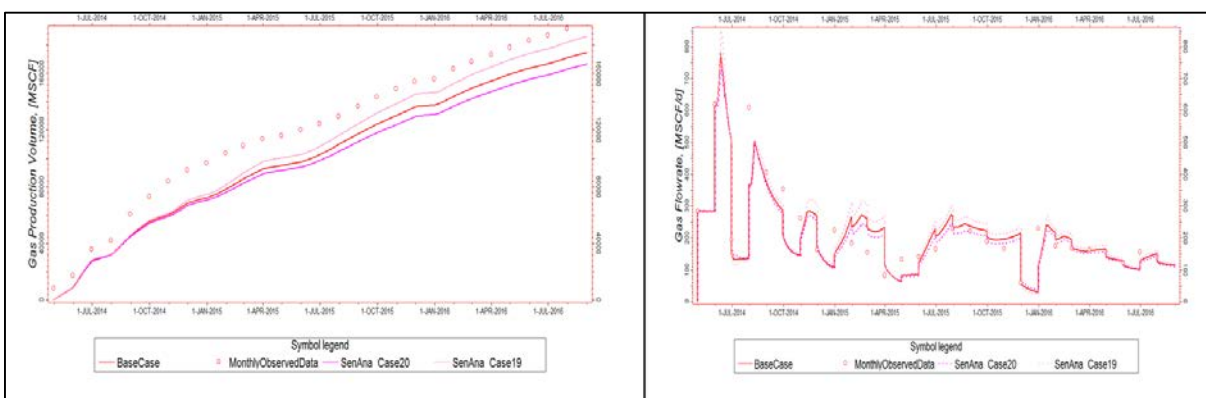


Figure 76: Gas production cumulative and gas production rate for water Corey exponent sensitivity analysis.

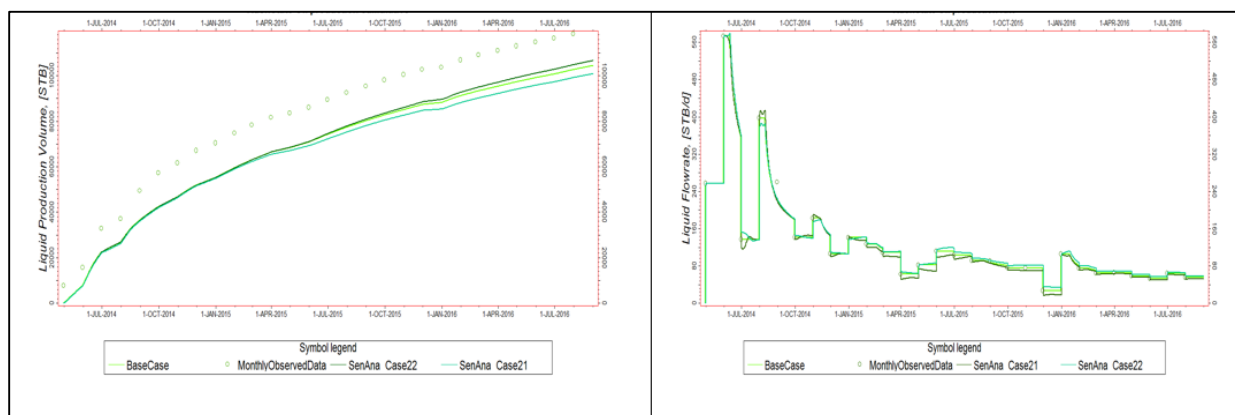


Figure 77: Oil production cumulative and oil production rate for gas Corey exponent sensitivity analysis

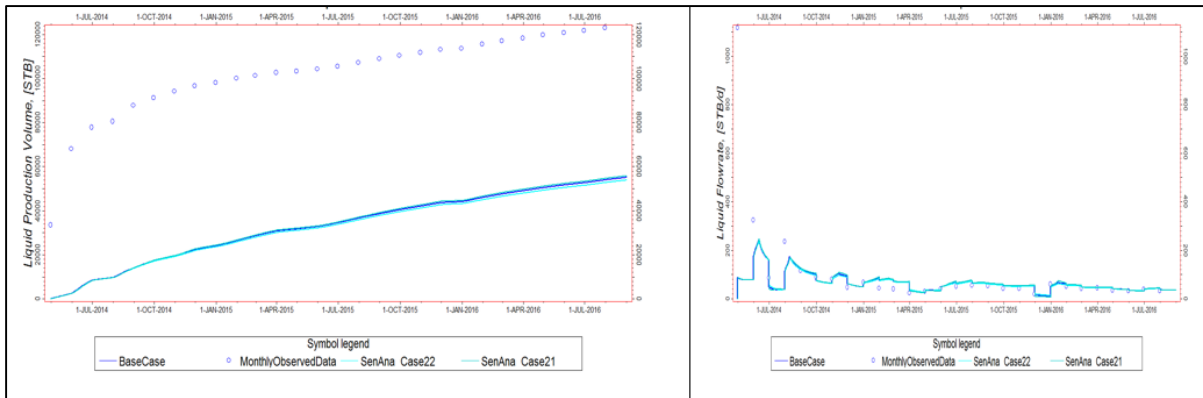


Figure 78: Water production cumulative and water production rate for gas Corey exponent sensitivity analysis

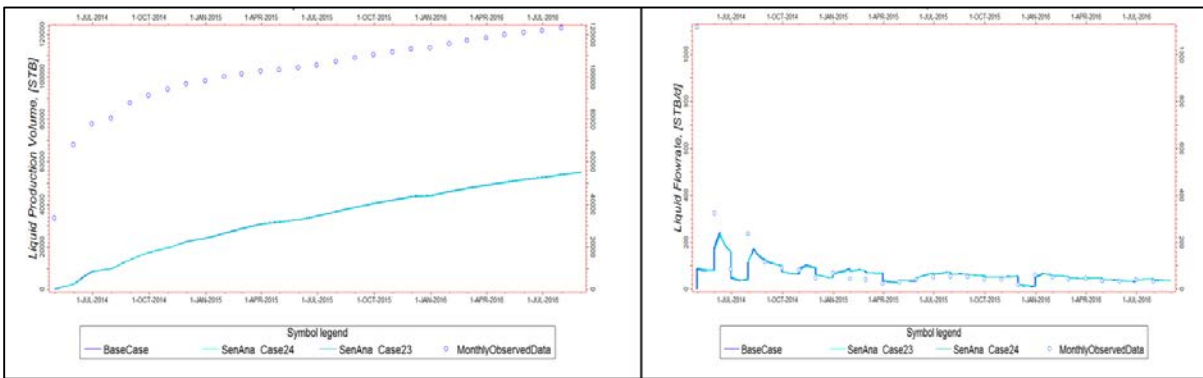


Figure 79: Water production cumulative and water production rate for K_{ro} at S_{omax} sensitivity analysis

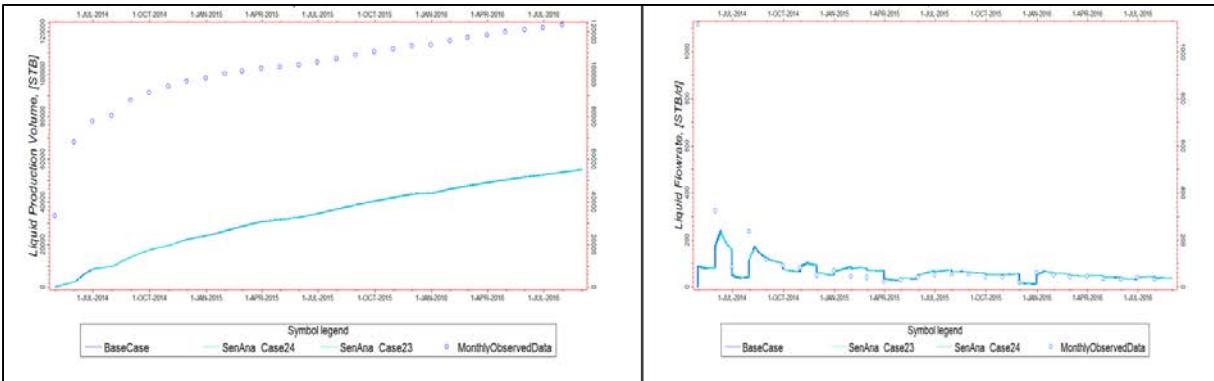


Figure 80: Water production cumulative and water production rate for K_{ro} at S_{omax} sensitivity analysis

9. Appendix B: High-resolution models and Flow Based Upscaling

Model 2A: Thin, Interbedded Sandstone with Siltstone/Mudstone

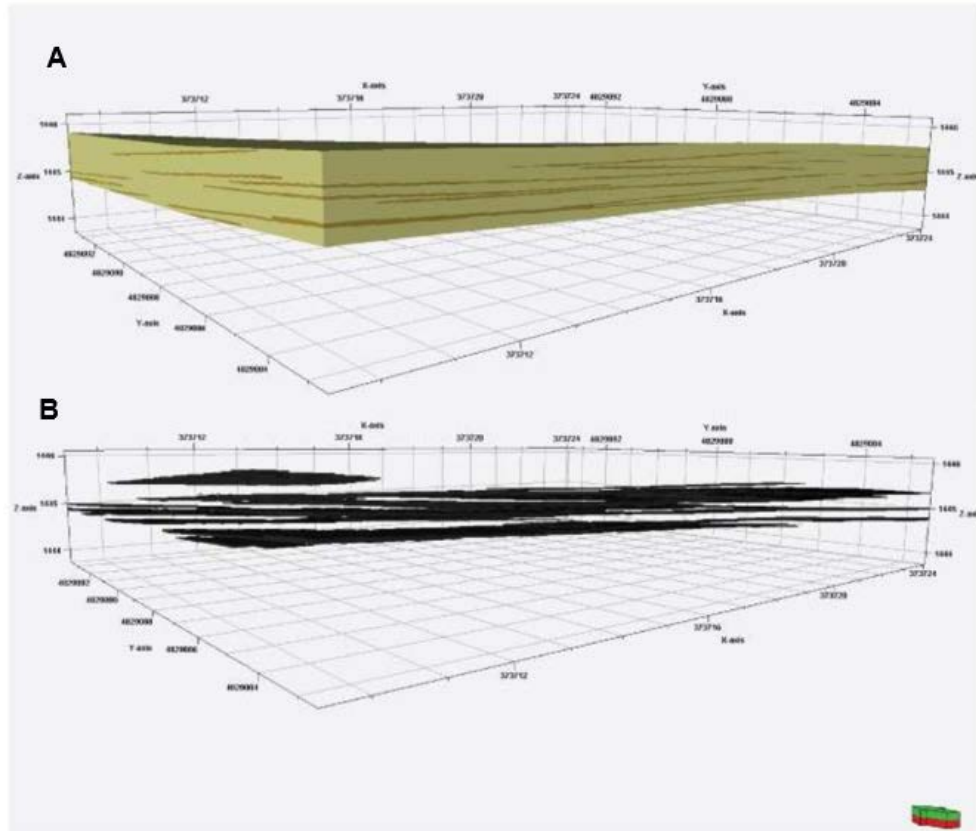


Figure 81: (A) Thin, interbedded sandstone and siltstone/mudstone facies model, and (B) mud drapes abundance illustrated by black traces.

| Case | Transmissibility Multiplier | ΔP | q | PermX | %Reduction |
|------|-----------------------------|------------|-----------|--------|------------|
| | | (psi) | (bbl/day) | (md) | |
| 1 | 0 | 7500 | 0.1106 | 0.0014 | 9.75 |
| 2 | 0.3 | 7500 | 0.1161 | 0.0014 | 5.28 |
| 3 | 0.5 | 7500 | 0.1180 | 0.0015 | 3.75 |
| 4 | 0.7 | 7500 | 0.1198 | 0.0015 | 2.25 |
| 5 | 1 | 7500 | 0.1226 | 0.0015 | 0.00 |

| | Perm | | Porosity |
|-------|-------|----|----------|
| WCR10 | 0.001 | md | 0.0403 |

Mud Drape Abundance = 7.51%

| Case | Transmissibility Multiplier | ΔP | q | PermY | %Reduction |
|------|-----------------------------|------------|-----------|--------|------------|
| | | (psi) | (bbl/day) | (md) | |
| 1 | 0 | 7500 | 0.1940 | 0.0014 | 8.73 |
| 2 | 0.3 | 7500 | 0.2049 | 0.0014 | 3.62 |
| 3 | 0.5 | 7500 | 0.2082 | 0.0015 | 2.09 |
| 4 | 0.7 | 7500 | 0.2114 | 0.0015 | 0.57 |
| 5 | 1 | 7500 | 0.2126 | 0.0015 | 0.00 |

| Case | Transmissibility Multiplier | ΔP | q | PermZ | %Reduction |
|------|-----------------------------|------------|-----------|--------|------------|
| | | (psi) | (bbl/day) | (md) | |
| 1 | 0 | 7500 | 0.4789 | 0.0000 | 97.88 |
| 2 | 0.3 | 7500 | 19.6960 | 0.0011 | 12.97 |
| 3 | 0.5 | 7500 | 21.2327 | 0.0011 | 6.18 |
| 4 | 0.7 | 7500 | 21.9984 | 0.0012 | 2.79 |
| 5 | 1 | 7500 | 22.6303 | 0.0012 | 0.00 |

Figure 82: Flow-based upscaling results for Thin, interbedded sandstone and siltstone/mudstone facies.

Model 2B: Shoreface Parasequences

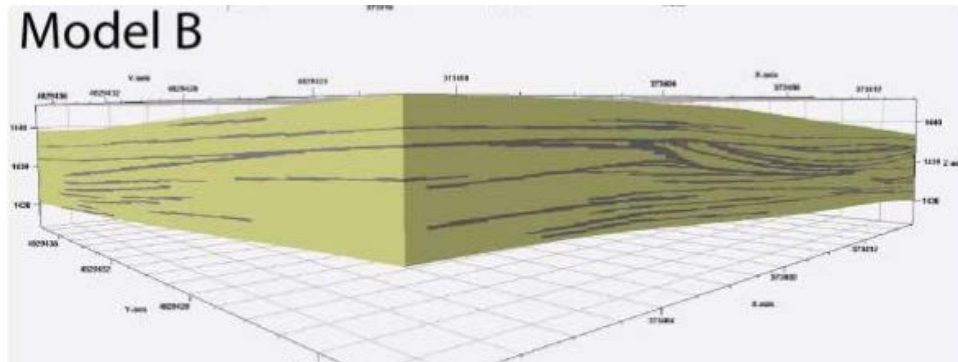


Figure 83: Shoreface Parasequences facies models

| Case | Transmissibility Multiplier | ΔP | q | PermX | %Reduction |
|------|-----------------------------|------------|-----------|--------|------------|
| | | (psi) | (bbl/day) | (md) | |
| 1 | 0 | 7500 | 0.2655 | 0.0010 | 23.96 |
| 2 | 0.3 | 7500 | 0.3128 | 0.0012 | 10.40 |
| 3 | 0.5 | 7500 | 0.3233 | 0.0012 | 7.40 |
| 4 | 0.7 | 7500 | 0.3337 | 0.0012 | 4.42 |
| 5 | 1 | 7500 | 0.3492 | 0.0013 | 9.00 |

| | Perm | | Porosity |
|--------|--------|----|----------|
| Upper | 0.002 | md | 0.0451 |
| Middle | 0.002 | md | 0.0451 |
| Bottom | 0.0015 | md | 0.0329 |

Mud Drape Abundance = 12.1%

| Case | Transmissibility Multiplier | ΔP | q | PermY | %Reduction |
|------|-----------------------------|------------|-----------|--------|------------|
| | | (psi) | (bbl/day) | (md) | |
| 1 | 0 | 7500 | 0.2756 | 0.0010 | 26.29 |
| 2 | 0.3 | 7500 | 0.3339 | 0.0012 | 10.69 |
| 3 | 0.5 | 7500 | 0.3456 | 0.0012 | 7.58 |
| 4 | 0.7 | 7500 | 0.3570 | 0.0012 | 4.52 |
| 5 | 1 | 7500 | 0.3739 | 0.0013 | 0.00 |

| Case | Transmissibility Multiplier | ΔP | q | PermZ | %Reduction |
|------|-----------------------------|------------|-----------|--------|------------|
| | | (psi) | (bbl/day) | (md) | |
| 1 | 0 | 7500 | 0.0000 | 0.0000 | 100.00 |
| 2 | 0.3 | 7500 | 17.0507 | 0.0016 | 23.23 |
| 3 | 0.5 | 7500 | 19.5671 | 0.0018 | 11.90 |
| 4 | 0.7 | 7500 | 20.9837 | 0.0019 | 5.52 |
| 5 | 1 | 7500 | 22.2102 | 0.0021 | 0.00 |

Figure 84: Flow-based upscaling results for Shoreface Parasequences facies.

Model 2C and 2D: Tidal Bar Base and Tidal Bar Top

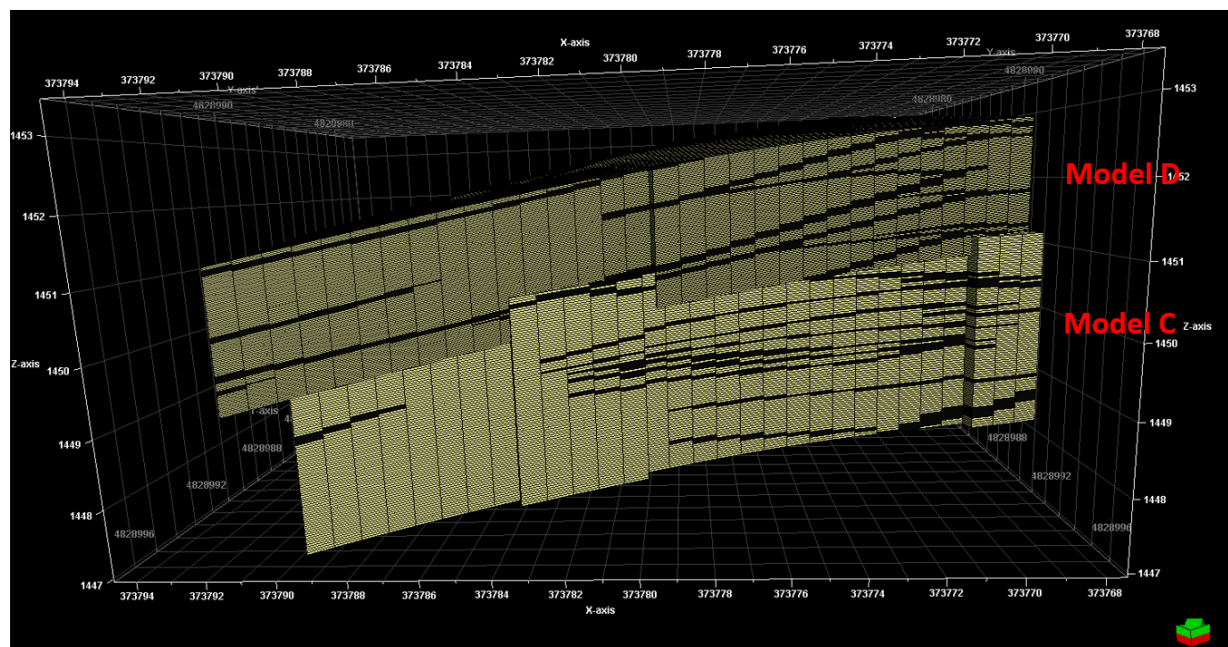


Figure 85: Tidal bar base and tidal bar top facies models. (Arrow illustrates the direction of the model)

| Case | Transmissibility Multiplier | ΔP | q | PermX | %Reduction |
|------|-----------------------------|------------|-----------|--------|------------|
| | | (psi) | (bbl/day) | (md) | |
| 1 | 0 | 6500 | 13.55 | 0.1212 | 33.19 |
| 2 | 0.3 | 6500 | 18.07 | 0.1616 | 10.97 |
| 3 | 0.5 | 6500 | 18.72 | 0.1674 | 7.79 |
| 4 | 0.7 | 6500 | 19.35 | 0.1731 | 4.65 |
| 5 | 1 | 6500 | 20.30 | 0.1815 | 0.00 |

| | Perm | Porosity |
|--------|--------|-----------|
| Facies | 0.1789 | md 0.0665 |

Mud Drape Abundance = 15.41%

| Case | Transmissibility Multiplier | ΔP | q | PermY | %Reduction |
|------|-----------------------------|------------|-----------|--------|------------|
| | | (psi) | (bbl/day) | (md) | |
| 1 | 0 | 6500 | 36.17 | 0.1101 | 38.91 |
| 2 | 0.3 | 6500 | 52.49 | 0.1597 | 11.34 |
| 3 | 0.5 | 6500 | 54.46 | 0.1658 | 8.01 |
| 4 | 0.7 | 6500 | 56.39 | 0.1716 | 4.76 |
| 5 | 1 | 6500 | 59.20 | 0.1802 | 0.00 |

| Case | Transmissibility Multiplier | ΔP | q | PermZ | %Reduction |
|------|-----------------------------|------------|-----------|--------|------------|
| | | (psi) | (bbl/day) | (md) | |
| 1 | 0 | 6500 | 267.16 | 0.0166 | 89.73 |
| 2 | 0.3 | 6500 | 2000.82 | 0.1243 | 23.07 |
| 3 | 0.5 | 6500 | 2291.71 | 0.1423 | 11.89 |
| 4 | 0.7 | 6500 | 2455.41 | 0.1525 | 5.60 |
| 5 | 1 | 6500 | 2601.00 | 0.1615 | 0.00 |

Figure 86: Flow-based upscaling results for tidal bar top facies.

| Case | Transmissibility Multiplier | ΔP | q | PermX | %Reduction |
|------|-----------------------------|------------|-----------|--------|------------|
| | | (psi) | (bbl/day) | (md) | |
| 1 | 0 | 6500 | 27.65 | 0.1492 | 15.48 |
| 2 | 0.3 | 6500 | 30.70 | 0.1656 | 6.18 |
| 3 | 0.5 | 6500 | 31.28 | 0.1688 | 4.39 |
| 4 | 0.7 | 6500 | 31.85 | 0.1719 | 2.62 |
| 5 | 1 | 6500 | 32.71 | 0.1765 | 0.00 |

| | | | |
|--------|--------|----|----------|
| | Perm | | Porosity |
| Facies | 0.1789 | md | 0.0665 |

Mud Drape Abundance = 8.59%

| Case | Transmissibility Multiplier | ΔP | q | PermY | %Reduction |
|------|-----------------------------|------------|-----------|--------|------------|
| | | (psi) | (bbl/day) | (md) | |
| 1 | 0 | 6500 | 71.77 | 0.1609 | 13.66 |
| 2 | 0.3 | 6500 | 77.66 | 0.1741 | 6.57 |
| 3 | 0.5 | 6500 | 79.28 | 0.1777 | 4.63 |
| 4 | 0.7 | 6500 | 80.84 | 0.1812 | 2.75 |
| 5 | 1 | 6500 | 83.13 | 0.1863 | 0.00 |

| Case | Transmissibility Multiplier | ΔP | q | PermZ | %Reduction |
|------|-----------------------------|------------|-----------|--------|------------|
| | | (psi) | (bbl/day) | (md) | |
| 1 | 0 | 6500 | 363.65 | 0.0349 | 66.05 |
| 2 | 0.3 | 6500 | 947.12 | 0.0909 | 11.58 |
| 3 | 0.5 | 6500 | 1008.09 | 0.0967 | 5.89 |
| 4 | 0.7 | 6500 | 1041.24 | 0.0999 | 2.80 |
| 5 | 1 | 6500 | 1071.18 | 0.1028 | 0.00 |

Figure 87: Flow-based upscaling results for tidal bar base facies.

10. Appendix C: Integrated Outcrop Model Analysis

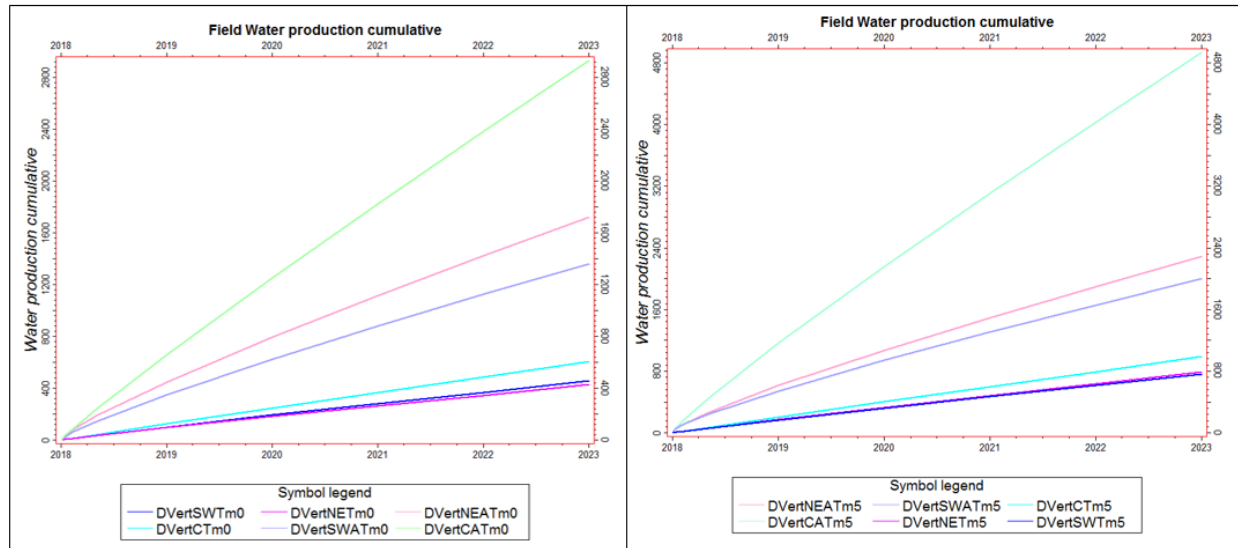


Figure 88: Results of vertical wells scenarios for geologic structural model (Model 3A) with $T_m=0$ and $T_m=0.5$. (D = Dipping, Vert = Vertical, A = All zones perforated, SW = South-West, NE = North-East, C = Center).

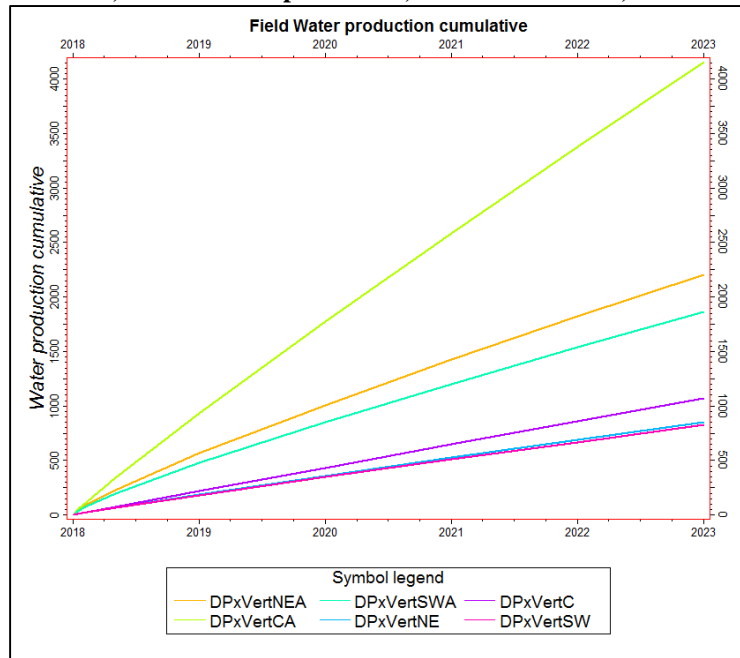


Figure 89: Results of vertical wells scenarios for proxy structural model (Model 3B). (D = Dipping, Px = Proxy, Vert = Vertical, A = All zones perforated, SW = South-West, NE = North-East, C = Center).

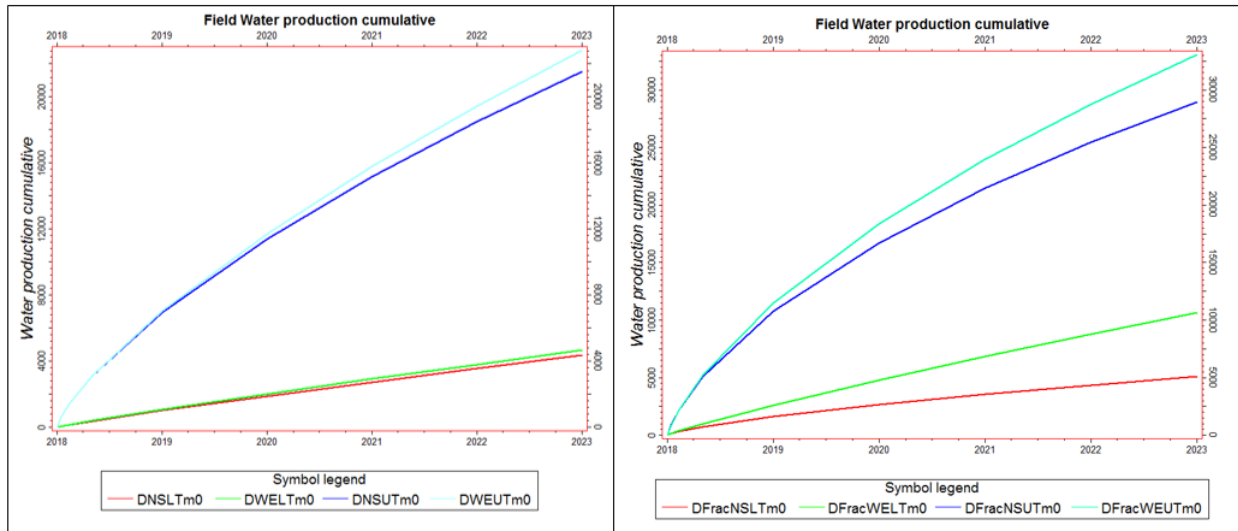


Figure 90: Results of horizontal wells scenarios for geologic structural model (Model 3A) with $T_m=0$. (D = Dipping, WE = West-East, NS = North-South, L = Lower zone, U = Upper zone, Frac = Hydraulic fractures).

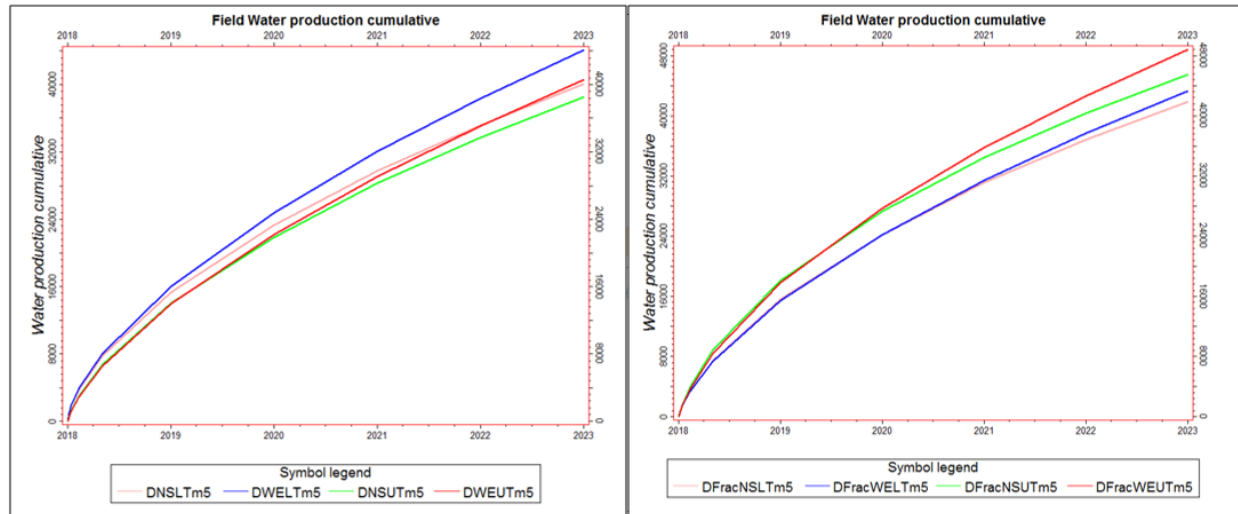


Figure 91: Results of horizontal wells scenarios for geologic structural model (Model 3A) with $T_m=5$. (D = Dipping, WE = West-East, NS = North-South, L = Lower zone, U = Upper zone, Frac = Hydraulic fractures).

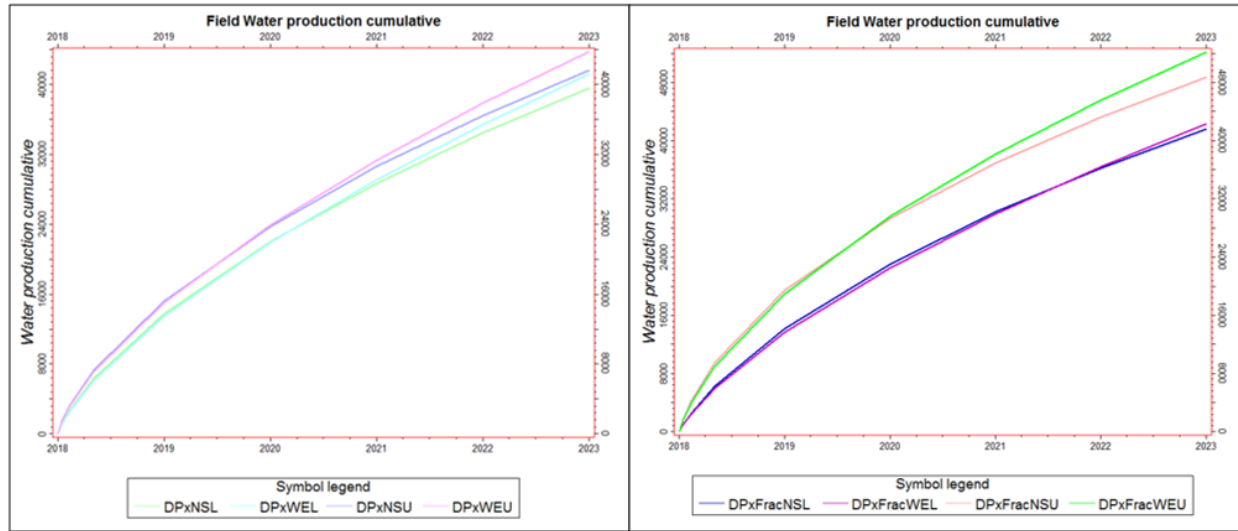


Figure 92: Results of horizontal wells scenarios for proxy structural model (Model 3B). (D = Dipping, Px = Proxy, WE = West-East, NS = North-South, L = Lower zone, U = Upper zone, Frac = Hydraulic fractures).

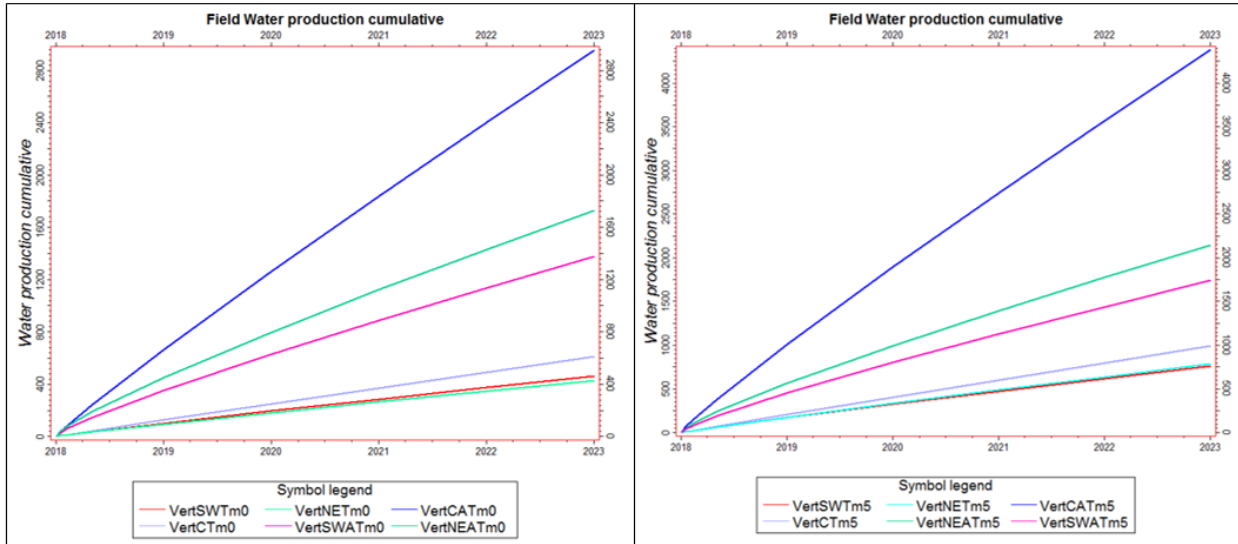


Figure 93: Results of vertical wells scenarios for geologic stratigraphic model (Model 3C) with $T_m=0$ and $T_m=0.5$. (Vert = Vertical, A = All zones perforated, SW = South-West, NE = North-East, C = Center).

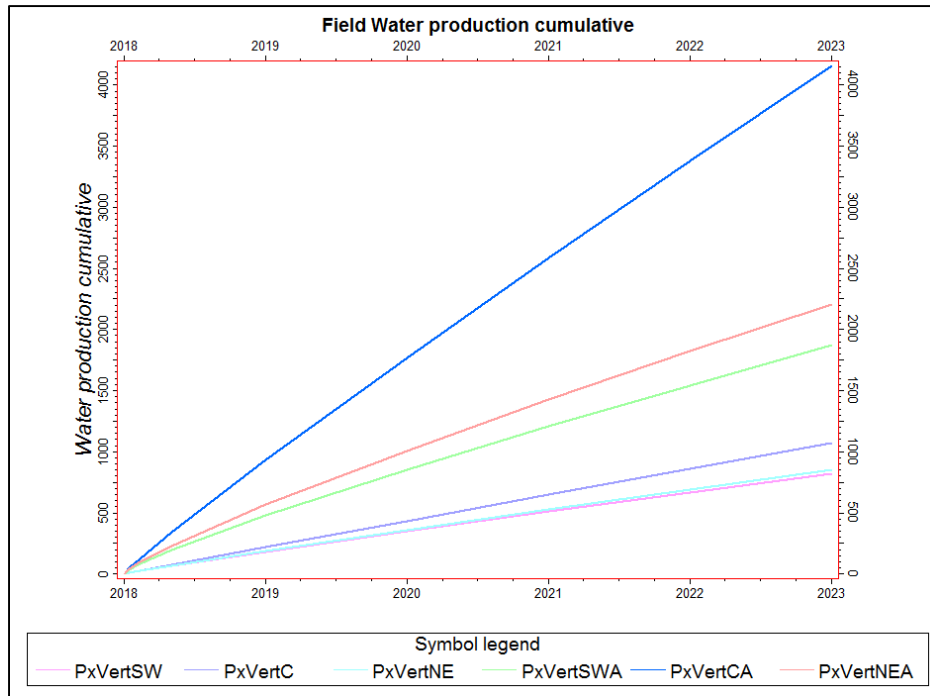


Figure 94: Results of vertical wells scenarios for proxy stratigraphic model (Model 3D). (Px = Proxy, Vert = Vertical, A = All zones perforated, SW = South-West, NE = North-East, C = Center).

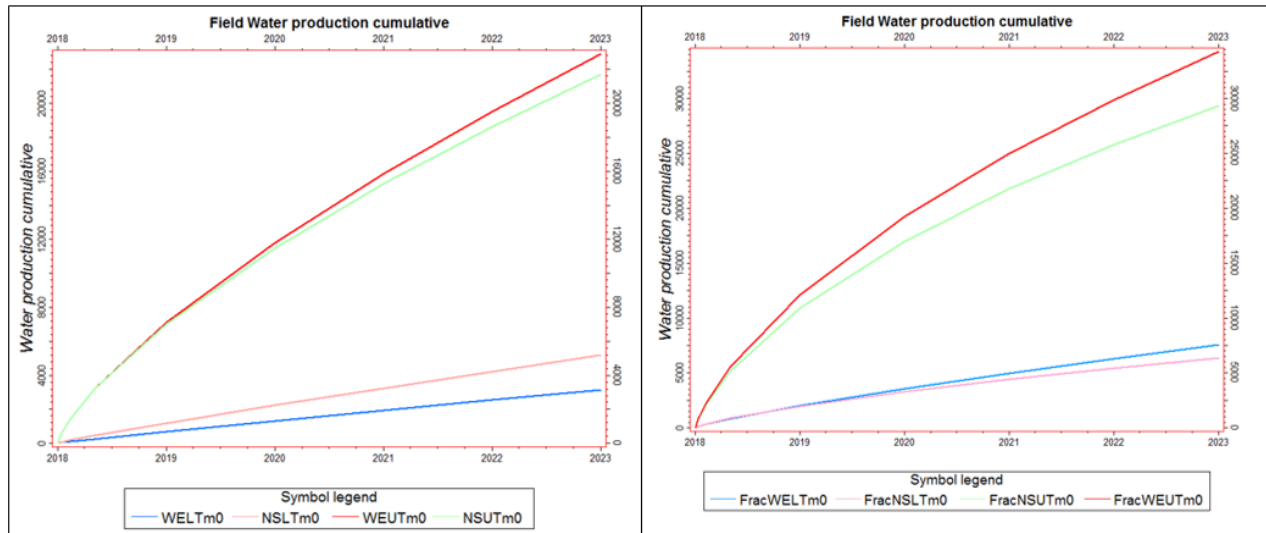


Figure 95: Results of horizontal wells scenarios for geologic stratigraphic model (Model 3C) with $T_m=0$. (WE = West-East, NS = North-South, L = Lower zone, U = Upper zone, Frac = Hydraulic fractures).

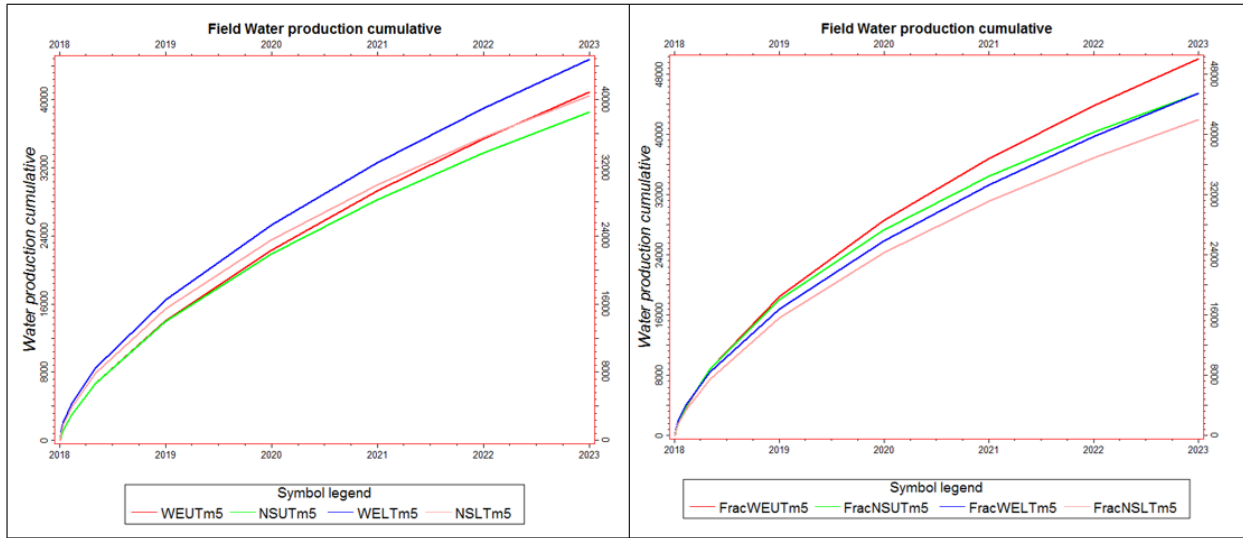


Figure 96: Results of horizontal wells scenarios for geologic stratigraphic model (Model 3C) with $T_m=5$. (WE = West-East, NS = North-South, L = Lower zone, U = Upper zone, Frac = Hydraulic fractures).

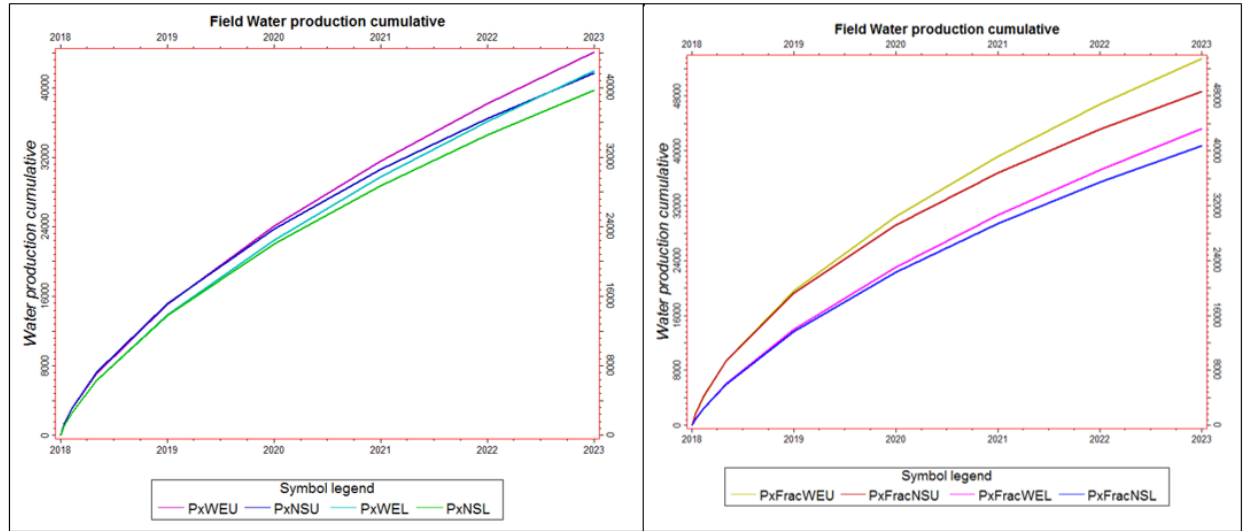
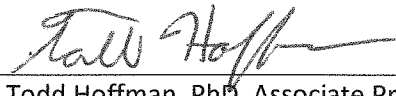


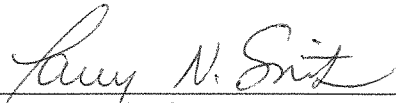
Figure 97: Results of horizontal wells scenarios for proxy stratigraphic model (Model 3D). (Px = Proxy, WE = West-East, NS = North-South, L = Lower zone, U = Upper zone, Frac = Hydraulic fractures).

SIGNATURE PAGE

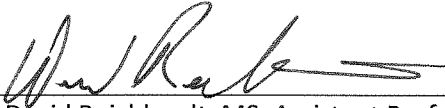
This is to certify that the thesis prepared by Tuan Le entitled "INTEGRATED STRATIGRAPHIC CONTROLS FOR FLOW SIMULATION OF THE WALL CREEK MEMBER OF FRONTIER FORMATION: WESTERN POWDER RIVER BASIN, WYOMING" has been examined and approved for acceptance by the Department of Petroleum Engineering, Montana Tech of The University of Montana, on this 5th day of April, 2018.



Todd Hoffman, PhD, Associate Professor
Department of Petroleum Engineering
Chair, Examination Committee



Larry Smith, PhD, Associate Professor and Department Head
Department of Geological Engineering
Member, Examination Committee



David Reichhardt, MS, Assistant Professor
Department of Petroleum Engineering
Member, Examination Committee